CONTROL OF CYCLING INDUCED BY FUNCTIONAL ELECTRICAL STIMULATION: A SWITCHED SYSTEMS THEORY APPROACH

By

MATTHEW JOHN BELLMAN

A DISSERTATION PRESENTED TO THE GRADUATE SCHOOL
OF THE UNIVERSITY OF FLORIDA IN PARTIAL FULFILLMENT
OF THE REQUIREMENTS FOR THE DEGREE OF
DOCTOR OF PHILOSOPHY

UNIVERSITY OF FLORIDA

2015

To my parents for making me who I am, and to my wife for building on their success

ACKNOWLEDGMENTS

I would like to acknowledge my advisor, Dr. Warren E. Dixon, for more than six years of guidance, without which this dissertation and, more importantly, my current position in life would not be possible. Dr. Dixon, along with my colleagues and the giants upon whose shoulders we all stand, have all played their parts in forging me into the engineer and scientist that I am today. No amount of gratitude could be sufficient to repay their contribution. All I can do is to take what they have given me and use those gifts to leave the world a better place than I found it. Thank you all.

TABLE OF CONTENTS

LIST OF TABLES

LIST OF FIGURES

Abstract of Dissertation Presented to the Graduate School
of the University of Florida in Partial Fulfillment of the
Requirements for the Degree of Doctor of Philosophy

CONTROL OF CYCLING INDUCED BY FUNCTIONAL ELECTRICAL STIMULATION: A SWITCHED SYSTEMS THEORY APPROACH

By

Matthew John Bellman

December 2015

Chair: Warren E. Dixon
Major: Mechanical Engineering

Functional electrical stimulation (FES) can be used to activate the dysfunctional lower limb muscles of individuals with some neurological disease or injury to produce cycling as a means of exercise, rehabilitation, and transportation. However, FES-cycling is metabolically inefficient and yields lower power output at the cycle crank than able-bodied cycling. Previous literature suggests that these problems are symptomatic of poor muscle control and non-physiological muscle fiber recruitment. The latter is a known problem with FES in general, and the former motivates investigation of better control methods for FES-cycling.

In Chapter 1, motivation for FES-cycling is introduced along with a survey of the challenges, approaches, and shortcomings of FES-cycling in the literature. In Chapter 2, a nonlinear model of a stationary FES-cycling system is developed that includes parametric uncertainty and an unknown, bounded, time-varying disturbance. A stimulation pattern for the gluteal, quadriceps femoris, and hamstrings muscle groups is designed based on the kinematic effectiveness of the rider's hip and knee joints to produce a forward torque about the cycle crank. In Chapter 3, a switched sliding mode controller is designed for the uncertain, nonlinear cycle-rider system with autonomous, state-dependent switching. The switched controller yields ultimately bounded tracking of a desired cadence, provided sufficient conditions on the control gains, desired trajectory, initial conditions, and stimulation pattern are satisfied. Stability is derived via a common

Lyapunov-like function, and experimental results demonstrate the performance of the switched controllers under typical FES-cycling conditions. In Chapter 4, the results of Chapter 3 are extended to include the control objective of crank position tracking, and experimental results demonstrate improved performance over cadence tracking alone. Chapter 5 builds on the results of Chapter 4 by including an electric motor in the FES-cycling system. In Chapter 6, a control system is developed that utilizes the electric motor to track a desired crank trajectory while FES of the rider's muscle groups is used to achieve a desired power output at the cycle crank. Chapter 7 concludes with a summary of the developed control systems, discussion of the challenges encountered, and guidance for future research.

CHAPTER 1
INTRODUCTION

Functional electrical stimulation (FES) is the application of electrical current across muscle fibers to artificially induce a muscle contraction and achieve a functional outcome (e.g., limb motion). Since the 1980s, FES has been applied to the lower limb muscles of people with upper motor neuron lesions (e.g., following spinal cord injury or stroke) to enable them to pedal a stationary cycle [1], and numerous physiological and psychological benefits have since been demonstrated [2]. To supplement these benefits with enhanced locomotion, mobile FES-cycling devices have been developed [3–9] and even commercialized[1] . Despite its success as a rehabilitative intervention, FES-cycling is still limited by lower efficiency and power output than volitional cycling by able-bodied individuals [10]. Low efficiency and power output limit the duration and workload achievable in FES-cycling, thereby limiting the training effect of stationary FES-cycling and the practicality of mobile FES-cycling [11], [12]. The direct cause of these limitations is still unknown, but it has been suggested that a primary factor affecting efficiency and power output is poor control of the stimulation parameters (e.g., frequency, intensity, timing) [13].

Early FES-cycling studies used open-loop or simple proportional-derivative (PD) feedback control of the stimulation intensity to achieve a desired cycling cadence [3–5, 7, 14–16]. In the late 1990s, researchers began using more sophisticated control methods in efforts to improve FES-cycling performance, including linear model identification and pole placement methods [8, 17, 18], fuzzy logic control [19, 20], neural network feedforward in addition to PD feedback control [21, 22], and higher-order sliding mode combined with fuzzy logic control [23]. All of these previous FES-cycling control studies

[1] http://www.hasomed.de/en/products/rehabike-cycling-with-fes.html; http://www.berkelbike.co.uk/

used a switched control input that alternated stimulation across different muscle groups according to a predefined stimulation pattern. The stimulation pattern defines the segments of the crank cycle over which each muscle group is stimulated to achieve the desired cycling motion and is: manually determined [1, 3, 7, 8, 15, 24], determined from offline numerical optimization [14, 21, 25–27], analytically determined [19], or based on able-bodied electromyography (EMG) measurements [4, 5, 16, 28].

FES-cycling systems that include electric motor assistance have been designed to facilitate controllability [4, 8, 15, 18, 20, 23, 29–31], as an electric motor has control authority across the entire joint space (i.e., not limited by dead points). In [4], an electric motor was added to ensure that the FES-cycling cadence did not fall below 25 revolutions per minute (RPM) and supplied a constant 5 Watts of power to compensate for losses in gearing. Similarly, in [20], a fuzzy logic control scheme was used to control a motor and FES to achieve a desired cadence. In [15], a motor controlled the cycling cadence while open-loop stimulation was applied to the rider's muscles to maximize power output. Similarly, in [8, 18, 23, 29–31], electric motors were used to maintain a desired cadence while FES was used to track a desired power output.

Switching the stimulation control input between multiple muscle groups and an electric motor according to the cycle crank angle makes the overall FES-cycling system a switched control system with autonomous, state-dependent switching ([32], Section 1.1.3). In general, during FES-cycling, there exist periods during which one or more muscle groups are active followed by periods during which no muscle groups are active. When muscle groups are actively controlled by stimulation, the system may stably track the desired trajectory, but when no muscle groups are active, the system may become unstable. This behavior is complicated by the fact that the dynamics of FES-cycling are nonlinear, time-varying, and uncertain, so that the system's state trajectories (e.g., cadence) are unknown a priori. None of the aforementioned studies have explored FES-cycling control while considering these properties of the FES-cycling system.

Investigating FES-cycling in the light of switched systems theory may yield control strategies that improve FES-cycling performance, thereby increasing the safety and effectiveness of FES-cycling.

Chapter 2 provides a detailed model of the stationary cycling system and two-legged rider undergoing FES-induced cycling. A nonlinear model of the cycle-rider system is developed that includes parametric uncertainty and unknown, bounded, time-varying disturbances. A stimulation pattern for the gluteal, quadriceps femoris, and hamstrings muscle groups is designed based on the kinematic effectiveness of the rider's hip and knee joints to produce a forward torque about the cycle crank. Based on the developed stimulation pattern, the FES control input is considered as a switched control input, making the overall cycle-rider system a switched system with autonomous, state-dependent switching.

Chapter 3 considers the control objective of crank velocity (cadence) tracking. A switched sliding mode controller is designed based on the model and stimulation pattern developed in Chapter 2. A common Lyapunov-like function is used to prove that the cadence tracking error is bounded by an exponentially decaying envelope in regions where muscle groups are activated and by an exponentially increasing envelope in regions where no muscle groups are activated. The overall error system is demonstrated to be ultimately bounded provided sufficient conditions on the control gains, desired trajectory, and stimulation pattern are satisfied. Experimental results on able-bodied subjects and one subject with Parkinson's disease demonstrate the switched controller's performance under typical FES-cycling conditions.

Chapter 4 extends the results of Chapter 3 to include the control objective of crank position tracking, motivated by the desire to minimize the steady state tracking error observed in the results of Chapter 3. A switched sliding mode controller is designed to yield simultaneous tracking of a desired crank position and cadence. A common

Lyapunov-like function is used to prove that the tracking error is bounded by an exponentially decaying envelope in regions where muscle groups are activated and by a tangentially increasing envelope with finite escape time in regions where no muscle groups are activated. The overall error system is demonstrated to be ultimately bounded, provided sufficient conditions on the control gains, the desired cadence, the initial conditions, and the stimulation pattern are satisfied. Experimental results on five able-bodied subjects demonstrate the switched controller's performance using FES of only the quadriceps femoris muscle groups under typical FES-cycling conditions. While the theoretical outcome of the stability analysis, ultimately bounded tracking error, is the same in Chapters 3 and 4, the controller developed in Chapter 4 demonstrates improved tracking performance, likely due to the inclusion of an integrator and filtered tracking error in the control input.

Chapter 5 builds on the results of Chapter 4 by including an electric motor in the FES-cycling system. The electric motor's current is controlled using the controller developed in Chapter 4 with the objective of tracking the desired crank position and cadence in the regions of the crank cycle where no muscle groups are activated. This approach removes the sufficient conditions from Chapter 4 that constrained the desired cadence, the initial conditions, and the stimulation pattern, as the electric motor grants controllability of the system throughout the entire crank cycle. The result is globally, exponentially stable tracking of the desired crank position and cadence, provided sufficient gain conditions are satisfied. Experimental results from five able-bodied, passive riders demonstrate that the motorized FES-cycling control system achieves an average cadence tracking error of 0.00 ± 2.91 revolutions per minute (rpm) for a desired trajectory of 50 rpm.

Chapter 6 considers the control objective of motor-controlled crank position and velocity and FES-controlled power output at the crank. As in Chapter 5, a sliding mode controller for the electric motor's current is developed to achieve stable tracking of the

desired crank trajectory, but in Chapter 6, it is assumed that a measure of the crank torque is available, which is then used as a feedforward term in the electric motor controller. Based on the model developed in Chapter 2, a sliding mode controller is designed for the FES control input with the objective of tracking a desired active torque, averaged over the crank cycle. A Lyapunov function is used to prove that the motor control system yields globally, exponentially stable tracking of the desired crank position and cadence, provide sufficient gain conditions are satisfied. A discrete Lyapunov function is used to prove that the average torque tracking error is ultimately bounded, provided sufficient conditions on the control gains are satisfied. Experimental results from three able-bodied, passive riders demonstrate that the developed control system is able to maintain an active power tracking error of 0.46 ± 2.6 Watts for a desired trajectory of 20 Watts at 50 rpm.

Chapter 7 concludes the dissertation. A summary of the dissertation is provided along with a discussion of challenges that were encountered throughout the development of Chapters 2-6 but that lie beyond the scope of this dissertation. Concluding remarks are made that may be useful in directing future research on FES-cycling.

CHAPTER 2
PRELIMINARIES

In this chapter, a nonlinear model of a stationary FES-cycling system is developed that includes parametric uncertainty and an unknown, bounded, time-varying disturbance. A stimulation pattern for the gluteal, quadriceps femoris, and hamstrings muscle groups is designed based on the kinematic effectiveness of the rider's hip and knee joints to produce a forward torque about the cycle crank.

2.1 Notation

Throughout the dissertation, functional dependencies are explicitly stated when terms are first introduced. Thereafter, for notational brevity, functional dependencies are suppressed, unless required for clarity of exposition. For example, the equation $\dot{x}(t) = f(x(t)) + g(x(t),\, t)$, where dot notation is used to denote derivatives with respect to time, is stated as such when first introduced but stated simply as $\dot{x} = f + g$ or $\dot{x} = f(x) + g(x,\, t)$ thereafter. The functions in $\dot{x} = f + g$ are denoted as $x : \mathbb{R}_{\geq 0} \to \mathbb{R}^n$, $f : \mathbb{R}^n \to \mathbb{R}^n$, and $f : \mathbb{R}^n \times \mathbb{R}_{\geq 0} \to \mathbb{R}^n$, where $\mathbb{R}^n$ denotes n-dimensional Euclidean space, $\mathbb{R}_{>a}$ denotes the set of real numbers strictly greater than $a \in \mathbb{R}$, and $\mathbb{R}_{\geq a}$ denotes the set of real numbers greater than or equal to $a \in \mathbb{R}$.

2.2 Stationary Cycle and Rider Dynamic Model

2.2.1 Kinematics

A two-legged rider pedaling a recumbent stationary cycle can be modeled as a single degree-of-freedom (DOF) system [33] comprised of two coupled, parallel, closed kinematic chains, as depicted in Fig. 2-1. Each kinematic chain includes four revolute joints, representing the hip, knee, pedal, and crank joints, connected by four rigid bodies, representing the thigh and shank limb segments as well as the cycle crank arm and frame. The ankle joint is assumed to be fixed in the anatomically neutral position in accordance with common clinical cycling practices for safety and mediolateral stability [34], and the rider's feet are assumed to be fixed to the pedals. The rigid

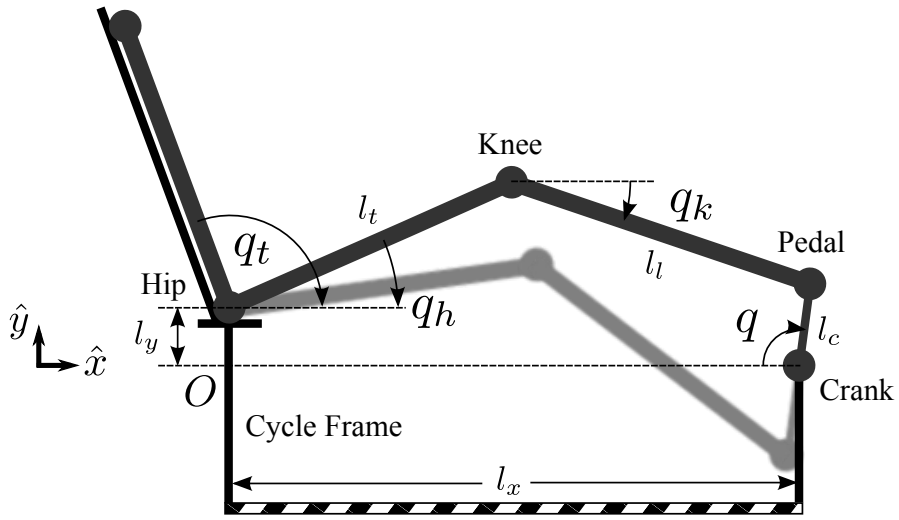

Figure 2-1. Diagram of the cycle-rider system.

body, or link, representing the cycle frame to which the rider's hip joints and the cycle crank joints are connected, is assumed to be fixed to the ground (where the ground is assumed to be an inertial reference frame) for stationary cycling. Cycling typically involves motion in only the sagittal plane, so the subsequent development assumes that both kinematic chains translate and rotate in planes parallel to the anatomically-defined sagittal plane. A closed kinematic chain of four planar links, one of which is fixed to the ground, each connected by four revolute joints, has only one DOF. Since both kinematic chains have one DOF, the total cycle-rider system would have two DOFs, except that cycles typically have their crank arms fixed 180 degrees out of phase with respect to each other. Coupling the crank arms in this manner leaves the total cycle-rider system with one DOF. Since the cycle-rider system has only one DOF, the position and orientation of all the links can be calculated using only knowledge of the link lengths and one joint angle with respect to ground. In practice, it is simplest to measure the crank angle, so the crank angle $q : \mathbb{R}_{\geq 0} \to \mathcal{Q}$ will be used in the subsequent development to parametrize the system, where $\mathcal{Q} \subseteq \mathbb{R}$ denotes the set of crank angles.

Since the cycle-rider system can be represented by a closed-loop mechanism, the closed-loop equation describing the joint positions relative to one another and the

ground for one kinematic chain, or one side of the cycle-rider system, can be expressed as

$$\vec{r}^{\,s}_{H/G} + \vec{r}^{\,s}_{K/H}\left(q\left(t\right)\right) + \vec{r}^{\,s}_{P/K}\left(q\left(t\right)\right) + \vec{r}^{\,s}_{C/P}\left(q\left(t\right)\right) + \vec{r}^{\,s}_{G/C} = \vec{0}, \quad s \in \mathcal{S}, \tag{2–1}$$

where $\vec{r}^{\,s}_{H/G} \in \mathbb{R}^2$ represents the vector from a point O fixed in the inertial reference frame to the hip joint, where the superscript $s \in \mathcal{S} \triangleq \{R,\ L\}$ indicates the right (R) or left (L) side of the cycle-rider system; $\vec{r}^{\,s}_{K/H},\ \vec{r}^{\,s}_{P/K},\ \vec{r}^{\,s}_{C/P} : \mathcal{Q} \to \mathbb{R}^2$ represent vectors from the hip joint to the knee joint, the knee joint to the pedal joint, and the pedal joint to the crank joint, respectively; $\vec{r}^{\,s}_{G/C} \in \mathbb{R}^2$ represents the vector from the crank joint back to O; and $\vec{0} \in \mathbb{R}^2$ represents the zero vector. The subsequent development considers the right side of the cycle-rider system first, then extends the results to include the left side, and the superscript s is omitted unless it adds clarity. Using the coordinate system depicted in Fig. 2-1, the vectors in (2–1) can be expressed as

$$\vec{r}^{\,s}_{H/G} \triangleq 0\hat{x} + l^s_y\hat{y}, \tag{2–2}$$

$$\vec{r}^{\,s}_{K/H}\left(q\left(t\right)\right) \triangleq l^s_t\cos\left(q^s_h\left(q\left(t\right)\right)\right)\hat{x} + l^s_t\sin\left(q^s_h\left(q\left(t\right)\right)\right)\hat{y}, \tag{2–3}$$

$$\vec{r}^{\,s}_{P/K}\left(q\left(t\right)\right) \triangleq l^s_l\cos\left(q^s_k\left(q\left(t\right)\right)\right)\hat{x} - l^s_l\sin\left(q^s_k\left(q\left(t\right)\right)\right)\hat{y}, \tag{2–4}$$

$$\vec{r}^{\,s}_{C/P}\left(q\left(t\right)\right) \triangleq l^s_c\cos\left(q\left(t\right)\right)\hat{x} - l^s_c\sin\left(q\left(t\right)\right)\hat{y}, \tag{2–5}$$

$$\vec{r}^{\,s}_{G/C} \triangleq -l^s_x\hat{x} + 0\hat{y}. \tag{2–6}$$

for $s \in \mathcal{S}$, where $q^s_h,\ q^s_k : \mathcal{Q} \to \mathbb{R}$ denote the hip and knee joint angles, measured as in Fig. 2-1; the constants $l^s_t,\ l^s_l,\ l^s_c \in \mathbb{R}_{>0}$ denote the lengths of the thigh, shank, and crank links, respectively; the constants $l^s_x,\ l^s_y \in \mathbb{R}_{>0}$ denote the x- and y-components, respectively, of the distance from the crank joint to the hip joint; and $\hat{x},\ \hat{y} \in \mathbb{R}^2$ represent unit vectors parallel to the x- and y-axes. Substituting the expressions from (2–2)-(2–6) into (2–1) and grouping the x- and y-components yields

$$\left(l_t\cos\left(q_h\right) + l_l\cos\left(q_k\right) + l_c\cos\left(q\right) - l_x\right)\hat{x} + \left(l_t\sin\left(q_h\right) - l_l\sin\left(q_k\right) - l_c\sin\left(q\right) + l_y\right)\hat{y} = 0\hat{x} + 0\hat{y},$$

which can be separated into the following independent, closed-loop kinematic equations:

$$l_t \cos(q_h) + l_l \cos(q_k) + l_c \cos(q) - l_x = 0, \tag{2–7}$$

$$l_t \sin(q_h) + l_l \sin(q_k) - l_c \sin(q) + l_y = 0. \tag{2–8}$$

To parametrize the cycle-rider system in terms of the crank angle, it is necessary to solve for q_h and q_k in terms of q, and this development begins by solving for q_h. Moving the terms including q_k to the right-hand sides of (2–7) and (2–8), squaring both equations, and adding them together yields a single equation of the form

$$k_1(q(t)) \sin(q_h(q(t))) + k_2(q(t)) \cos(q_h(q(t))) + k_3(q(t)) = 0, \tag{2–9}$$

where the coefficients $k_i : \mathcal{Q} \to \mathbb{R}$, $i \in \{1, 2, 3\}$, are defined as

$$\begin{aligned} k_1(q(t)) &\triangleq -2l_t(l_c \sin(q(t)) - l_y), \\ k_2(q(t)) &\triangleq 2l_t(l_c \cos(q(t)) - l_x), \\ k_3(q(t)) &\triangleq l_x^2 + l_y^2 + l_t^2 - l_l^2 + l_c^2 - 2l_c(l_x \cos(q(t)) + l_y \sin(q(t))). \end{aligned}$$

Equation (2–9) can be solved for q_h using the trigonometric solution technique described in [35, Section 6.7]. This technique is preferred over other closed-form solution techniques like the tan-half-angle technique because it will yield proper solutions in special cases where the other techniques will not. Dividing (2–9) by $\sqrt{k_1^2 + k_2^2}$ yields

$$\frac{k_1}{\sqrt{k_1^2 + k_2^2}} \sin(q_h) + \frac{k_2}{\sqrt{k_1^2 + k_2^2}} \cos(q_h) + \frac{k_3}{\sqrt{k_1^2 + k_2^2}} = 0. \tag{2–10}$$

Recognizing that $\sqrt{k_1^2 + k_2^2}$ is the hypotenuse of a right triangle with sides of length k_1 and k_2, a unique angle $\gamma : \mathcal{Q} \to \mathbb{R}$ can be defined with the following relations:

$$\gamma(q(t)) \triangleq \arctan\left(\frac{k_1(q(t))}{k_2(q(t))}\right), \tag{2–11}$$

$$\sin(\gamma) = \frac{k_1}{\sqrt{k_1^2 + k_2^2}}, \tag{2–12}$$

$$\cos(\gamma) = \frac{k_2}{\sqrt{k_1^2 + k_2^2}}. \tag{2–13}$$

Substituting (2–11)-(2–13) into (2–10) yields

$$\cos(\gamma)\cos(q_h) + \sin(\gamma)\sin(q_h) + \frac{k_3}{\sqrt{k_1^2 + k_2^2}} = 0. \tag{2–14}$$

Using the trigonometric identity $\cos(u - v) = \cos(u)\cos(v) + \sin(u)\sin(v)$ in (2–14) and grouping terms yields

$$\cos(q_h - \gamma) = \frac{-k_3}{\sqrt{k_1^2 + k_2^2}}. \tag{2–15}$$

Two solutions for $(q_h - \gamma)$ can be found for (2–15), and, because γ is unique, two values for q_h can subsequently be found which are equal to the two solutions of

$$q_h = \pm\arccos\left(\frac{-k_3}{\sqrt{k_1^2 + k_2^2}}\right) + \gamma. \tag{2–16}$$

The two solutions of (2–16) can viewed from an anatomical perspective, with the negative solution representing hip flexion and the positive solution representing hyper-extension of the hip with respect to Fig. 2-1. Therefore, the subsequent development proceeds using the negative solution in (2–16).

The knee angle can be found as a function of both the hip angle and the crank angle. Isolating the terms containing q_k in (2–7) and (2–8), dividing (2–8) by (2–7), and applying the inverse tangent yields

$$q_k = -\arctan\left(\frac{l_t\sin(q_h) - l_c\sin(q) + l_y}{l_t\cos(q_h) + l_c\cos(q) - l_x}\right). \tag{2–17}$$

To parametrize the velocities of the cycle-rider system in terms of the crank angle, the first time derivative of both (2–7) and (2–8) are determined, the terms containing q are isolated, and the resulting equations are expressed in matrix form as

$$\begin{bmatrix} -l_t \sin(q_h) & -l_l \sin(q_k) \\ l_t \cos(q_h) & -l_l \cos(q_k) \end{bmatrix} \begin{bmatrix} \dot{q}_h \\ \dot{q}_k \end{bmatrix} = \begin{bmatrix} l_c \sin(q) \\ l_c \cos(q) \end{bmatrix} \dot{q}. \tag{2–18}$$

Solving (2–18) for $\dot{q}_h$ and $\dot{q}_k$ in terms of $\dot{q}$ yields

$$\begin{bmatrix} \dot{q}_h(q(t),\ \dot{q}(t)) \\ \dot{q}_k(q(t),\ \dot{q}(t)) \end{bmatrix} = \begin{bmatrix} S_1(q(t)) \\ S_2(q(t)) \end{bmatrix} \dot{q}(t), \tag{2–19}$$

where $S_1,\ S_2 : \mathcal{Q} \to \mathbb{R}$ denote velocity transformation terms defined as

$$S_1(q(t)) \triangleq \frac{l_c}{l_t} \frac{\sin(q_k(q(t)) - q(t))}{\sin(q_k(q(t)) + q_h(q(t)))}, \quad S_2(q(t)) \triangleq -\frac{l_c}{l_l} \frac{\sin(q_h(q(t)) + q(t))}{\sin(q_k(q(t)) + q_h(q(t)))}.$$

The solution in (2–19) is achieved by performing a matrix inversion, which is only possible if $q_k + q_h \neq n\pi, n \in \mathbb{Z}$, which is always satisfied provided that the rider is positioned such that the knee joint never reaches full extension. It is useful to note that the joint velocities may also be expressed as

$$\dot{q}_h = \frac{\partial q_h}{\partial q}\dot{q}, \quad \dot{q}_k = \frac{\partial q_k}{\partial q}\dot{q}. \tag{2–20}$$

Combining (2–20) with (2–19) demonstrates that

$$S_1 = \frac{\partial q_h}{\partial q}, \quad S_2 = \frac{\partial q_k}{\partial q}. \tag{2–21}$$

These relationships will be used in the subsequent development to determine the contribution of torque applied about the rider's joints to the resultant torque about the crank axis.

2.2.2 Dynamics

Now that kinematics of the cycle-rider system have been parametrized in terms of the crank angle, the dynamics of the cycle-rider system can be expressed in terms

of the crank angle, crank velocity, and crank acceleration. The kinetic and potential energy of the right side of the cycle-rider system are subsequently derived and used in a Lagrangian formulation to determine the total system's equation of motion.

The kinetic energy of the right side of the cycle-rider system can be expressed as

$$\begin{aligned} T\left(q\left(t\right),\ \dot{q}\left(t\right)\right) \triangleq & \left(\frac{1}{2}m_t\vec{v}_t\left(q\left(t\right),\ \dot{q}\left(t\right)\right)\cdot\vec{v}_t\left(q\left(t\right),\ \dot{q}\left(t\right)\right)+\frac{1}{2}I_t\dot{q}_h^2\left(q\left(t\right),\ \dot{q}\left(t\right)\right)\right) \\ & +\left(\frac{1}{2}m_l\vec{v}_l\left(q\left(t\right),\ \dot{q}\left(t\right)\right)\cdot\vec{v}_l\left(q\left(t\right),\ \dot{q}\left(t\right)\right)+\frac{1}{2}I_l\dot{q}_k^2\left(q\left(t\right),\ \dot{q}\left(t\right)\right)\right) \\ & +\left(\frac{1}{2}m_c\vec{v}_c\left(q\left(t\right),\ \dot{q}\left(t\right)\right)\cdot\vec{v}_c\left(q\left(t\right),\ \dot{q}\left(t\right)\right)+\frac{1}{2}I_c\dot{q}^2\left(t\right)\right), \end{aligned} \tag{2–22}$$

where $T\ :\ \mathcal{Q}\times\mathbb{R}\to\mathbb{R}$ denotes the kinetic energy of the kinematic chain; $m_t,\ m_l,\ m_c\in\mathbb{R}_{>0}$ denote the mass of the thigh, shank, and crank arm, respectively; $\vec{v}_t,\ \vec{v}_l,\ \vec{v}_c\ :\ \mathcal{Q}\times\mathbb{R}\to\mathbb{R}^2$ represent the velocity vectors of the center of mass of the thigh, shank, and crank arm, respectively, and are obtained by differentiation of the positions of each center of mass with respect to the inertial reference frame; and $I_t,\ I_l,\ I_c\in\mathbb{R}_{>0}$ denote the principle moments of inertia about the center of mass of the thigh, shank, and crank arm, respectively. The thigh and shank can be modeled as conical cylinders with principle moments of inertia given as [36]

$$I_i\triangleq\frac{2A_im_i^2}{\delta_il_i},\quad i\in\left\{t,\ l\right\}, \tag{2–23}$$

where $A_i,\ \mu_i,\ \delta_i\in\mathbb{R}_{>0}$, $i\in\{t,\ l\}$, are defined as

$$\begin{aligned} A_i &\triangleq \frac{9}{20\pi}\left[\frac{1+\mu_i+\mu_i^2+\mu_i^3+\mu_i^4}{\left(1+\mu_i+\mu_i^2\right)^2}\right], \\ \mu_i &\triangleq r_i/R_i, \\ \delta_i &\triangleq \frac{3m_i}{\pi l_i\left(R_i^2+R_ir_i+r_i^2\right)}, \end{aligned}$$

and $r_i,\ R_i\ \in\ \mathbb{R}_{>0}$ denote the distal and proximal circumferences of each limb segment, respectively. The crank arm is modeled as a slender rod with a uniform mass

distribution, and its principle moment of inertia with respect to its mass center is

$$I_c \triangleq \frac{1}{12} m_c l_c^2. \tag{2–24}$$

Defining $l_{c,t},\ l_{c,l},\ l_{c,c} \in \mathbb{R}_{>0}$ to denote the distances from the hip joint, knee joint, and crank joint to the thigh, shank, and crank arm centers of mass, respectively, the positions of the center of mass of each link can be expressed as

$$\vec{r}_{c,t}\left(q\left(t\right)\right) \triangleq l_{c,t}\cos\left(q_h\left(q\left(t\right)\right)\right)\hat{x} + l_{c,t}\sin\left(q_h\left(q\left(t\right)\right)\right)\hat{y}, \tag{2–25}$$

$$\begin{aligned}\vec{r}_{c,l}\left(q\left(t\right)\right) \triangleq\ & \left(l_t\cos\left(q_h\left(q\left(t\right)\right)\right) + l_{c,l}\cos\left(q_k\left(q\left(t\right)\right)\right)\right)\hat{x} \\ & + \left(l_t\sin\left(q_h\left(q\left(t\right)\right)\right) - l_{c,l}\sin\left(q_k\left(q\left(t\right)\right)\right)\right)\hat{y},\end{aligned} \tag{2–26}$$

$$\vec{r}_{c,c}\left(q\left(t\right)\right) \triangleq \left(l_x - l_{c,c}\cos\left(q\left(t\right)\right)\right)\hat{x} + \left(l_{c,c}\sin\left(q\left(t\right)\right) + l_y\right)\hat{y}, \tag{2–27}$$

where $\vec{r}_{c,t},\ \vec{r}_{c,l},\ \vec{r}_{c,c} : \mathcal{Q} \to \mathbb{R}^2$ represent the positions of the center of mass of the thigh, shank, and crank of the first leg, respectively. Then, the velocities of the center of mass of each link can be expressed as

$$\begin{aligned}\vec{v}_t\left(q\left(t\right),\ \dot{q}\left(t\right)\right) =\ & -l_{c,t}\sin\left(q_h\left(q\left(t\right)\right)\right)\dot{q}_h\left(q\left(t\right),\ \dot{q}\left(t\right)\right)\hat{x} \\ & + l_{c,t}\cos\left(q_h\left(q\left(t\right)\right)\right)\dot{q}_h\left(q\left(t\right),\ \dot{q}\left(t\right)\right)\hat{y},\end{aligned} \tag{2–28}$$

$$\begin{aligned}\vec{v}_l\left(q\left(t\right),\ \dot{q}\left(t\right)\right) =\ & \left(-l_t\sin\left(q_h\left(q\left(t\right)\right)\right)\dot{q}_h\left(q\left(t\right),\ \dot{q}\left(t\right)\right) - l_{c,l}\sin\left(q_k\left(q\left(t\right)\right)\right)\dot{q}_k\left(q\left(t\right),\ \dot{q}\left(t\right)\right)\right)\hat{x} \\ & + \left(l_t\cos\left(q_h\left(q\left(t\right)\right)\right)\dot{q}_h\left(q\left(t\right),\ \dot{q}\left(t\right)\right)\right. \\ & \left. - l_{c,l}\cos\left(q_k\left(q\left(t\right)\right)\right)\dot{q}_k\left(q\left(t\right),\ \dot{q}\left(t\right)\right)\right)\hat{y},\end{aligned} \tag{2–29}$$

$$\vec{v}_c\left(q\left(t\right),\ \dot{q}\left(t\right)\right) = l_{c,c}\sin\left(q\left(t\right)\right)\dot{q}\left(t\right)\hat{x} + l_{c,c}\cos\left(q\left(t\right)\right)\dot{q}\left(t\right)\hat{y}. \tag{2–30}$$

Substituting the expressions in (2–28)-(2–30) into the kinetic energy in (2–22) gives

$$\begin{aligned}T =\ & \frac{1}{2}\left(m_t l_{c,t}^2 + I_t\right)\dot{q}_h^2 + \frac{1}{2}\left(m_l l_t^2 \dot{q}_h^2 + \left(m_l l_{c,l}^2 + I_l\right)\dot{q}_k^2 - 2m_l l_t l_{c,l}\cos\left(q_k - q_h\right)\dot{q}_h\dot{q}_k\right) \\ & + \frac{1}{2}\left(m_c l_{c,c}^2 + I_c\right)\dot{q}^2,\end{aligned}$$

which can be rewritten using (2–19) as

$$T\left(q\left(t\right),\ \dot{q}\left(t\right)\right) = \left(J_1\left(q\left(t\right)\right) + J_2\left(q\left(t\right)\right) + J_3\right)\dot{q}^2\left(t\right), \tag{2–31}$$

where $J_1,\ J_2\ :\ \mathcal{Q} \to \mathbb{R}_{>0}$, $J_3 \in \mathbb{R}_{>0}$ denote the effective moment of inertia of the thigh, shank, and crank arm about the crank joint axis and are defined as

$$\begin{aligned} J_1\left(q\left(t\right)\right) &\triangleq \frac{1}{2}\left(m_t l_{c,t}^2 + I_t\right) S_1^2\left(q\left(t\right)\right), \\ J_2\left(q\left(t\right)\right) &\triangleq \frac{1}{2} m_l l_t^2 S_1^2\left(q\left(t\right)\right) + \frac{1}{2}\left(m_l l_{c,l}^2 + I_l\right) S_2^2\left(q\left(t\right)\right) \\ &\quad - m_l l_t l_{c,l} \cos\left(q_k\left(q\left(t\right)\right) - q_h\left(q\left(t\right)\right)\right) S_1\left(q\left(t\right)\right) S_2\left(q\left(t\right)\right), \\ J_3 &\triangleq \frac{1}{2}\left(m_c l_{c,c}^2 + I_c\right). \end{aligned}$$

The potential energy of the right side of the cycle-rider system, $U\ :\ \mathcal{Q} \to \mathbb{R}_{\geq 0}$, can be expressed as

$$U\left(q\left(t\right)\right) \triangleq -\vec{r}_{c,t}\left(q\left(t\right)\right) \cdot \vec{g}_t - \vec{r}_{c,l}\left(q\left(t\right)\right) \cdot \vec{g}_l - \vec{r}_{c,c}\left(q\left(t\right)\right) \cdot \vec{g}_c, \tag{2–32}$$

where $\vec{g}_i \triangleq m_i g\left(-\hat{y}\right),\ i \in \{t,\ l,\ c\}$, and $g \in \mathbb{R}_{>0}$ denotes the acceleration due to gravity. Equation (2–32) can be expressed using (2–25)-(2–27) as

$$U = \left(m_t l_{c,t} \sin\left(q_h\right) + m_l l_t \sin\left(q_h\right) + m_l l_{c,l} \sin\left(q_k\right) + m_c l_{c,c} \sin\left(q\right) + m_c l_y\right) g. \tag{2–33}$$

The Lagrangian for the right side of the cycle-rider system can be defined as $L\left(q\left(t\right),\ \dot{q}\left(t\right)\right) \triangleq T\left(q\left(t\right),\ \dot{q}\left(t\right)\right) - U\left(q\left(t\right)\right)$. Defining the crank angle q as the generalized coordinate, Lagrange's equation can be applied as

$$\frac{d}{dt}\left(\frac{\partial L\left(q\left(t\right),\ \dot{q}\left(t\right)\right)}{\partial \dot{q}\left(t\right)}\right) - \frac{\partial L\left(q\left(t\right),\ \dot{q}\left(t\right)\right)}{\partial q\left(t\right)} = \tau_{crank}\left(t\right), \tag{2–34}$$

where $\tau_{crank}\ :\ \mathbb{R}_{\geq 0} \to \mathbb{R}$ denotes external torques applied about the crank joint axis (e.g., torques applied by friction, muscle contractions, etc.). The step-by-step solution of

(2–34) is

$$\begin{aligned}
\frac{\partial L}{\partial q} &= \frac{\partial T}{\partial q} - \frac{\partial U}{\partial q} = \left(\frac{\partial J_1}{\partial q} + \frac{\partial J_2}{\partial q}\right)\dot{q}^2 - \frac{\partial U}{\partial q}. \\
\frac{\partial L}{\partial \dot{q}} &= \frac{\partial T}{\partial \dot{q}} = 2\left(J_1 + J_2 + J_3\right)\dot{q}. \\
\frac{d}{dt}\left(\frac{\partial L}{\partial \dot{q}}\right) &= 2\left(\frac{dJ_1}{dt} + \frac{dJ_2}{dt}\right)\dot{q} + 2\left(J_1 + J_2 + J_3\right)\ddot{q}, \\
&= 2\left(\frac{\partial J_1}{\partial q} + \frac{\partial J_2}{\partial q}\right)\dot{q}^2 + 2\left(J_1 + J_2 + J_3\right)\ddot{q}. \\
\frac{d}{dt}\left(\frac{\partial L}{\partial \dot{q}}\right) - \frac{\partial L}{\partial q} &= 2\left(J_1 + J_2 + J_3\right)\ddot{q} + \left(\frac{\partial J_1}{\partial q} + \frac{\partial J_2}{\partial q}\right)\dot{q}^2 + \frac{\partial U}{\partial q} = \tau_{crank}. \qquad \text{(2–35)}
\end{aligned}$$

Equation (2–35) can be written compactly as

$$M^R\left(q\left(t\right)\right)\ddot{q}\left(t\right) + V^R\left(q\left(t\right),\ \dot{q}\left(t\right)\right)\dot{q}\left(t\right) + G^R\left(q\left(t\right)\right) = \tau^R_{crank}\left(t\right), \qquad \text{(2–36)}$$

where $M^s : \mathcal{Q} \to \mathbb{R}_{>0}$, $V^s : \mathcal{Q} \times \mathbb{R} \to \mathbb{R}$, $G^s : \mathcal{Q} \to \mathbb{R}$, $s \in \mathcal{S}$, denote inertial, centripetal and Coriolis, and gravitational effects, respectively, of one side of the cycle-rider system about the crank joint axis and are defined as

$$\begin{aligned}
M^s\left(q\left(t\right)\right) &\triangleq 2\left(J^s_1\left(q\left(t\right)\right) + J^s_2\left(q\left(t\right)\right) + J^s_3\right), \qquad \text{(2–37)} \\
V^s\left(q\left(t\right)\right) &\triangleq \left(\frac{\partial J^s_1\left(q\left(t\right)\right)}{\partial q\left(t\right)} + \frac{\partial J^s_2\left(q\left(t\right)\right)}{\partial q\left(t\right)}\right)\dot{q}\left(t\right), \qquad \text{(2–38)} \\
G^s\left(q\left(t\right)\right) &\triangleq -\frac{\partial U^s\left(q\left(t\right)\right)}{\partial q\left(t\right)}. \qquad \text{(2–39)}
\end{aligned}$$

Detailed expressions for M^s, V^s, and G^s are provided in Appendix 7.

Now that the equation of motion for the right side of the cycle-rider system has been defined in (2–36), the left side of the system can be easily included in the equation of motion, since it is also defined by the crank angle, though lagged by π radians as depicted in Fig. 2-1. Repeating the same previous development using the parameters of the left side of the cycle-rider system (e.g., m^L_t, l^L_l) and substituting $(q + \pi)$ for q yields the equation of motion for the left side of the system as

$$M^L\ddot{q} + V^L\dot{q} + G^L = \tau^L_{crank}, \qquad \text{(2–40)}$$

Since the two sides of the cycle-rider system are coupled together at the crank joint, and since the crank angle is used as the generalized coordinate parametrization the equation of motion for each side, (2–36) and (2–40) can be added together to yield the overall system equation of motion as

$$M\left(q\left(t\right)\right)\ddot{q}\left(t\right)+V\left(q\left(t\right),\ \dot{q}\left(t\right)\right)\dot{q}\left(t\right)+G\left(q\left(t\right)\right)=\tau_{crank}\left(t\right), \tag{2–41}$$

where $M\ :\ \mathcal{Q}\rightarrow\mathbb{R}_{>0},\ V\ :\ \mathcal{Q}\times\mathbb{R}\rightarrow\mathbb{R},\ G\ :\ \mathcal{Q}\rightarrow\mathbb{R}$, are defined as

$$\begin{aligned} M &\triangleq M^{R}+M^{L}, \\ V &\triangleq V^{R}+V^{L}, \\ G &\triangleq G^{R}+G^{L}, \\ \tau_{crank} &\triangleq \tau_{crank}^{R}+\tau_{crank}^{L}. \end{aligned}$$

2.2.3 Motorized Cycle-Rider System

The equation of motion in (2–41) describes the dynamics of a set of rigid bodies configured as a cycle-rider system. An FES-cycling system includes the effects of the cycle itself (e.g., friction in the crank bearings), viscoelastic tissue in the rider's joints, activation of the rider's muscles, an auxiliary electric motor, and unknown disturbances. Specifically, a motorized FES-cycling system can be modeled as

$$\tau_{cycle}\left(\dot{q}\left(t\right),\ \ddot{q}\left(t\right),\ t\right)+\tau_{rider}\left(q\left(t\right),\ \dot{q}\left(t\right),\ \ddot{q}\left(t\right),\ t\right)=\tau_{motor}\left(t\right), \tag{2–42}$$

where $\tau_{cycle}\ :\ \mathbb{R}\times\mathbb{R}\times\mathbb{R}_{\geq 0}\rightarrow\mathbb{R}$ denotes the effects of inertia, friction, and disturbances in the motorized cycle; $\tau_{rider}\ :\ \mathcal{Q}\times\mathbb{R}\times\mathbb{R}\times\mathbb{R}_{\geq 0}\rightarrow\mathbb{R}$ denotes the effects of the rider's passive limb dynamics, active muscle contractions, and disturbances from the rider; and $\tau_{motor}\ :\ \mathbb{R}_{\geq 0}\rightarrow\mathbb{R}$ denotes the torque applied about the cycle crank axis by the electric motor. The net cycle torque $\tau_{cycle}\left(\dot{q}\left(t\right),\ \ddot{q}\left(t\right),\ t\right)$ can be modeled as

$$\tau_{cycle}\left(\dot{q}\left(t\right),\ \ddot{q}\left(t\right),\ t\right)\triangleq J_{cycle}\ddot{q}\left(t\right)+b_{cycle}\dot{q}\left(t\right)+d_{cycle}\left(t\right), \tag{2–43}$$

where $J_{cycle} \in \mathbb{R}_{>0}$ is the unknown cycle inertia, $b_{cycle} \in \mathbb{R}_{>0}$ is the unknown coefficient of viscous damping in the cycle, and $d_{cycle} : \mathbb{R}_{\geq 0} \to \mathbb{R}$ denotes unknown disturbances such as changes in load. The net rider torque $\tau_{rider}(q(t), \dot{q}(t), \ddot{q}(t), t)$ can be modeled as

$$\tau_{rider}(q(t), \dot{q}(t), \ddot{q}(t), t) = \tau_p(q(t), \dot{q}(t), \ddot{q}(t)) - \tau_a(q(t), \dot{q}(t), t) + d_{rider}(t), \quad (2\text{–}44)$$

where $\tau_p : \mathcal{Q} \times \mathbb{R} \times \mathbb{R} \to \mathbb{R}$ denotes the net torque produced by the rider's passive limb dynamics, $\tau_a : \mathcal{Q} \times \mathbb{R} \times \mathbb{R}_{\geq 0} \to \mathbb{R}$ denotes the net torque produced by active contractions of the rider's muscles, and $d_{rider} : \mathbb{R}_{\geq 0} \to \mathbb{R}$ denotes the effects of unknown disturbances from the rider such as muscle spasms.

Assumption 1. The unknown disturbances $d_{cycle}(t)$ and $d_{rider}(t)$ and their first time derivatives have known bounds such that $|d_{cycle}(t)| \leq c_{d,cycle}$ and $|d_{rider}(t)| \leq c_{d,rider}$, where $c_{d,cycle}, c_{d,rider} \in \mathbb{R}_{>0}$ are known constants, and $\left|\dot{d}_{cycle}(t)\right| \leq c_{\dot{d},cycle}$ and $\left|\dot{d}_{rider}(t)\right| \leq c_{\dot{d},rider}$, where $c_{\dot{d},cycle}, c_{\dot{d},rider} \in \mathbb{R}_{>0}$ are known constants.

The rider's passive limb dynamics can be modeled as a single degree-of-freedom system [33] of rigid links with viscoelastic pin joints rotating in the sagittal plane, which can be expressed as

$$\tau_p(q(t), \dot{q}(t), \ddot{q}(t)) \triangleq M(q(t))\ddot{q}(t) + V(q(t), \dot{q}(t))\dot{q}(t) + G(q(t)) + P(q(t), \dot{q}(t)), \quad (2\text{–}45)$$

where $P : \mathcal{Q} \times \mathbb{R} \to \mathbb{R}$ denotes the effects of passive viscoelastic tissue forces in the rider's joints. The passive viscoelastic effects of the tissues surrounding the hip and knee joints can be expressed as

$$P(q(t), \dot{q}(t)) \triangleq \sum_{j \in \mathcal{J}} T_j(q(t)) p_j(q(t), \dot{q}(t)),$$

where $T_j : \mathcal{Q} \to \mathbb{R}$ are the known joint torque transfer ratios [26] with subscript $j \in \mathcal{J} \triangleq \{RHip, RKnee, LHip, LKnee\}$ indicating right and left hip and knee joints, and $p_j : \mathcal{Q} \times \mathbb{R} \to \mathbb{R}$ denotes the resultant torque about the rider's joint from viscoelastic

tissue forces. The joint torque transfer ratios are the Jacobian elements that translate torque from one joint to another and can be expressed as

$$\begin{aligned} T_{*Hip}\left(q\left(t\right)\right) &= -\frac{\partial q_{*Hip}\left(q\left(t\right)\right)}{\partial q\left(t\right)} = -\frac{l_c}{l_t}\frac{\sin\left(q_{*Knee}\left(q\left(t\right)\right) - q\left(t\right)\right)}{\sin\left(q_{*Knee}\left(q\left(t\right)\right) + q_{*Hip}\left(q\left(t\right)\right)\right)}, \\ T_{*Knee}\left(q\left(t\right)\right) &= \frac{\partial q_{*Hip}\left(q\left(t\right)\right)}{\partial q\left(t\right)} + \frac{\partial q_{*Knee}\left(q\left(t\right)\right)}{\partial q\left(t\right)}, \\ &= \left(\frac{l_c}{l_l l_t}\right)\frac{l_l \sin\left(q_{*Knee}\left(q\left(t\right)\right) - q\left(t\right)\right) - l_t \sin\left(q_{*Hip}\left(q\left(t\right)\right) + q\left(t\right)\right)}{\sin\left(q_{*Knee}\left(q\left(t\right)\right) + q_{*Hip}\left(q\left(t\right)\right)\right)}, \end{aligned}$$

where the measurable constants $l_t,\ l_l,\ l_c \in \mathbb{R}_{>0}$ are the thigh and shank lengths of the rider and the cycle crank arm length, respectively, assuming that these lengths are symmetric with respect to the left and right sides of the system; $q_j : \mathcal{Q} \to \mathbb{R}$ denotes the rider's joint angles with respect to the horizontal plane; and the notation $*$ indicates that the expression holds for both right and left sides of the model (i.e., $*$ can be replaced by R or L to create distinct expressions). Based on [37] and [38], $p_j\left(q\left(t\right),\ \dot{q}\left(t\right)\right)$ can be modeled as

$$\begin{aligned} p_j\left(q\left(t\right),\ \dot{q}\left(t\right)\right) \triangleq\ & k_{j,1}\exp\left(k_{j,2}\gamma_j\left(q\left(t\right)\right)\right)\left(\gamma_j\left(q\left(t\right)\right) + k_{j,3}\right) \\ & + b_{j,1}\tanh\left(b_{j,2}\dot{\gamma}_j\left(q\left(t\right),\ \dot{q}\left(t\right)\right)\right) + b_{j,3}\dot{\gamma}_j\left(q\left(t\right),\ \dot{q}\left(t\right)\right), \end{aligned}$$

for $j \in \mathcal{J}$, where $k_{j,i},\ b_{j,i} \in \mathbb{R}$, $i \in \{1,\ 2,\ 3\}$, are unknown, constant coefficients, and $\gamma_j : \mathcal{Q} \to \mathbb{R}$ denotes the rider's relative hip and knee joint angles, defined as

$$\gamma_{*Hip}\left(q\left(t\right)\right) \triangleq q_{*Hip}\left(q\left(t\right)\right) - q_t + \pi \quad , \quad \gamma_{*Knee}\left(q\left(t\right)\right) \triangleq q_{*Hip}\left(q\left(t\right)\right) - q_{*Knee}\left(q\left(t\right)\right),$$

where $q_t \in \mathbb{R}$ is the measurable, constant trunk angle.

The active torque resulting from the rider's muscles can be expressed as

$$\tau_a \triangleq \sum_{m \in \mathcal{M}} B_m\left(q\left(t\right),\ \dot{q}\left(t\right)\right) u_m\left(t\right) + \tau_r\left(t\right), \tag{2–46}$$

where $B_m : \mathcal{Q} \times \mathbb{R} \to \mathbb{R}$ denotes the uncertain control effectiveness of a muscle group with subscript $m \in \mathcal{M} \triangleq \{RGlute,\ RQuad,\ RHam,\ LGlute,\ LQuad,\ LHam\}$ indicating

the right (R) and left (L) gluteal ($Glute$), quadriceps femoris ($Quad$), and hamstrings (Ham) muscle groups, respectively; $u_m : \mathbb{R}_{\geq 0} \to \mathbb{R}$ denotes the electrical stimulation intensity applied to each muscle group; and $\tau_r : \mathbb{R}_{\geq 0} \to \mathbb{R}$ denotes torque applied about the crank axis through the rider's volitional cycling effort. The control effectiveness for each muscle group can be defined as

$$B_m\left(q\left(t\right),\ \dot{q}\left(t\right)\right) \triangleq \Omega_m\left(q\left(t\right),\ \dot{q}\left(t\right)\right) T_m\left(q\left(t\right)\right), \tag{2–47}$$

or $m \in \mathcal{M}$, where $\Omega_m : \mathcal{Q} \times \mathbb{R} \to \mathbb{R}$ denotes the uncertain relationship between stimulation intensity and a muscle group's resultant torque about the joint it spans, and $T_m : \mathcal{Q} \to \mathbb{R}$ denotes the torque transfer ratio for a muscle group, which can be determined according to the primary joint that each muscle group spans as

$$T_{*Glute}\left(q\left(t\right)\right) = T_{*Hip}\left(q\left(t\right)\right), \quad T_{*Quad}\left(q\left(t\right)\right) = T_{*Ham}\left(q\left(t\right)\right) = T_{*Knee}\left(q\left(t\right)\right),$$

given that the following assumption holds.

Assumption 2. The biarticular effects of the rectus femoris and hamstring muscles are negligible (i.e., activation of the quadriceps and hamstrings muscle groups produces torque about the knee joints only).

The uncertain function $\Omega_m\left(q\left(t\right),\ \dot{q}\left(t\right)\right)$ can be modeled as in [39], neglecting the effects of muscle fatigue, as

$$\Omega_m\left(q\left(t\right),\ \dot{q}\left(t\right)\right) \triangleq \lambda_m\left(q\left(t\right)\right) \eta_m\left(q\left(t\right),\ \dot{q}\left(t\right)\right) \cos\left(a_m\left(q\left(t\right)\right)\right), \tag{2–48}$$

for $m \in \mathcal{M}$, where $\lambda_m : \mathcal{Q} \to \mathbb{R}$ denotes the uncertain moment arm of a muscle's output force about the joint it spans; $\eta_m : \mathcal{Q} \times \mathbb{R} \to \mathbb{R}$ denotes the uncertain, nonlinear function relating stimulation intensity to muscle fiber force; and $a_m : \mathcal{Q} \to \mathbb{R}$ denotes the uncertain pennation angle of the muscle fibers.

Property 1. The moment arm of the muscle group about the joint it spans $\lambda_m(q(t))$ depends on the joint angle and is nonzero and continuously differentiable with a bounded first time derivative for all $m \in \mathcal{M}$ [40].

Property 2. The function relating stimulation voltage to muscle fiber force $\eta_m(q(t),\ \dot{q}(t))$ depends on the force-length and force-velocity relationships of the muscle being stimulated and is lower and upper bounded by known positive constants $\underline{\eta},\ \overline{\eta} \in \mathbb{R}_{>0}$, respectively, for all $m \in \mathcal{M}$, provided the muscle is not fully stretched [41] or contracting concentrically at its maximum shortening velocity.

Property 3. The muscle fiber pennation angle $a_m(q(t)) \neq (n\pi + \pi/2),\ n \in \mathbb{Z}$, (i.e., $\cos(a_m(q(t))) \neq 0$) for all $m \in \mathcal{M}$ [42].

Property 4. Based on (2–48) and Properties 1-3, the function relating the electrical stimulation intensity applied to a muscle group and the resulting torque about the joint is nonzero and bounded. In other words, $0 < \underline{\Omega} < |\Omega_m(q(t),\ \dot{q}(t))| \leq \overline{\Omega}$, where $\underline{\Omega},\ \overline{\Omega} \in \mathbb{R}_{>0}$ are known positive constants, for all $m \in \mathcal{M}$.

Torque about the crank axis provided by an electric motor is modeled as

$$\tau_{motor}(t) \triangleq B_e u_e(t), \tag{2–49}$$

where $B_e \in \mathbb{R}$ is a constant relating the current in the electric motor's windings to the resulting torque about the crank axis, and $u_e : \mathbb{R}_{\geq 0} \to \mathbb{R}$ is the control current applied to the electric motor windings. The control effectiveness for the electric motor is defined as $B_e \triangleq K_\tau r_g$, where $K_\tau \in \mathbb{R}$ is the constant coefficient relating armature current to torque about the crank axis, and $r_g \in \mathbb{R}_{>0}$ is the gear ratio between the motor output and the crank axis. It is assumed that $0 < c_e \leq B_e$, where $c_e \in \mathbb{R}_{>0}$ is a known constant.

2.3 Switched System Model

2.3.1 Stimulation Pattern Development

The muscle torque transfer ratios T_m indicate how each muscle group should be activated to induce forward pedaling. Multiplying the joint torque yielded by a

muscle contraction with T_m transforms that torque to a resultant torque about the crank. Therefore, if only forward pedaling is desired, then each muscle group should only be activated when it yields a clockwise (with respect to Fig. 2-1) torque about the crank. In other words, stimulation should only activate the quadriceps when T_{*Quad} is negative, the hamstrings when T_{*Ham} is positive, and the gluteal muscles when T_{*Glute} is positive. However, this stimulation pattern would require stimulation of the muscle groups for vanishingly small values of T_m (i.e., near the so-called dead points of the crank cycle) and may therefore activate the muscles inefficiently, in the sense that large values of stimulation and metabolic power output would result in little power output at the cycle crank. Therefore, to increase FES-cycling efficiency, motivation exists to only stimulate a muscle group when its torque transfer ratio is sufficiently large. Indeed, evidence in [26] suggests that the stimulation interval for each muscle group should be minimized to optimize metabolic efficiency.

The control input can be generated by stimulation of the muscle groups or by an electric motor. A common question that arises in human-machine interaction is: How should the person's effort be balanced with the machine to accomplish a task cooperatively? In this case, the person's effort is the electrically stimulated muscle input and the machine's is the electric motor input. In the present development, the electric motor contribution is considered to be a generic torque input, but in Chapter 5, the human-machine effort is balanced by only activating the muscle groups where they can effectively contribute to pedaling and activating the electric motor everywhere else, and in Chapter 6, the human-machine effort is balanced by assigning each system a different control objective (i.e., the electric motor is tasked with tracking a desired crank position and cadence while FES is used to track a desired crank torque to achieve a desired power output). Switching the control input in this manner yields an autonomous, state-dependent, switched control system [32].

The portion of the crank cycle over which a particular muscle group is stimulated is denoted $\mathcal{Q}_m \subset \mathcal{Q}$ for $m \in \mathcal{M}$, and the union of the stimulation regions is the controlled region, denoted $\mathcal{Q}_c \triangleq \underset{m \in \mathcal{M}}{\cup} \mathcal{Q}_m$. The uncontrolled region (i.e., the region of the crank cycle in which no muscle groups are stimulated) is denoted $\mathcal{Q}_u \triangleq \mathcal{Q} \backslash \mathcal{Q}_c$. Similarly, the portion of the crank cycle over which the electric motor actively contributes torque is denoted $\mathcal{Q}_e \subseteq \mathcal{Q}$. In this development, $\mathcal{Q}_m$ is defined for each muscle group as

$$\mathcal{Q}_{*Glute} \triangleq \{q(t) \mid T_{*Glute}(q(t)) > \varepsilon_{*Glute}(t)\}, \tag{2–50}$$

$$\mathcal{Q}_{*Quad} \triangleq \{q(t) \mid -T_{*Quad}(q(t)) > \varepsilon_{*Quad}(t)\}, \tag{2–51}$$

$$\mathcal{Q}_{*Ham} \triangleq \{q(t) \mid T_{*Ham}(q(t)) > \varepsilon_{*Ham}(t)\}, \tag{2–52}$$

where $\varepsilon_m : \mathbb{R}_{\geq 0} \to \left(0, \max\left(T_m(q(t))\right)\right]$ is a time-varying signal defined for $m \in \mathcal{M}$. Defining the stimulation regions as in (2–50)-(2–52) limits stimulation to portions of the crank cycle where the ratio of the torque produced by stimulation of the muscle group and the resultant torque about the crank axis is bounded below by $\varepsilon_m(t)$, which is designed a priori, and prevents backpedaling, as the muscle groups may only be stimulated when the resultant torque about the crank axis is positive (i.e., forward pedaling). Note that a negative sign is included in (2–51) because knee extensor torque is defined to be negative.

2.3.2 Switched Control Input

To stimulate the rider's muscle groups according to the stimulation pattern defined by (2–50)-(2–52), the stimulation input to each muscle must be switched on and off at appropriate points along the crank cycle. Based on these switching laws, piecewise constant switching signals can be developed for $m \in \mathcal{M}$, $\sigma_m : \mathcal{Q} \to \{0, 1\}$, and for the

electric motor, $\sigma_e : \mathcal{Q} \to \{0, 1\}$, as

$$\sigma_m(q(t)) \triangleq \begin{cases} 1 & \text{if } q(t) \in \mathcal{Q}_m \\ 0 & \text{if } q(t) \notin \mathcal{Q}_m \end{cases}, \quad \sigma_e(q(t)) \triangleq \begin{cases} 1 & \text{if } q(t) \in \mathcal{Q}_e \\ 0 & \text{if } q(t) \notin \mathcal{Q}_e \end{cases}. \tag{2–53}$$

Using these state-dependent switching signals, the stimulation input to the muscles groups and the current input to the motor windings can be defined as

$$u_m(t) \triangleq k_m \sigma_m(q(t)) u_{FES}(t), \quad u_e(t) \triangleq k_e \sigma_e(q(t)) u_{motor}(t), \tag{2–54}$$

where $k_m,\ k_e \in \mathbb{R}_{>0},\ m \in \mathcal{M}$, are positive, constant control gains, and $u_{FES},\ u_{motor} : \mathbb{R}_{\geq 0} \to \mathbb{R}$ are the subsequently designed stimulation and electric motor control inputs, respectively. Substituting (2–43)-(2–46), (2–49), and (2–54) into (2–42) and rearranging terms yields

$$\begin{aligned} J_{cycle}\ddot{q}(t) + b_{cycle}\dot{q}(t) + M(q(t))\ddot{q}(t) + V(q(t), \dot{q}(t))\dot{q}(t) + G(q(t)) + P(q(t), \dot{q}(t)) \\ + d_{cycle}(t) + d_{rider}(t) = \tau_r(t) + B_{FES}(q(t), \dot{q}(t)) u_{FES}(t) + B_{motor}(q(t)) u_{motor}(t), \end{aligned} \tag{2–55}$$

where $B_{FES} : \mathcal{Q} \times \mathbb{R} \to \mathbb{R}_{>0},\ B_{motor} : \mathcal{Q} \to \mathbb{R}$ are lumped, switched control effectiveness terms defined as

$$B_{FES} \triangleq \sum_{m \in \mathcal{M}} B_m k_m \sigma_m, \quad B_{motor} \triangleq B_e k_e \sigma_e.$$

The switched system in (2–55) has the following properties.

Property 5. $\underline{J} \leq J_{cycle} \leq \overline{J}$, where $\underline{J},\ \overline{J} \in \mathbb{R}_{>0}$ are known constants

Property 6. $0 < b_{cycle} \leq \overline{b}$, where $\overline{b} \in \mathbb{R}_{>0}$ is a known constant.

Property 7. $\underline{M} \leq M(q(t)) \leq \overline{M}$, where $\underline{M},\ \overline{M} \in \mathbb{R}_{>0}$ are known constants.

Property 8. $|V(q(t), \dot{q}(t))| \leq c_V |\dot{q}(t)|$, where $c_V \in \mathbb{R}_{>0}$ is a known constant.

Property 9. $|G(q(t))| \leq c_G$, where $c_G \in \mathbb{R}_{>0}$ is a known constant.

Property 10. $|P(q(t),\ \dot{q}(t))| \leq c_{P1} + c_{P2}|\dot{q}(t)|$, where $c_{P1},\ c_{P2} \in \mathbb{R}_{>0}$ are known constants.

Property 11. For all $m \in \mathcal{M}$, $\underline{B} \leq B_m(q(t),\ \dot{q}(t)) \leq \overline{B}$ for $q(t) \in \mathcal{Q}_m$, where $\underline{B},\ \overline{B} \in \mathbb{R}_{>0}$ are known constants, $|B_m(q(t),\ \dot{q}(t))| \leq c_B$ for all $q(t) \in \mathcal{Q}$, where $c_B \in \mathbb{R}_{>0}$ is a known constant, and $\left|\dot{B}_m(q(t),\ \dot{q}(t),\ \ddot{q}(t))\right| \leq c_{\dot{B}1}|\dot{q}(t)| + c_{\dot{B}2}|\ddot{q}(t)|$ for all $q(t) \in \mathcal{Q}$, where $c_{\dot{B}1},\ c_{\dot{B}2} \in \mathbb{R}_{>0}$ are known constants.

Property 12. $|\tau_r(t)| \leq c_r$ and $|\dot{\tau}_r(t)| \leq c_{\dot{r}}$, where $c_r,\ c_{\dot{r}} \in \mathbb{R}_{>0}$ are known constants.

Property 13. $\dot{M}(q(t),\ \dot{q}(t)) - 2V(q(t),\ \dot{q}(t)) = 0$.

2.3.3 Switching States and Times

Assuming that the initial crank angle $q_0^{on} \in \mathcal{Q}$ is an element of $\mathcal{Q}_c$, the known sequence of switching states for the electrical stimulation, which are precisely the limit points of $\mathcal{Q}_u$, is defined as $\left\{q_n^{on},\ q_n^{off} \in \mathcal{Q}\right\}_{n=0}^{\infty}$, where the superscripts on and off indicate that the sum of signals σ_m is switching from zero to nonzero or nonzero to zero, respectively. The corresponding sequence of unknown switching times $\left\{t_n^{on},\ t_n^{off} \in \mathbb{R}_{\geq 0}\right\}_{n=0}^{\infty}$ is defined such that each on-time t_n^{on} and off-time t_n^{off} denotes the instant when q reaches the corresponding on-angle q_n^{on} and off-angle q_n^{off}, respectively. Fig. 2-2 exemplifies the stimulation pattern and the associated switching states.

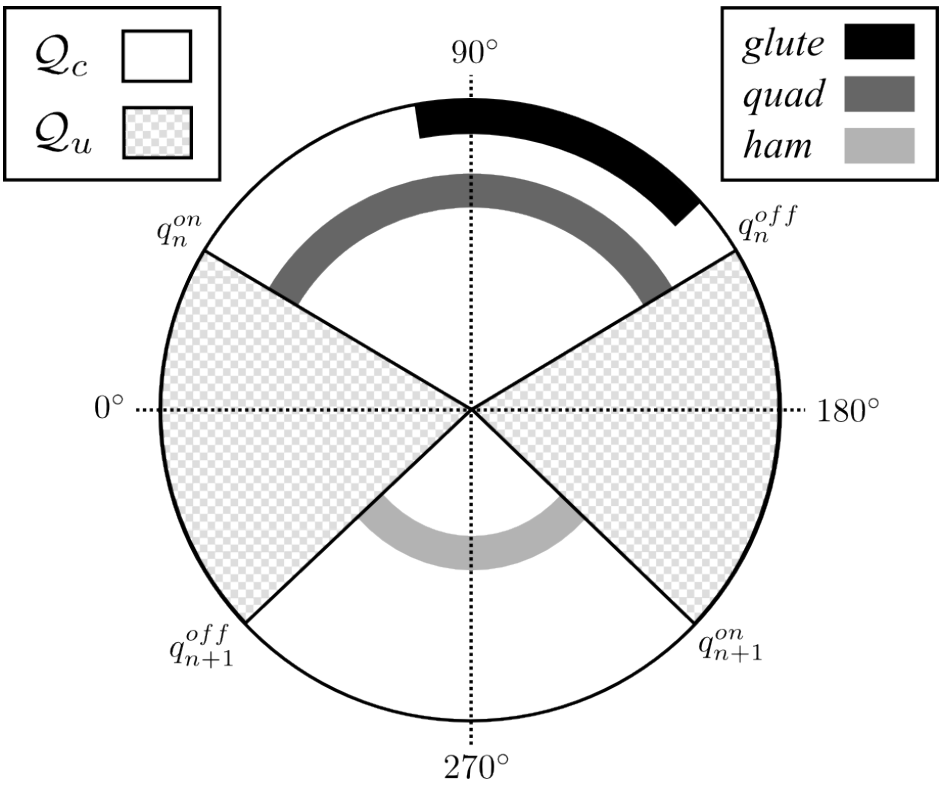

Figure 2-2. Example stimulation pattern depicting intervals of the crank cycle over which the muscle groups of one leg are stimulated.

CHAPTER 3
SWITCHED CONTROL OF CADENCE DURING STATIONARY CYCLING INDUCED BY FUNCTIONAL ELECTRICAL STIMULATION

In this chapter, a switched sliding mode control input is developed, based on the stimulation pattern developed in Chapter 2, with the objective that the rider pedal at a desired cadence (crank velocity). A common Lyapunov-like function is used, in conjunction with the switched FES-cycling system model developed in Chapter 2, to prove that the cadence tracking error is bounded by an exponentially decaying envelope in regions where muscle groups are activated and by an exponentially increasing envelope in regions where no muscle groups are activated. The overall error system is shown to be ultimately bounded provided sufficient conditions on the control gains, desired trajectory, and stimulation pattern are satisfied. Experimental results on able-bodied subjects and one subject with Parkinson's disease demonstrate the switched controller's performance under typical FES-cycling conditions.

3.1 Control Development

In this development, no electric motor input is provided (i.e., $u_{motor} = 0$) and the cycle inertia J_{cycle} is lumped together with the rider inertia M (i.e., here $M \triangleq M + J_{cycle}$).

3.1.1 Open-Loop Error System

The control objective is to track a desired crank cadence with performance quantified by the tracking error signal $r : \mathbb{R}_{\geq 0} \to \mathbb{R}$, defined as

$$r(t) \triangleq \dot{q}_d(t) - \dot{q}(t), \tag{3–1}$$

where $\dot{q}_d : \mathbb{R}_{\geq 0} \to \mathbb{R}$ denotes the desired cadence, designed so that its derivatives exist and $\dot{q}_d,\ \ddot{q}_d \in \mathcal{L}_\infty$. Without loss of generality, $\dot{q}_d$ is designed to be non-negative, i.e., backpedaling is not desired.

Taking the time derivative of (3–1), multiplying by M, and using (2–55) and (3–1) yields the open-loop error system

$$M\left(q\left(t\right)\right)\dot{r}\left(t\right)=\chi\left(q\left(t\right),\ \dot{q}\left(t\right),\ t\right)-V\left(q\left(t\right),\ \dot{q}\left(t\right)\right)r\left(t\right)-B_{FES}\left(q\left(t\right),\ \dot{q}\left(t\right)\right)u_{FES}\left(t\right), \quad (3\text{–}2)$$

where the auxiliary term $\chi : \mathcal{Q}\times\mathbb{R}\times\mathbb{R}_{\geq 0}\to\mathbb{R}$ is defined as

$$\chi \triangleq M\ddot{q}_d + V\dot{q}_d + b_{cycle}\dot{q} + G + P + d_{cycle} + d_{rider} - \tau_r. \quad (3\text{–}3)$$

Based on Assumption 1 and Properties 5-12, χ can be bounded as

$$|\chi| \leq c_1 + c_2\left|r\right|, \quad (3\text{–}4)$$

where $c_1,\ c_2\in\mathbb{R}_{>0}$ are known constants defined as

$$\begin{aligned} c_1 &\triangleq \overline{M}c_{d2} + c_G + c_{P1} + c_{d,cycle} + c_{d,rider} + c_r + c_V c_{d1}^2 + \left(\overline{b} + c_{P2}\right)c_{d1}, \\ c_2 &\triangleq c_V c_{d1} + \overline{b} + c_{P2}. \end{aligned}$$

3.1.2 Closed-Loop Error System

Based on (3–2) and the subsequent stability analysis, the control input is designed as

$$u_{FES} \triangleq k_1 r + k_2 \text{sgn}\left(r\right), \quad (3\text{–}5)$$

where sgn $: \mathbb{R}\to[-1,\ 1]$ denotes the signum function and $k_1,\ k_2\in\mathbb{R}_{>0}$ are constant control gains. After substituting (3–5) into the open-loop error system in (3–2), the following switched closed-loop error system is obtained:

$$M\dot{r} = \chi - Vr - B_{FES}\left(k_1 r + k_2\text{sgn}\left(r\right)\right). \quad (3\text{–}6)$$

3.2 Stability Analysis

Let $V_L : \mathbb{R}\to\mathbb{R}_{\geq 0}$ be a positive definite, continuously differentiable, common Lyapunov-like function defined as

$$V_L\left(r\left(t\right)\right) \triangleq \frac{1}{2}M\left(q\left(t\right)\right)r^2\left(t\right). \quad (3\text{–}7)$$

The common Lyapunov-like function V_L is radially unbounded and satisfies the following inequalities:

$$\left(\frac{1}{2}\underline{M}\right) r^2 \leq V_L \leq \left(\frac{1}{2}\overline{M}\right) r^2. \tag{3–8}$$

Theorem 3.1. *For $q \in \mathcal{Q}_c$, the tracking error is bounded by an exponentially decaying envelope given by*

$$|r(t)| \leq \sqrt{\overline{M}\underline{M}^{-1}}\, |r(t_n^{on})|\, \textit{exp}\left(-\frac{1}{2}\lambda_c (t - t_n^{on})\right), \tag{3–9}$$

for all $t \in \left[t_n^{on},\, t_n^{off}\right)$ and for all n, where $\lambda_c \in \mathbb{R}_{>0}$ is defined as

$$\lambda_c \triangleq 2\overline{M}^{-1}(k_1 \underline{B} - c_2), \tag{3–10}$$

provided the following sufficient gain conditions are satisfied:

$$k_1 > c_2 \left(\textit{min}\,(k_m)\,\underline{B}\right)^{-1}, \quad k_2 \geq c_1 \left(\textit{min}\,(k_m)\,\underline{B}\right)^{-1}. \tag{3–11}$$

Proof. Let $r(t)$ for $t \in \left[t_n^{on},\, t_n^{off}\right)$ be a Filippov solution to the differential inclusion $\dot{r}(t) \in K[h](r(t))$, where $K[\cdot]$ is defined as in [43] and where $h : \mathbb{R} \to \mathbb{R}$ is defined by (3–6) as

$$h \triangleq M^{-1}\left(\chi - Vr - B_{FES}\left(k_1 r + k_2 \textsf{sgn}\,(r)\right)\right). \tag{3–12}$$

The time derivative of (3–7) exists almost everywhere (a.e.), i.e., for almost all $t \in \left[t_n^{on},\, t_n^{off}\right)$, and $\dot{V}_L \overset{a.e.}{\in} \dot{\tilde{V}}_L$, where $\dot{\tilde{V}}_L$ is the generalized time derivative of (3–7) along the Filippov trajectories of $\dot{r} \in h(r)$ and is defined as [44]

$$\dot{\tilde{V}}_L \triangleq \bigcap_{\xi \in \partial V_L} \xi^T K \begin{bmatrix} h \\ 1 \end{bmatrix},$$

where ∂V_L is the generalized gradient of V_L. Since V_L is continuously differentiable in r, $\partial V_L = \{\nabla V_L\}$; thus,

$$\dot{\tilde{V}}_L \subseteq \begin{bmatrix} Mr \\ \frac{1}{2}\dot{M}r^2 \end{bmatrix}^T K \begin{bmatrix} h \\ 1 \end{bmatrix}.$$

Using the calculus of $K[\cdot]$ from [44] and substituting (3–12) into the result yields

$$\dot{\tilde{V}}_L \subseteq (\chi - Vr - k_1 K[B_{FES}] r - k_2 K[B_{FES} \cdot \text{sgn}](r)) r + \frac{1}{2}\dot{M} r^2. \tag{3–13}$$

First, (3–13) is evaluated between instants where B_{FES} switches to prove that V_L is a common Lyapunov function in the controlled regions. In other words, consider $q \in \mathcal{Q}_m$ for an arbitrary $m \in \mathcal{M}$, where B_{FES} is continuous and nonzero, so that (3–13) can be expressed as

$$\dot{\tilde{V}}_L \subseteq (\chi - Vr - k_1 B_{FES} r - k_2 B_{FES} K[\text{sgn}](r)) r + \frac{1}{2}\dot{M} r^2, \tag{3–14}$$

for $q \in \mathcal{Q}_m$, where $K[B_{FES} \cdot \text{sgn}](r) = B_{FES} \cdot \text{SGN}(r)$ and

$$\text{SGN}(r) \triangleq \begin{cases} 1 & \text{if } r > 0 \\ [-1,\ 1] & \text{if } r = 0 \\ -1 & \text{if } r < 0 \end{cases}. \tag{3–15}$$

Using Property 13 allows (3–14) to be rewritten as

$$\dot{\tilde{V}}_L \subseteq \chi r - k_1 B_{FES} r^2 - k_2 B_{FES} \cdot \text{SGN}(r) r. \tag{3–16}$$

The singleton supremum of (3–16) can be found using Property 11, (3–4), and (3–15), and the fact that $\dot{V}_L \overset{a.e.}{\in} \dot{\tilde{V}}_L$ can subsequently be used to prove that

$$\dot{V}_L \overset{a.e.}{\leq} -(k_2 \text{min}(k_m) \underline{B} - c_1)|r| - (k_1 \text{min}(k_m) \underline{B} - c_2) r^2, \tag{3–17}$$

where $\text{SGN}(r) r$ was replaced with $|r|$ since $\text{SGN}(r)$ is only set-valued for $r = 0$. From Property 11, it can be demonstrated that the inequality in (3–17) holds for all subsets $\mathcal{Q}_m$ of the controlled region $\mathcal{Q}_c$, so it can be concluded that V_L is a common Lyapunov function in the controlled region. Provided the conditions on the control gains in (3–11)

are satisfied, (3–8) can be used to upper bound (3–17) as

$$\dot{V}_L \overset{a.e.}{\leq} -\lambda_c V_L, \tag{3–18}$$

where λ_c was defined in (3–10). The inequality in (3–18) can be rewritten as

$$\exp\left(\lambda_c \left(t - t_n^{on}\right)\right)\left(\dot{V}_L + \lambda_c V_L\right) \overset{a.e.}{\leq} 0,$$

which is equivalent to the following expression:

$$\frac{d}{dt}\left(V_L \exp\left(\lambda_c \left(t - t_n^{on}\right)\right)\right) \overset{a.e.}{\leq} 0. \tag{3–19}$$

Taking the Lebesgue integral of (3–19) and recognizing that the integrand on the left-hand side is absolutely continuous allows the Fundamental Theorem of Calculus to be used to yield

$$V_L\left(r\left(t\right)\right) \leq V_L\left(r\left(t_n^{on}\right)\right) \exp\left(-\lambda_c \left(t - t_n^{on}\right)\right), \tag{3–20}$$

for all $t \in \left[t_n^{on},\, t_n^{off}\right)$ and for all n. Rewriting (3–20) using (3–8) and performing some algebraic manipulation yields (3–9). □

Remark 3.1. Theorem 3.1 guarantees that the desired cadence can be tracked with exponential convergence, provided that the crank angle does not exit the controlled region. Thus, if the stimulation pattern and desired cadence are designed such that the crank is not required to exit the controlled region, the controller in (3–5) may yield exponential tracking for all time. If the desired cadence is designed such that the crank must exit the controlled region, the system may become uncontrolled and the following theorem details the resulting error system behavior.

Theorem 3.2. *For $q \in \mathcal{Q}_u$, the tracking error can be bounded as*

$$\left|r\left(t\right)\right| \leq \left\{\underline{M}^{-1}\left(\overline{M} r^2\left(t_n^{off}\right) + 1\right) \exp\left(\lambda_u \left(t - t_n^{off}\right)\right) - \underline{M}^{-1}\right\}^{\frac{1}{2}}, \tag{3–21}$$

for all $t \in \left[t_n^{off},\ t_{n+1}^{on}\right)$ *and for all* n*, where* $\lambda_u \in \mathbb{R}_{>0}$ *is defined as*

$$\lambda_u \triangleq 2max\left\{c_1\sqrt{2\underline{M}^{-1}},\ 2c_2\underline{M}^{-1}\right\}. \tag{3–22}$$

Proof. In the uncontrolled region, the time derivative of (3–7) can be expressed using (3–6), Property 11, and Property 13 as

$$\dot{V}_L = \chi r,$$

which can be upper bounded using (3–4) and (3–8) as

$$\dot{V}_L \leq c_2\left(2\underline{M}^{-1}\right)V_L + c_1\sqrt{2\underline{M}^{-1}}V_L^{\frac{1}{2}}. \tag{3–23}$$

The right-hand side of (3–23) can be upper bounded in a piecewise manner as

$$\dot{V}_L \leq \begin{cases} \frac{1}{2}\lambda_u\left(V_L+1\right) & \text{if } V_L \leq 1 \\ \lambda_u V_L & \text{if } V_L > 1 \end{cases}, \tag{3–24}$$

where λ_u was defined in (3–22). Since both V_L and λ_u are positive, (3–24) can always be upper bounded as

$$\dot{V}_L \leq \lambda_u\left(V_L + \frac{1}{2}\right). \tag{3–25}$$

The solution to (3–25) over the interval $t \in \left[t_n^{off},\ t_{n+1}^{on}\right)$ yields the following upper bound on V_L in the uncontrolled region:

$$V_L\left(r\left(t\right)\right) \leq V_L\left(r\left(t_n^{off}\right)\right)\exp\left(\lambda_u\left(t-t_n^{off}\right)\right) + \frac{1}{2}\left(\exp\left(\lambda_u\left(t-t_n^{off}\right)\right)-1\right), \tag{3–26}$$

for all $t \in \left[t_n^{off},\ t_{n+1}^{on}\right)$ and for all n. Rewriting (3–26) using (3–8) and performing some algebraic manipulation yields (3–21). □

Remark 3.2. The exponential bound in (3–21) indicates that in the uncontrolled regions, the error norm is bounded by an exponentially increasing envelope. Since the error norm decays at an exponential rate in the controlled regions, as described by (3–9),

sufficient conditions for stability of the overall system can be developed based on the exponential time constants λ_c and λ_u and the time that the crank dwells in each region (dwell-times) $\Delta t_n^{on} \triangleq t_n^{off} - t_n^{on}$ and $\Delta t_n^{off} \triangleq t_{n+1}^{on} - t_n^{off}$. However, a challenge is that the dwell-time Δt_n^{on} and reverse dwell-time Δt_n^{off} (nomenclature derived from [45]) depend on the switching times, which are unknown a priori. The following propositions introduce bounds on the uncertain dwell-times.

Proposition 3.1. *The n^{th} dwell-time Δt_n^{on} has a known, constant lower bound $\Delta t_{min}^{on} \in \mathbb{R}_{>0}$ such that*

$$\min_n \Delta t_n^{on} \geq \Delta t_{min}^{on}, \tag{3–27}$$

where Δt_{min}^{on} is defined as

$$\Delta t_{min}^{on} \triangleq \frac{\min_n \left(q_n^{off} - q_n^{on} \right)}{\dot{q}_{max}}, \tag{3–28}$$

provided

$$\dot{q}\left(t\right) \leq \dot{q}_{max}, \tag{3–29}$$

for all $t \in \left[t_n^{on},\ t_n^{off}\right]$, where $\dot{q}_{max} \in \mathbb{R}_{>0}$ is a selected safety limit.

Proof. The dwell-time Δt_n^{on} can be precisely expressed as

$$\Delta t_n^{on} = \frac{q_n^{off} - q_n^{on}}{\dot{q}_{avg,n}^{on}}, \tag{3–30}$$

where $\dot{q}_{avg,n}^{on} \in \mathbb{R}$ is the average cadence through the n^{th} controlled region. The numerator of (3–30) depends on the choice of ε_m, introduced in (2–50)-(2–52), and the initial conditions; therefore, q_n^{off} and q_n^{on} are known a priori. However, the average cadence through a region of the crank cycle depends on future velocity states and is therefore unknown a priori. Then, the expression in (3–30) can be lower bounded using the cadence limit $\dot{q}_{max}$ as

$$\Delta t_n^{on} \geq \frac{q_n^{off} - q_n^{on}}{\dot{q}_{max}}, \tag{3–31}$$

provided (3–29) is satisfied for all $t \in \left[t_n^{on},\ t_n^{off}\right]$. Finally, (3–31) can be bounded for all n as in (3–28). □

Assumption 3. If the velocity at each off-time is greater than or equal to some known critical velocity $\dot{q}_{crit} \in \mathbb{R}_{>0}$, then the crank will exit the uncontrolled region in a finite amount of time for all n. In other words, $\dot{q}\left(t_n^{off}\right) \geq \dot{q}_{crit} \Rightarrow \Delta t_n^{off} \leq \Delta t_{crit}^{off}, \forall n$, where $\Delta t_{crit}^{off} \in \mathbb{R}_{>0}$ is a known constant. The critical velocity and the corresponding critical reverse dwell-time Δt_{crit}^{off} can be numerically determined for a wide range of system configurations or experimentally determined for a specific configuration.

Proposition 3.2. *The n^{th} reverse dwell-time Δt_n^{off} has a known, constant upper bound $\Delta t_{max}^{off} \in \mathbb{R}_{>0}$ such that*

$$\max_n \Delta t_n^{off} \leq \Delta t_{crit}^{off} = \Delta t_{max}^{off}, \tag{3–32}$$

provided

$$\dot{q}\left(t_n^{off}\right) \geq \dot{q}^{crit}, \tag{3–33}$$

for all n.

Proof. According to Assumption 3, each Δt_n^{off} is bounded by a known constant, provided the initial crank velocity is sufficiently large upon entering the uncontrolled regions. Therefore, if (3–33) is satisfied for all n, then $\max_n \Delta t_n^{off} \leq \Delta t_{crit}^{off}$. The critical off-duration is therefore also the maximum off-duration, i.e., $\Delta t_{crit}^{off} = \Delta t_{max}^{off}$, provided the critical velocity is also the minimum velocity for all off-times, i.e., (3–33). □

Remark 3.3. Propositions 3.1 and 3.2 introduce sufficient conditions (3–29) and (3–33) that, if satisfied, guarantee known bounds on the dwell-times Δt_n^{on} and reverse dwell-times Δt_n^{off}, despite uncertainty in the switching times. The following theorems describe how these sufficient conditions can be satisfied a priori.

Theorem 3.3. *The crank velocity satisfies (3–29) for all $t \in \left[t_n^{on},\ t_n^{off}\right]$, provided the following conditions are satisfied for all n:*

$$\max_{t \in \left[t_n^{on},\ t_n^{off}\right]} \dot{q}_d(t) < \dot{q}_{max}, \tag{3–34}$$

$$\left|r\left(t_n^{on}\right)\right| \leq \sqrt{2\overline{DM}^{-1}}, \tag{3–35}$$

where $\overline{D} \in \mathbb{R}_{\geq 0}$ *is defined as*

$$\overline{D} \triangleq \frac{1}{2}\underline{M}\left(\dot{q}_{max} - \max_{t \in \left[t_n^{on},\, t_n^{off}\right]} \dot{q}_d(t)\right)^2. \tag{3–36}$$

Proof. The conditions in (3–34) and (3–35) can be used with (3–8) to demonstrate that $V_L(r(t_n^{on})) \leq \overline{D}$, which can then be used with (3–20) to upper bound $V_L(r(t))$ as

$$V_L(r(t)) \leq \overline{D}\exp\left(-\lambda_c\left(t - t_n^{on}\right)\right), \tag{3–37}$$

for all $t \in \left[t_n^{on},\, t_n^{off}\right]$. Using (3–8), (3–1), and (3–37), and assuming the worst case scenario where $r(t) < 0$, the following upper bound on the crank velocity in the controlled regions can be obtained:

$$\dot{q}(t) \leq \dot{q}_d(t) + \sqrt{2\overline{DM}^{-1}\exp\left(-\lambda_c\left(t - t_n^{on}\right)\right)}, \tag{3–38}$$

for all $t \in \left[t_n^{on},\, t_n^{off}\right]$. To satisfy (3–29), it is sufficient to demonstrate that the right-hand side of (3–38) is upper bounded by $\dot{q}_{max}$. The right-hand side of (3–38) can be upper bounded further as

$$\dot{q}(t) \leq \max_{t \in \left[t_n^{on},\, t_n^{off}\right]} \dot{q}_d(t) + \sqrt{2\overline{DM}^{-1}}, \tag{3–39}$$

for all $t \in \left[t_n^{on},\, t_n^{off}\right]$. From the definition in (3–36), the right-hand side of (3–39) is equal to $\dot{q}_{max}$. Therefore, it can be concluded via (3–39) and the definition in (3–36) that (3–29) is satisfied for all $t \in \left[t_n^{on},\, t_n^{off}\right]$, which allows the dwell-time to be lower bounded as in Proposition 3.1. □

Theorem 3.4. *The crank velocity at the* n^{th} *off-time satisfies (3–33) provided the sufficient conditions in Theorem 3.3 and the following conditions are satisfied for all* n*:*

$$\dot{q}_d\left(t_n^{off}\right) > \dot{q}_{crit}, \tag{3–40}$$

$$\lambda_c \geq -\frac{1}{\Delta t_{min}^{on}} ln\left(\underline{D}\overline{D}^{-1}\right), \tag{3–41}$$

where $\underline{D} \in \mathbb{R}_{\geq 0}$ *is defined as*

$$\underline{D} \triangleq \frac{1}{2}\underline{M}\left(\min_n \dot{q}_d\left(t_n^{off}\right) - \dot{q}_{crit}\right)^2. \tag{3–42}$$

Proof. To ensure that (3–33) is satisfied for all n, (3–40) must be satisfied; otherwise, the tracking error may converge to zero at the off-time, according to (3–9), which could result in a crank velocity at the off-time that is slower than the critical velocity. In addition, (3–40) also guarantees that $\underline{D}$ is nonzero, which would otherwise require $\lambda_c \to \infty$ via (3–41). If (3–40) is satisfied, then it is sufficient to show that the actual velocity is sufficiently close to the desired velocity at the off-time, which can be guaranteed by a sufficiently large convergence rate λ_c. Specifically, if the conditions in Theorem 3.3 are satisfied, the worst case scenario where $\Delta t_n^{on} = \Delta t_{min}^{on}$ for all n can be considered, so that (3–37) can be used to demonstrate that

$$V_L\left(r\left(t_n^{off}\right)\right) \leq \overline{D}\exp\left(-\lambda_c \Delta t_{min}^{on}\right). \tag{3–43}$$

Then, (3–41) can be used to demonstrate that the right-hand side of (3–43) is upper bounded by $\underline{D}$, so that (3–43) can be further bounded as

$$V_L\left(r\left(t_n^{off}\right)\right) \leq \underline{D}. \tag{3–44}$$

Assuming the worst case scenario where $r\left(t_n^{off}\right) > 0$ and using (3–8) with (3–44), the crank velocity at the n^{th} off-time can be lower bounded as

$$\dot{q}\left(t_n^{off}\right) \geq \min_n \dot{q}_d\left(t_n^{off}\right) - \sqrt{2\underline{D}\underline{M}^{-1}}. \tag{3–45}$$

From the definition in (3–42), the right-hand side of (3–45) is equal to $\dot{q}_{crit}$. Therefore, it can be concluded that the conditions in Theorem 3.3, Theorem 3.4, (3–40), and (3–41) are sufficient to satisfy (3–33) for an arbitrary n, which, from Assumption 3, allows the reverse dwell-time Δt_n^{off} to be upper bounded as in Proposition 3.2. □

Remark 3.4. Theorems 3.3 and 3.4 give sufficient conditions which ensure boundedness of the crank velocity, and thereby the dwell-time Δt_n^{on} and reverse dwell-time Δt_n^{off}, over a single crank cycle. To ensure boundedness across all crank cycles, it must be shown that the tracking error does not grow so much in the uncontrolled regions that the crank velocity could exceed $\dot{q}_{max}$ upon re-entering the controlled regions. In other words, given that the sufficient conditions in the previous theorems are satisfied for $n = 0$, and if $\left|r\left(t_{n+1}^{on}\right)\right| \leq \sqrt{2\overline{DM}^{-1}}$, then the results of Theorems 3.3 and 3.4 hold for all n.

Theorem 3.5. *The tracking error upon exiting the uncontrolled regions* $r\left(t_{n+1}^{on}\right)$ *is bounded as*

$$\left|r\left(t_{n+1}^{on}\right)\right| \leq \sqrt{2\overline{DM}^{-1}} \tag{3–46}$$

for all n*, provided the sufficient conditions in Theorems 3.3 and 3.4 and the following conditions are satisfied:*

$$\lambda_c \geq \lambda_u \frac{\Delta t_{max}^{off}}{\Delta t_{min}^{on}} - \frac{1}{\Delta t_{min}^{on}} ln\left(\underline{M}\overline{M}^{-1} - b\overline{D}^{-1}\right), \tag{3–47}$$

$$\overline{D} > b\overline{M}\underline{M}^{-1}, \tag{3–48}$$

where $b \in \mathbb{R}_{>0}$ *is defined as*

$$b \triangleq \frac{1}{2}\left(exp\left(\lambda_u \Delta t_{max}^{off}\right) - 1\right).$$

Consequently, the dwell-times Δt_n^{on} *and reverse dwell-times* Δt_n^{off} *are bounded as in Propositions 3.1 and 3.2 for all* n.

Proof. Assuming the worst case scenario for the n^{th} cycle where $\Delta t_n^{on} = \Delta t_{min}^{on}$ and $\Delta t_n^{off} = \Delta t_{max}^{off}$ (i.e., minimum decay and maximum growth of the tracking error), (3–35), (3–20), (3–26), and (3–8) can be used to demonstrated that

$$\frac{1}{2}\overline{M}\left|r\left(t_{n+1}^{on}\right)\right|^2 \leq a\overline{DM}\underline{M}^{-1} + b, \tag{3–49}$$

where $a \in \mathbb{R}_{>0}$ is defined as

$$a \triangleq \exp\left(\lambda_u \Delta t_{max}^{off} - \lambda_c \Delta t_{min}^{on}\right).$$

Provided (3–47) is satisfied, it can be demonstrated that the right-hand side of (3–49) is bounded above by $\overline{D}$, i.e., (3–46). Provided (3–48) is satisfied, it can be demonstrated that the argument of ln $(\cdot)$ in (3–47) is positive, so that λ_c can always be selected to satisfy (3–47). Finally, if (3–46) is satisfied, Theorems 3.3-3.5 can be applied for all n. □

Remark 3.5. The condition in (3–48) arises due to the fact that the tracking error will always have a nonzero upper bound, derived from (3–21), when exiting the uncontrolled region. Therefore, $\overline{D}$ must be sufficiently large. Based on the definition in (3–36), $\overline{D}$ can be made arbitrarily large by selection of $\dot{q}_{max}$ and the design of $\dot{q}_d$.

Remark 3.6. Propositions 3.1 and 3.2 propose known bounds on the dwell-times and reverse dwell-times, and Theorems 3.3-3.5 give sufficient conditions to validate the Propositions for all n. With known bounds on the time between switches and known rates of convergence and divergence of the tracking error, a known ultimate bound on the tracking error can be calculated. The following Theorem gives the value of this ultimate bound along with a sufficient condition for convergence of the tracking error to that bound.

Theorem 3.6. *The tracking error is ultimately bounded in the sense that* $|r(t)|$ *converges to a ball with constant radius* $d \in \mathbb{R}_{>0}$ *as the number of crank cycles approaches infinity (i.e., as* $n \to \infty$*), where* d *is defined as*

$$d \triangleq \sqrt{\frac{2b}{\underline{M}(1-a)}}, \tag{3–50}$$

provided the sufficient conditions in Theorems 3.3-3.5 and the following condition are satisfied:

$$\lambda_c > \lambda_u \frac{\Delta t_{max}^{off}}{\Delta t_{min}^{on}}. \tag{3–51}$$

Proof. Using (3–20) and (3–26) sequentially and assuming the worst case scenario for each cycle where $\Delta t_n^{on} = \Delta t_{min}^{on}$ and $\Delta t_n^{off} = \Delta t_{max}^{off}$, an upper bound for $V_L\left(r\left(t_n^{on}\right)\right)$ after $N \in \mathbb{N}_{>0}$ cycles can be developed as

$$V_L\left(r\left(t_N^{on}\right)\right) \leq V_L\left(r\left(t_0^{on}\right)\right) a^N + b\sum_{n=0}^{N-1} a^n. \tag{3–52}$$

The right-hand side of (3–52) can be viewed as a series whose elements form the sequence $\{x_n \in \mathbb{R}_{\geq 0}\}_0^N$, defined for $n \in \{1,\ 2,\ ...,\ N\}$ as

$$x_n \triangleq x_0 a^n + b\sum_{k=0}^{n-1} a^k, \tag{3–53}$$

where $x_0 \triangleq V_L\left(r\left(t_0^{on}\right)\right)$. Then, the sequence $\{V_L\left(r\left(t_n^{on}\right)\right)\}$ is upper-bounded by $\{x_n\}$ for each n. The sequence $\{x_n\}$ is positive, monotonic, and bounded, provided (3–51) is satisfied (i.e., $a < 1$); therefore, the limit of $\{x_n\}$ exists and can be expressed as

$$\lim_{n\to\infty} x_n = \overline{d},$$

where $\overline{d} \in \mathbb{R}_{>0}$ is a known constant defined as

$$\overline{d} \triangleq \frac{b}{1-a}. \tag{3–54}$$

Therefore, since $V_L\left(r\left(t_n^{on}\right)\right) \leq x_n$ for each n, $V_L\left(r\left(t_n^{on}\right)\right)$ is ultimately bounded by $\overline{d}$ in the sense that as $n \to \infty,\ V_L\left(r\left(t_n^{on}\right)\right) \leq x_n \to \overline{d}$. Similarly, $V_L\left(r\left(t_n^{off}\right)\right)$ is ultimately bounded by $\underline{d} \in \mathbb{R}_{\geq 0}$, which is a known constant defined as

$$\underline{d} \triangleq \overline{d}\exp\left(-\lambda_c \Delta t_{min}^{on}\right). \tag{3–55}$$

Monotonicity of the bounds in (3–20) and (3–26) can be used to demonstrate that $V_L\left(r\left(t\right)\right) \leq \max\left\{x_n,\ x_{n+1}\right\}$ for $t \in \left[t_n^{on},\ t_{n+1}^{on}\right]$, so it can be concluded that V_L is ultimately bounded by $\overline{d}$. It can also be concluded that $V_L\left(r\left(t\right)\right) \leq \overline{d}$ for all $t \geq t_N^{off}$ when $V_L\left(r\left(t_N^{off}\right)\right) \leq \underline{d}$, or, similarly, for all $t \geq t_N^{on}$ when $V_L\left(r\left(t_N^{on}\right)\right) \leq \overline{d}$. In other words, if the controller is switched on when $V_L\left(r\left(t_N^{on}\right)\right) \leq \overline{d}$, V_L will remain within that ball for

all subsequent time. Using (3–8), it can then be demonstrated that as $n \to \infty$, $|r(t)|$ converges to a ball with constant radius d, where d was defined in (3–50). □

Remark 3.7. The size of the ultimate bound d depends on the bounds of the inertial term given in Property 7, the bounds of χ in (3–4), the minimum dwell-time Δt_{min}^{on}, the maximum reverse dwell-time Δt_{max}^{off}, and the control gain k_1 via λ_c. However, the effect of the control gain is limited; consider the following:

$$\lim_{\lambda_c \to \infty} \overline{d} = b, \tag{3–56}$$

$$\lim_{\lambda_c \to \infty} \underline{d} = 0. \tag{3–57}$$

Based on (3–56) and (3–57), the lower limit of V_L can be driven to zero by choosing the gains to be arbitrarily large, but V_L will always have a nonzero upper bound. The size of the ultimate bound can be further minimized by decreasing the length of the uncontrolled regions via ε_m or by ensuring larger $\dot{q}\left(t_n^{off}\right)$ for each n to reduce Δt_{max}^{off}. Note also that (3–47) is a sufficient condition for $\overline{d} \leq \overline{D}$.

Remark 3.8. The conditions in (3–41), (3–47), and (3–51), together with (3–11), all impose constraints on the selection of k_1 via λ_c and can therefore be combined as

$$k_1 \geq \max\left\{ c_2 \left(\min\left(k_m\right) \underline{B}\right)^{-1} - \frac{\overline{M}}{2\min\left(k_m\right) \underline{B} \Delta t_{min}^{on}} \ln\left(\underline{D}\overline{D}^{-1}\right), \right.$$
$$\left. c_2 \left(\min\left(k_m\right) \underline{B}\right)^{-1} + \frac{\overline{M}}{2\min\left(k_m\right) \underline{B} \Delta t_{min}^{on}} \left(\lambda_u \Delta t_{max}^{off} - \ln\left(1 - b\overline{D}^{-1}\right)\right) \right\}, \tag{3–58}$$

where the fact that (3–47) is a sufficient condition for (3–51) was used.

3.3 Experiments

FES-cycling experiments were conducted with the primary objective of evaluating the performance of the switched controller given in (3–5) and distributed to the gluteal, quadriceps femoris, and hamstrings muscle groups according to (2–54). The experiments were divided into Protocol A and Protocol B. The objective of both protocols was to demonstrate the controller's cadence tracking performance in the presence

of parametric uncertainty and unmodeled disturbances. The FES-cycling trials were stopped if the control input saturated, the subject reported significant discomfort, the cadence fell below 0 RPM, the trial runtime expired, or the cadence exceeded 60 RPM. The experiments could also be ended at any time by the subjects via an emergency stop switch.

3.3.1 Methods

Four able-bodied male subjects 25-27 years old were recruited from the student population at the University of Florida, and one male subject with PD, 60 years old, with a modified Hoehn and Yahr disability score of 2.5 [46], was recruited from the University of Florida Center for Movement Disorders and Neurorestoration. Each subject gave written informed consent approved by the University of Florida Institutional Review Board. Able-bodied subjects were recruited to validate the controller design, and the subject with PD was recruited to demonstrate feasibility of the proposed approach in a potential patient population.

The subject with PD in this experiment exhibited mild bilateral motor impairment with evident tremor. It was observed during preliminary testing that the subject's right side was more affected (i.e., greater tremor) and exhibited bradykinesia during cycling (i.e., when the right leg was supposed to pedal, cadence decreased significantly). In addition, preliminary testing revealed that subject could not tolerate the level of stimulation intensity necessary for FES-induced cycling (i.e., FES-cycling without volitional effort from the rider). It was hypothesized that FES-assisted cycling (i.e., FES-cycling with volitional effort from the rider) would be a more appropriate protocol for subjects with PD. It was further hypothesized that FES-assistance would provide sensory cues and muscle activation assistance during cycling and thereby decrease variability in the subject's cadence.

A commercially available, stationary, recumbent exercise cycle (AudioRider R400, NordicTrack) was modified for the purposes of the FES-cycling experiments and is

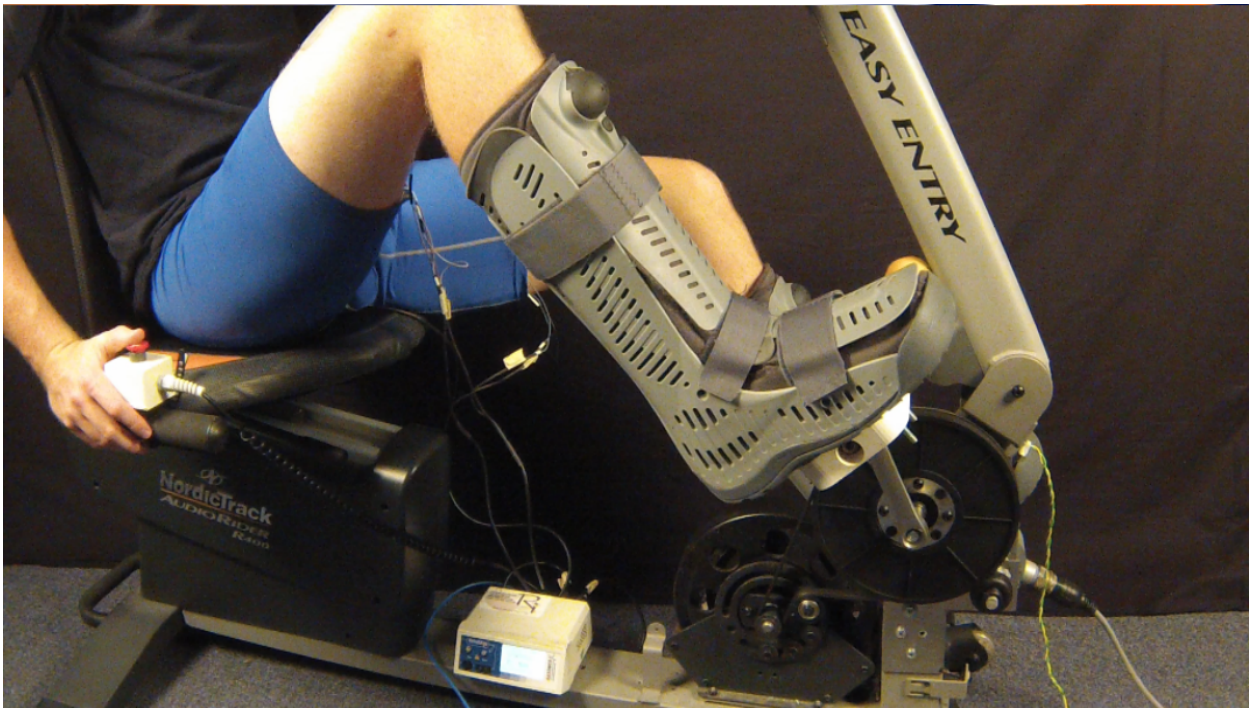

Figure 3-1. FES-cycling test bed. Photo courtesy of author.

depicted in Figure 3-1. The cycle originally had a flywheel which was driven by a freewheel. The freewheel was then replaced with a fixed gear so that the crankshaft was directly coupled to the flywheel, allowing the flywheel to contribute its momentum to the cycle-rider momentum and improving the system energetics [47]. The cycle has an adjustable seat and a magnetic hysteresis brake on the flywheel with 16 incremental levels of resistance (resistance was set to Level 1 unless otherwise noted). Custom pedals were constructed that allowed high-top orthotic boots (Rebound Air Walker, Össur) to be affixed to them; these orthotic pedals served to fix the rider's feet to the pedals, prevent dorsiflexion and plantarflexion of the ankles, and maintain sagittal alignment of the lower legs. An optical, incremental encoder (HS35F, BEI Sensors, resolution $0.018°$) was added to the cycle and coupled to the crank shaft to measure the cycling cadence. The cycle was equipped with a Hall effect sensor and magnet on the crank that provided an absolute position reference once per cycle.

A current-controlled stimulator (RehaStim, Hasomed) delivered biphasic, symmetric, rectangular pulses to the subject's muscle groups via bipolar, self-adhesive electrodes (PALS 3x5).[1] A personal computer equipped with data acquisition hardware and software was used to read the encoder signal, calculate the control input, and command the stimulator. Stimulation frequency was fixed at 60 Hz to leverage the results found in [48]. Stimulation intensity was controlled by fixing the pulse amplitude for each muscle group and controlling the pulsewidth according to (3–5). Pulse amplitude was determined for each subject's muscle groups in preliminary testing and ranged from 50-110 mA.

Electrodes were placed over the subjects' gluteal, quadriceps femoris, and hamstrings muscle groups, according to Axelgaard's electrode placement manual[2] , while subjects were standing upright. Subjects were then seated on the stationary cycle, and their feet were inserted securely into the orthotic pedals. The cycle seat position was adjusted for each subject's comfort while ensuring that hyperextension of the knees could not be achieved while cycling. The subject's hip position relative to the cycle crank axis was measured along with the distances between the subjects' greater trochanters and lateral femoral condyles (l_t) and between the subjects' lateral femoral condyles and the pedal axes of rotation (l_l). These distances were used to calculate the torque transfer ratios for the subjects' muscle groups and to thereby determine the stimulation pattern.

The desired crank velocity was defined in radians per second as

$$\dot{q}_d \triangleq \frac{5\pi}{3}\left(1 - \exp\left(-\phi t\right)\right), \tag{3–59}$$

[1] Surface electrodes for this study were provided compliments of Axelgaard Manufacturing Co., Ltd.

[2] http://www.palsclinicalsupport.com/videoElements/videoPage.php

where $\phi \in \mathbb{R}_{>0}$ was a selectable constant used to control the acceleration of the desired trajectory and $t_0^{on} = 0$ seconds. The trajectory in (3–59) ensured that the desired velocity started at 0 RPM and smoothly approached 50 RPM. The control gains, introduced in (2–54) and (3–5), were tuned to yield acceptable tracking performance for each subject in preliminary testing and ranged as follows: $k_1 \in [70,\ 150]$, $k_2 \in [7,\ 15]$, $k_{*Glute} \in [0.5625,\ 1.125]$, $k_{*Quad} \in [0.9,\ 1.125]$, $k_{*Ham} \in [0.816,\ 1.2375]$.

Protocol A was completed by all able-bodied subjects and consisted of a voluntary cycling phase followed by five minutes of rest and a subsequent FES-cycling phase. During the voluntary cycling phase, subjects were shown a computer screen with a real-time plot of their actual cadence, as measured by the encoder, versus the desired cadence given in (3–59), and each subject was asked to voluntarily pedal so that the two plots coincided with one another (i.e., minimize the tracking error r). After 175 seconds had elapsed, the flywheel resistance was increased from Level 1 directly to Level 9 for a period of 30 seconds, after which the resistance was decreased back to Level 1 for the remainder of the cycling phase. The voluntary cycling phase lasted five minutes.

Following five minutes of rest, the FES-cycling phase was initiated, wherein cycling was only controlled by stimulation of the gluteal, quadriceps femoris, and hamstrings muscle groups (i.e., a completely passive rider). The stimulation pattern (i.e., the range of crank angles over which each muscle was stimulated) for Protocol A was defined by selecting $\varepsilon_{*Glute} = 0.2,\ \varepsilon_{*Quad} = 0.3,\ \varepsilon_{*Ham} = 0.38$, which was found to yield satisfactory performance in preliminary testing. While the same values of ε_m were used for all subjects, the stimulation pattern resulting from the choice of each ε_m was slightly different for each subject because each subject had different leg lengths and preferred seating positions. The subjects' limbs were then positioned manually so that the initial crank position was in the controlled region, and then the controller was activated. The subjects were instructed to relax as much as possible throughout this

phase and to make no effort to voluntarily control the cycling motion; additionally, the subjects were not given any indication of the control performance (i.e., subjects could no longer see the actual or desired trajectory). As in the voluntary cycling phase, the flywheel resistance was increased from Level 1 to Level 9 for $t \in [175,\ 205]$ seconds to demonstrate the controller's robustness to an unknown, bounded, time-varying disturbance. The FES-cycling phase lasted five minutes.

Protocol B was completed by the subject with PD and was the same as Protocol A, with the exception that the subject was allowed to voluntarily pedal during the FES-cycling phase (i.e., FES-assisted cycling) and could see the actual and desired cadence. While Protocol A was intended to demonstrate the controller's performance with a completely passive rider, as would be the case with a subject with motor complete spinal cord injury, Protocol B demonstrates feasibility of the developed controller for a broader patient population with intact, albeit diminished, motor control, such as those with incomplete spinal cord injury, hemiparetic stroke, traumatic brain injury, and PD. This voluntary assistance from the rider is modeled as τ_r in (2–55). Although disturbances are generally neither assistive nor resistive, voluntary effort from the rider during FES-cycling is generally assistive and is therefore expected to decrease the control input needed to track the desired cadence.

3.3.2 Results

3.3.2.1 Protocol A results

Fig. 3-2 depicts one able-bodied subject's tracking performance, quantified by the cadence tracking error r, and the stimulation intensity (pulsewidth) input to each muscle group u_m during the FES-cycling phase of Protocol A. In Fig. 3-2 and subsequent figures, the shaded region marks the period of time during which the ergometer's resistance was increased from Level 1 to Level 9. Fig. 3-3 provides an enhanced view of the control input over a single crank cycle to illustrate the controller switching and distribution of the control input across the muscle groups. Table 3-1 compares the

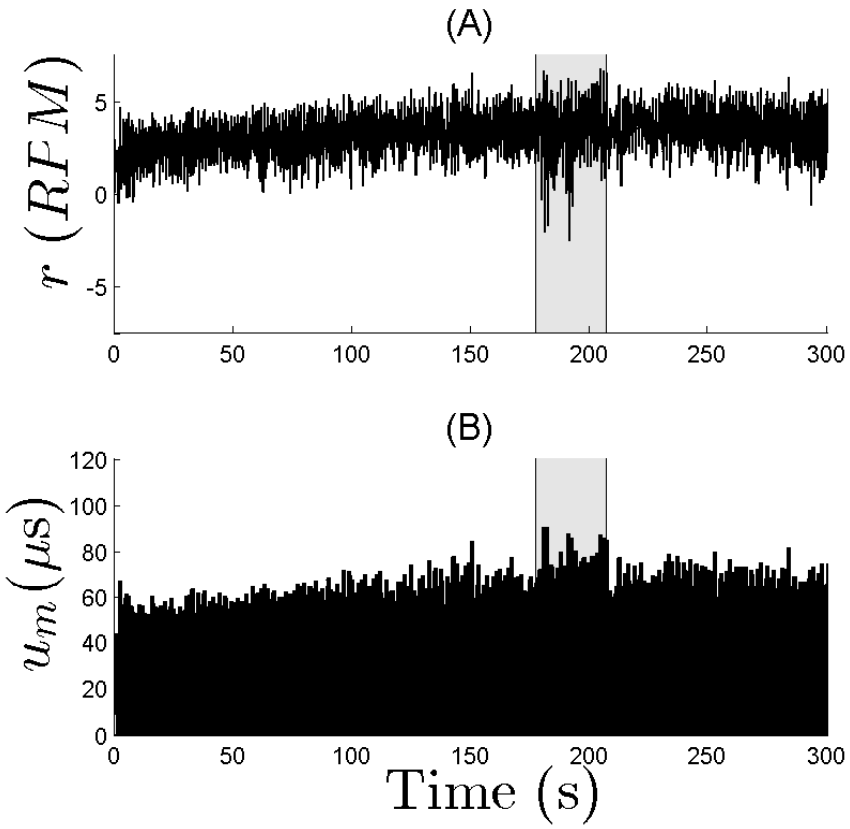

Figure 3-2. One subject's cadence tracking error and control input to each muscle group during the FES-cycling trial of Protocol A. A) Cadence tracking error. B) Stimulation intensity input to each muscle group.

subjects' volitional and FES-induced tracking performance, quantified by the mean and standard deviation of the cadence tracking error in RPM, over the total trial ($t \in [0,\ 300]$ seconds) and during several phases of each trial: the transient phase ($t \in [0,\ 40]$ seconds), the steady state phase ($t \in (40,\ 175)$ seconds), the added disturbance phase ($t \in [175,\ 205]$ seconds), and the final phase ($t \in (205,\ 300]$ seconds). Fig. 3-4 compares another subject's cadence tracking error in the voluntary and FES-induced cycling phases. All trials went to completion.

3.3.2.2 Protocol B results

Fig. 3-5 depicts the tracking performance of the subject with PD, quantified by the cadence tracking error r, and the stimulation intensity (pulsewidth) input to each muscle group u_m during the FES-assisted phase of Protocol B. An enhanced view of the control

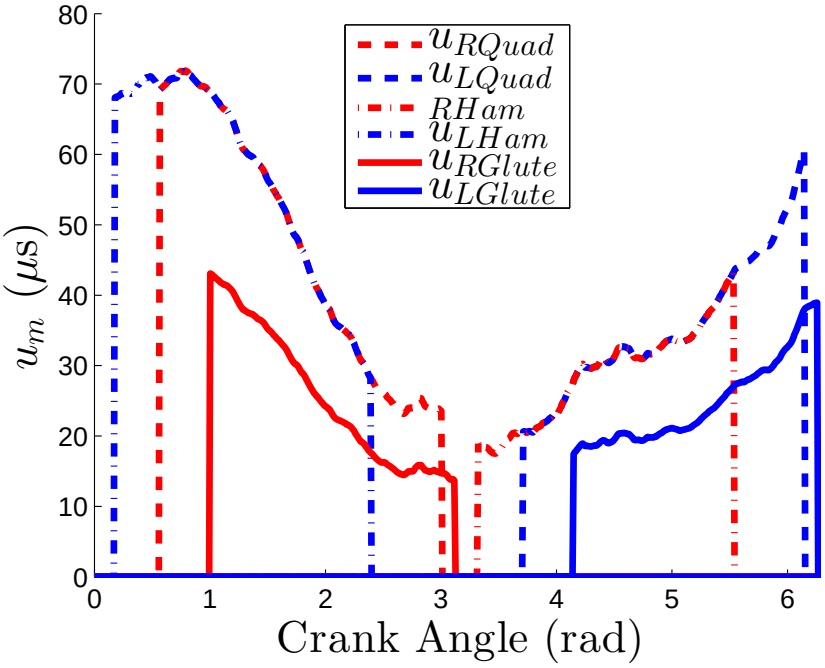

Figure 3-3. Control input over a single crank cycle during the FES-cycling trial of Protocol A for Subject AB3.

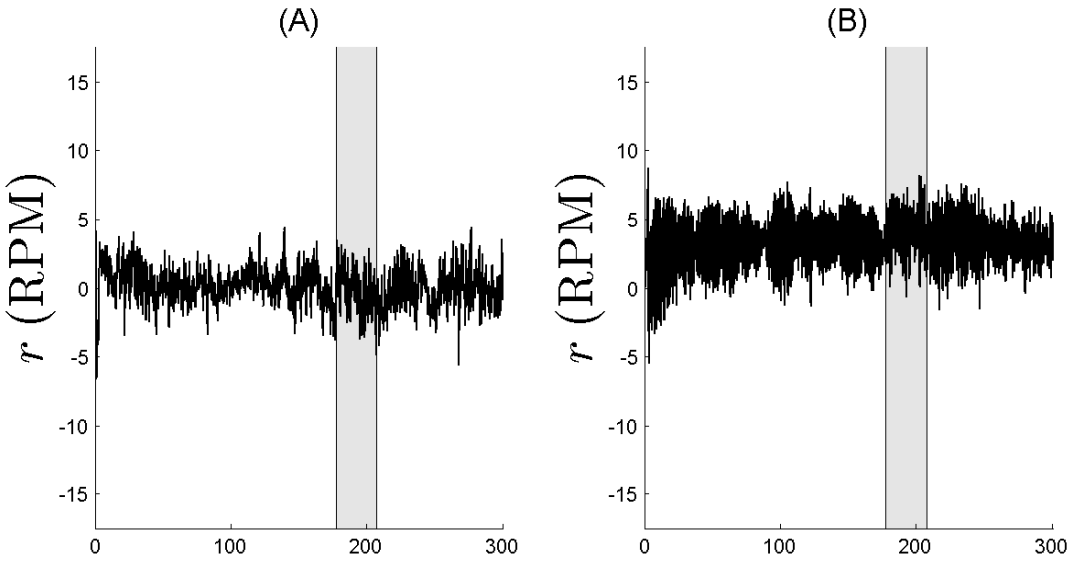

Figure 3-4. Cadence tracking error for the voluntary and FES-cycling phases of Protocol A for Subject AB3. A) Voluntary tracking phase. B) FES-cycling phase.

Table 3-1. Comparison of cadence tracking error for all able-bodied subjects' volitional and FES-cycling.

Subject	Phase	Volitional error (RPM)	FES error (RPM)
AB1	Transient	1.04±1.58	2.41±1.08
	Steady state	-0.06±1.59	3.12±1.04
	Disturbance	0.04±2.01	3.39±1.61
	Final	-0.43±1.70	3.47±1.21
	Total trial	-0.02±1.73	3.16±1.22
AB2	Transient	0.28±3.26	6.03±2.07
	Steady state	-0.07±1.15	9.78±1.58
	Disturbance	0.01±1.43	14.56±1.78
	Final	-0.01±1.17	12.68±1.21
	Total trial	0.01±1.63	10.68±2.92
AB3	Transient	0.62±1.68	2.31±2.54
	Steady state	0.01±1.06	3.12±1.70
	Disturbance	-0.21±1.51	4.14±1.52
	Final	-0.31±1.38	3.19±1.63
	Total trial	-0.03±1.34	3.14±1.85
AB4	Transient	1.22±2.72	3.51±2.75
	Steady state	-0.01±1.36	3.93±1.78
	Disturbance	0.40±1.56	4.74±3.52
	Final	0.18±1.34	4.41±2.97
	Total trial	0.25±1.67	4.11±2.57
All	Transient	0.79±2.31	3.56±2.11
	Steady state	-0.03±1.29	4.99±1.53
	Disturbance	0.06±1.63	6.71±2.11
	Final	-0.14±1.40	5.94±1.76
	Total trial	0.05±1.59	5.27±2.14

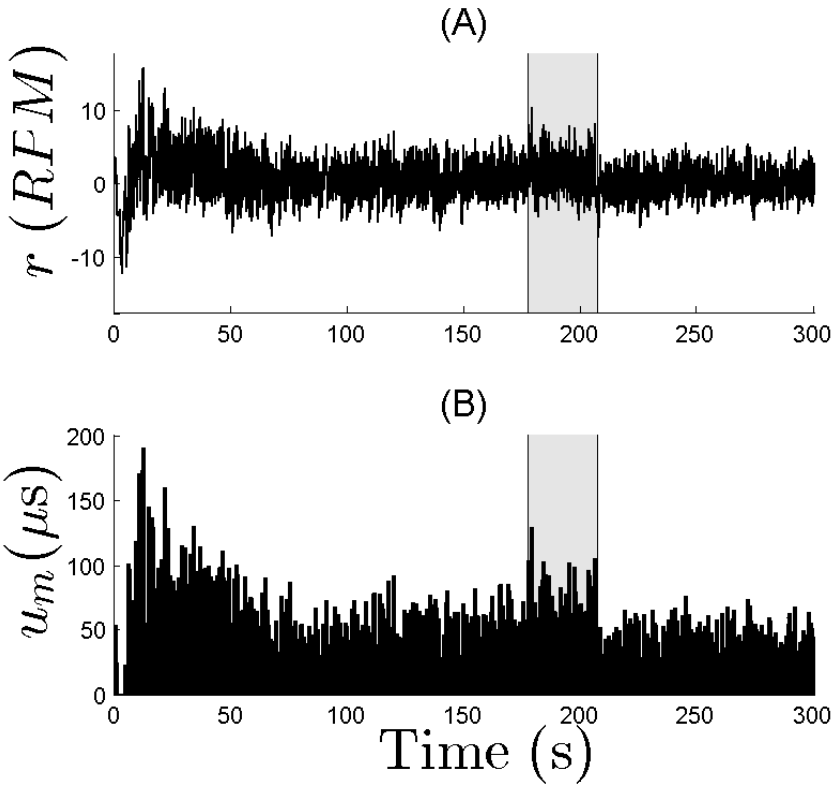

Figure 3-5. Cadence tracking error and control input to each muscle group during the FES-assisted phase of Protocol B. A) Cadence tracking error. B) Stimulation intensity input to each muscle group.

input over a single crank cycle is provided in Fig. 3-6 to illustrate the controller switching and distribution of the control input across the muscle groups. Table 3-2 summarizes the volitional and FES-assisted cadence tracking performance of the subject with PD using the same metrics as described in Section 3.3.2.1. Fig. 3-7 compares the subject's cadence tracking error in the voluntary and FES-assisted cycling phases. All trials went to completion.

3.3.3 Discussion

The results of Protocol A successfully demonstrate the ability of the controller in (3–5), distributed across the muscle groups according to (2–54), to achieve ultimately bounded tracking of the desired cadence despite parametric uncertainty (e.g., uncertain rider limb mass) and unknown disturbances. Ultimately bounded tracking was achieved

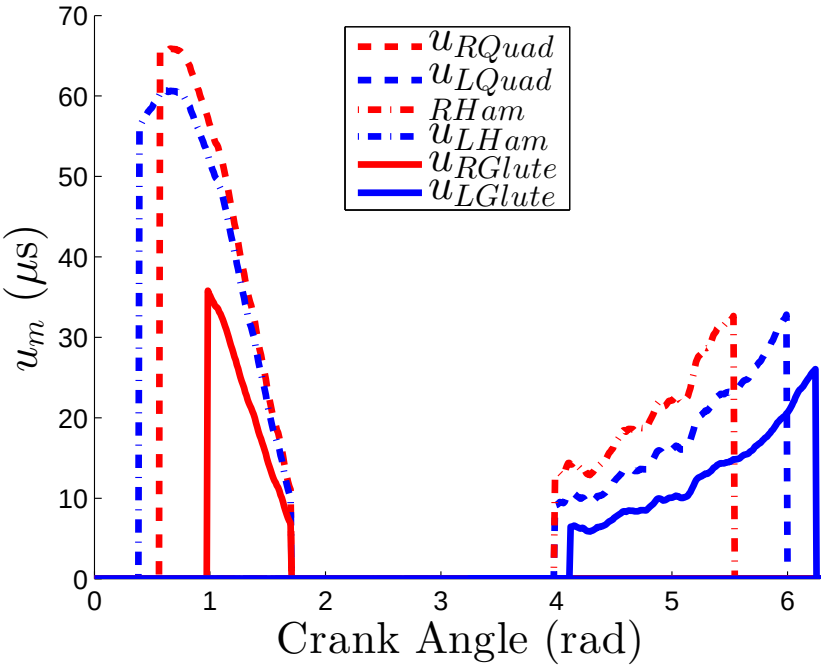

Figure 3-6. Control input over a single crank cycle during the FES-assisted cycling trial of Protocol B.

Table 3-2. Comparison of cadence tracking error of the subject with PD during volitional and FES-assisted cycling.

Subject	Phase	Volitional error (RPM)	FES error (RPM)
PD	Transient	-1.28±7.41	1.28±4.87
	Steady state	0.80±3.21	0.07±2.82
	Disturbance	2.10±3.88	1.15±2.91
	Final	0.11±2.65	-0.46±2.32
	Total trial	0.43±4.06	0.17±3.11

even across a range of stimulation patterns. Although the ultimate bound on the tracking error was higher for FES-cycling than volitional cycling by all subjects in Protocol A, this was likely due to the steady state offset in the tracking error and not due to large variations in cycling cadence, as quantified in Table 3-1. The cadence tracking error of all able-bodied subjects during voluntary and FES-induced cycling was 0.05 ± 1.59 RPM and 5.27 ± 2.14 RPM, respectively. The steady state error observed in the FES-cycling phase may be caused by a lack of adaptation in the FES-cycling controller. During volitional cycling, riders can learn how to modulate the force output of the muscles involved in cycling to improve tracking performance over time. Therefore, to achieve cadence tracking performance during FES-cycling that is similar to that observed during volitional cycling, motivation arises to use adaptive control methods during the controlled regions. However, this is challenging because adaptive control methods usually only achieve asymptotic convergence of the tracking error, but stability of a switched system with stable and unstable subsystems can only be guaranteed if the convergence and divergence rates are known (as is the case with exponential convergence, for example).

The results of Protocol B demonstrate the controller's tracking performance despite the presence of an additional unknown disturbance (manifested as volitional effort from the subject with PD). The data given in Table 3-2 indicate that the addition of FES-assistance to the subject's volitional effort improved cadence tracking performance measurably (60.5% and 23.4% improvement in mean and standard deviation of the cadence tracking error across the total trial). The improvement in tracking performance may be due to the bias of the stimulation input towards the subject's affected right leg (as depicted in Fig. 3-6), providing both assistance in activating the appropriate muscle groups and a sensory cue to volitionally pedal faster. More data is needed to determine if these results are statistically significant, but the results nonetheless indicate the potential of FES-assistance to improve the ability of a person with PD to pedal at a desired cadence.

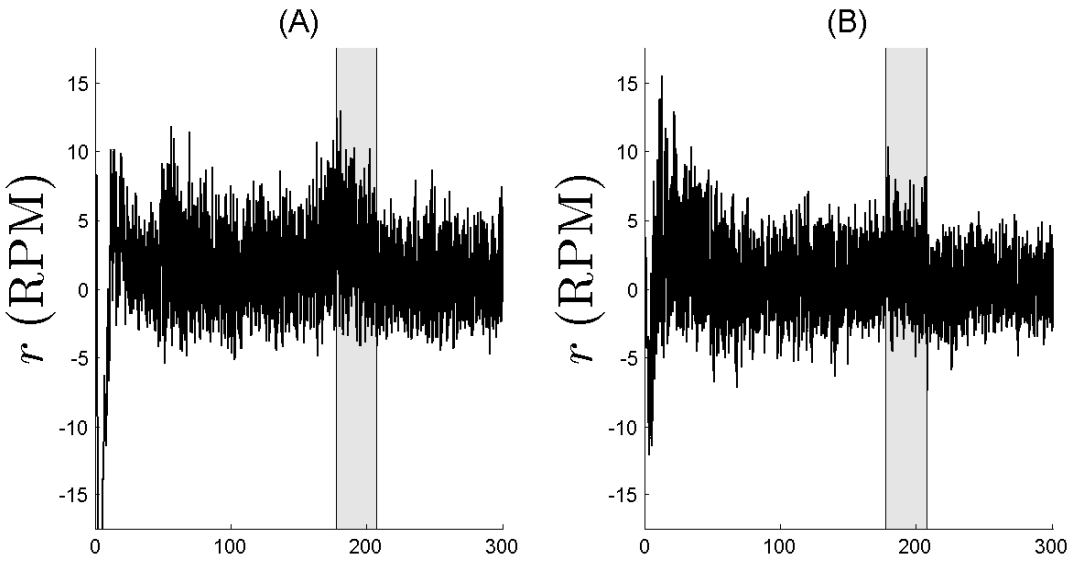

Figure 3-7. Cadence tracking error of the subject with PD during the voluntary and FES-assisted phases of Protocol B. A) Voluntary tracking phase. B) FES-cycling phase.

3.4 Concluding Remarks

A common Lyapunov-like function was used to prove that the developed controller, given in (3–5), yields ultimately bounded tracking of a desired cadence (i.e., crank velocity), provided the desired cadence, control gains, and stimulation pattern satisfy sufficient conditions. Experiments were conducted on four able-bodied subjects, and the results both demonstrate the robustness and stability of the developed switched controller and corroborate the theoretical relationships, described in Theorems 3.3-3.5, between the desired cadence, control gains, and stimulation pattern. Experiments were also conducted on one subject with PD, and the results suggest that FES-assisted cycling using the developed switched controller may improve the ability of people with PD to track a desired cadence.

Motivated by the need to minimize the steady state cadence tracking error observed in this chapter, the next chapter will add crank position tracking to the control objective of cadence tracking.

CHAPTER 4
SWITCHED CONTROL OF CRANK POSITION AND CADENCE TRACKING DURING STATIONARY CYCLING INDUCED BY FUNCTIONAL ELECTRICAL STIMULATION

In this chapter, a switched sliding mode controller is designed for the switched system in (2–55) with the objective that the FES control input achieves tracking of a desired crank position and cadence, simultaneously. A common Lyapunov-like function is used to demonstrate that the tracking error is ultimately bounded, despite uncertainty and bounded disturbances in the system and despite autonomous, state-dependent switching, provided sufficient conditions on the control gains, the desired cadence, the initial conditions, and the stimulation pattern are satisfied. Experimental results are provided which demonstrate the controller's tracking performance for a range of stimulation patterns.

4.1 Control Development

In this development, no electric motor input is provided (i.e., $u_{motor} = 0$) and the cycle inertia J_{cycle} is lumped together with the rider inertia M (i.e., here $M \triangleq M + J_{cycle}$).

4.1.1 Open-Loop Error System

The control objective is to simultaneously track a desired crank position and cadence, with performance quantified by the tracking error signals $e_1,\ e_2 \ : \ \mathbb{R}_{\geq 0} \to \mathbb{R}$, defined as

$$e_1(t) \triangleq q_d(t) - q(t), \tag{4–1}$$

$$e_2(t) \triangleq \dot{e}_1(t) + \alpha e_1(t), \tag{4–2}$$

where $q_d \ : \ \mathbb{R}_{\geq 0} \to \mathbb{R}$ is the desired crank position, designed so that its derivatives exist and $|\dot{q}_d| \leq c_{d1},\ |\ddot{q}_d| \leq c_{d2}$, where $c_{d1},\ c_{d2} \in \mathbb{R}_{>0}$ are known constants, and $\alpha \in \mathbb{R}_{>0}$ is a selectable constant. Without loss of generality, q_d is designed to monotonically increase, i.e., backpedaling is not desired. Taking the time derivative of (4–2), multiplying by M, and using (2–55) with (4–1) and (4–2) yields the following open-loop error system:

$$M\left(q\left(t\right)\right)\dot{e}_2\left(t\right) = \chi\left(q\left(t\right),\ \dot{q}\left(t\right),\ t\right) - V\left(q\left(t\right),\ \dot{q}\left(t\right)\right)e_2\left(t\right) - B_{FES}\left(q\left(t\right),\ \dot{q}\left(t\right)\right)u_{FES}\left(t\right), \tag{4–3}$$

where the auxiliary term $\chi : \mathcal{Q} \times \mathbb{R} \times \mathbb{R}_{\geq 0} \to \mathbb{R}$ is defined as

$$\chi \triangleq M\left(\ddot{q}_d + \alpha\dot{e}_1\right) + V\left(\dot{q}_d + \alpha e_1\right) + b_{cycle}\dot{q} + G + P + d_{cycle} + d_{rider} - \tau_r. \tag{4–4}$$

Based on Assumption 1 and Properties 5-12, χ can be bounded as

$$\left|\chi\left(q\left(t\right),\ \dot{q}\left(t\right),\ t\right)\right| \leq c_1 + c_2\left\|z\left(t\right)\right\| + c_3\left\|z\left(t\right)\right\|^2, \tag{4–5}$$

where $c_1,\ c_2,\ c_3 \in \mathbb{R}_{>0}$ are known constants defined as

$$\begin{aligned} c_1 &\triangleq \overline{M}c_{d2} + c_G + c_{P1} + c_{d,cycle} + c_{d,rider} + c_r + c_V c_{d1}^2 + \left(\overline{b} + c_{P2}\right)c_{d1}, \\ c_2 &\triangleq \alpha^2\overline{M} + \left(\overline{M} + 2c_V c_{d1} + \overline{b} + c_{P2}\right)\alpha + c_{d1}c_V + \overline{b} + c_{P2}, \\ c_3 &\triangleq c_V\left(\alpha^2 + \alpha\right), \end{aligned}$$

and the error vector $z : \mathbb{R}_{\geq 0} \to \mathbb{R}^2$ is defined as

$$z \triangleq \begin{bmatrix} e_1 & e_2 \end{bmatrix}^T. \tag{4–6}$$

4.1.2 Closed-Loop Error System

Based on (4–3) and the subsequent stability analysis, the control input is designed as

$$u_{FES} \triangleq k_1 e_2 + \left(k_2 + k_3\left\|z\right\| + k_4\left\|z\right\|^2\right)\text{sgn}\left(e_2\right), \tag{4–7}$$

where sgn $: \mathbb{R} \to [-1,\ 1]$ denotes the signum function and $k_1,\ k_2,\ k_3,\ k_4 \in \mathbb{R}_{>0}$ are constant control gains. After substituting (4–7) into the open-loop error system in (4–3),

the following switched closed-loop error system is obtained:

$$M\dot{e}_2 = \chi - Ve_2 - B_{FES}\left(k_1 e_2 + \left(k_2 + k_3\left\|z\right\| + k_4\left\|z\right\|^2\right)\text{sgn}\left(e_2\right)\right). \tag{4–8}$$

4.2 Stability Analysis

Let $V_L : \mathbb{R}^2 \to \mathbb{R}$ denote a continuously differentiable, positive definite, radially unbounded, common Lyapunov-like function defined as

$$V_L\left(z\left(t\right)\right) \triangleq \frac{1}{2} z^T\left(t\right) W\left(q\left(t\right)\right) z\left(t\right), \tag{4–9}$$

where the positive definite matrix $W : \mathcal{Q} \to \mathbb{R}^{2\times 2}$ is defined as

$$W \triangleq \begin{bmatrix} 1 & 0 \\ 0 & M \end{bmatrix}. \tag{4–10}$$

V_L satisfies the following inequalities:

$$\lambda_1\left\|z\right\|^2 \leq V_L \leq \lambda_2\left\|z\right\|^2, \tag{4–11}$$

where $\lambda_1,\ \lambda_2 \in \mathbb{R}_{>0}$ are known constants defined as

$$\lambda_1 \triangleq \min\left\{\frac{1}{2},\ \frac{1}{2}\underline{M}\right\}, \quad \lambda_2 \triangleq \max\left\{\frac{1}{2},\ \frac{1}{2}\overline{M}\right\}.$$

Theorem 4.1. *For $q \in \mathcal{Q}_c$, the tracking error is bounded by an exponentially decaying envelope given by*

$$\left\|z\left(t\right)\right\| \leq \sqrt{\frac{\lambda_2}{\lambda_1}}\left\|z\left(t_n^{on}\right)\right\| \exp\left(-\frac{\gamma_1}{2\lambda_2}\left(t - t_n^{on}\right)\right), \tag{4–12}$$

for all $t \in \left[t_n^{on},\ t_n^{off}\right)$ and for all n, where $\gamma_1 \in \mathbb{R}_{>0}$ is defined as

$$\gamma_1 \triangleq \min\left\{\alpha - \frac{1}{2},\ k_1 \min\left(k_m\right)\underline{B} - \frac{1}{2}\right\}, \tag{4–13}$$

provided the following gain conditions are satisfied:

$$\alpha > \tfrac{1}{2}, \quad k_1 > \tfrac{1}{2}\left(\textit{min}\left(k_m\right)\underline{B}\right)^{-1}, \quad k_2 \geq c_1\left(\textit{min}\left(k_m\right)\underline{B}\right)^{-1},$$
$$k_3 \geq c_2\left(\textit{min}\left(k_m\right)\underline{B}\right)^{-1}, \quad k_4 \geq c_3\left(\textit{min}\left(k_m\right)\underline{B}\right)^{-1}. \tag{4–14}$$

Proof. Let $z\left(t\right)$ for $t \in \left[t_n^{on},\, t_n^{off}\right)$ be a Filippov solution to the differential inclusion $\dot{z}\left(t\right) \in K\left[h\right]\left(z\left(t\right)\right)$, where $K\left[\cdot\right]$ is defined as in [43] and where $h : \mathbb{R}^2 \to \mathbb{R}^2$ is defined by (4–2) and (3–6) as

$$h \triangleq \begin{bmatrix} \dot{e}_1 \\ \dot{e}_2 \end{bmatrix} = \begin{bmatrix} e_2 - \alpha e_1 \\ M^{-1}\left(\chi - Ve_2 - B_{FES}\left(k_1 e_2 + \left(k_2 + k_3\left\|z\right\| + k_4\left\|z\right\|^2\right)\textsf{sgn}\left(e_2\right)\right)\right) \end{bmatrix}. \tag{4–15}$$

The time derivative of (4–9) exists almost everywhere (a.e.), i.e., for almost all $t \in \left[t_n^{on},\, t_n^{off}\right)$, and $\dot{V}_L \overset{a.e.}{\in} \dot{\tilde{V}}_L$, where $\dot{\tilde{V}}_L$ is the generalized time derivative of (4–9) along the Filippov trajectories of $\dot{z} \in h\left(z\right)$ and is defined as [44]

$$\dot{\tilde{V}}_L \triangleq \bigcap_{\xi \in \partial V_L} \xi^T K \begin{bmatrix} h \\ 1 \end{bmatrix},$$

where ∂V_L is the generalized gradient of V_L. Since V_L is continuously differentiable in z, $\partial V_L = \left\{\nabla V_L\right\}$; thus,

$$\dot{\tilde{V}}_L \subseteq \begin{bmatrix} z^T W \\ \frac{1}{2} z^T \dot{W} z \end{bmatrix}^T K \begin{bmatrix} h \\ 1 \end{bmatrix}.$$

Using the calculus of $K\left[\cdot\right]$ from [44], substituting (4–15), and using (4–10) to simplify the resulting expression yields

$$\begin{aligned} \dot{\tilde{V}}_L \;\subseteq\; & -\alpha e_1^2 + e_1 e_2 + \chi e_2 + \frac{1}{2}\left(\dot{M} - V\right)e_2^2 - K\left[B_{FES}\right]\left(k_1 e_2^2\right) \\ & - \left(k_2 + k_3\left\|z\right\| + k_4\left\|z\right\|^2\right) K\left[B_{FES} \cdot \textsf{sgn}\right]\left(e_2\right) e_2. \end{aligned} \tag{4–16}$$

The expression in (4–16) is evaluated between instants where B_{FES} switches to prove that V_L is a common Lyapunov function in the controlled regions. In other words,

consider $q \in \mathcal{Q}_m$ for an arbitrary $m \in \mathcal{M}$, where B_{FES} is continuous and nonzero, so that (4–16) can be expressed as

$$\begin{aligned} \dot{\tilde{V}}_L &\subseteq -\alpha e_1^2 + e_1 e_2 + \chi e_2 + \frac{1}{2}\left(\dot{M} - V\right) e_2^2 - B_{FES}\left(k_1 e_2^2\right) \\ &\quad - \left(k_2 + k_3 \|z\| + k_4 \|z\|^2\right) B_{FES} \cdot \mathrm{SGN}\left(e_2\right) e_2, \end{aligned} \tag{4–17}$$

where $K\left[B_{FES} \cdot \mathrm{sgn}\right](e_2) = B_{FES} \cdot \mathrm{SGN}\left(e_2\right)$. Using Property 13 allows (4–17) to be rewritten as

$$\begin{aligned} \dot{\tilde{V}}_L &\subseteq -\alpha e_1^2 + e_1 e_2 + \chi e_2 - B_{FES}\left(k_1 e_2^2\right) \\ &\quad - \left(k_2 + k_3 \|z\| + k_4 \|z\|^2\right) B_{FES} \cdot \mathrm{SGN}\left(e_2\right) e_2. \end{aligned} \tag{4–18}$$

Since $\dot{V}_L \overset{a.e.}{\in} \dot{\tilde{V}}_L$, (4–18) can be used to demonstrate that

$$\begin{aligned} \dot{V}_L &\overset{a.e.}{=} -\alpha e_1^2 + e_1 e_2 + \chi e_2 - B_{FES}\left(k_1 e_2^2\right) \\ &\quad - B_{FES}\left(k_2 + k_3 \|z\| + k_4 \|z\|^2\right) |e_2|, \end{aligned} \tag{4–19}$$

where $\mathrm{SGN}\left(e_2\right) e_2$ was replaced with $|e_2|$ since $\mathrm{SGN}\left(e_2\right)$ is only set-valued for $e_2 = 0$. By using Young's inequality, Property 11, and (3–4), (4–19) can be upper bounded as

$$\begin{aligned} \dot{V}_L &\overset{a.e.}{\leq} -\left(\alpha - \frac{1}{2}\right) e_1^2 - \left(k_1 \underline{m}\left(k_m\right) \underline{B} - \frac{1}{2}\right) e_2^2 - \left(k_2 \underline{m}\left(k_m\right) \underline{B} - c_1\right) |e_2| \\ &\quad - \left(k_3 \underline{m}\left(k_m\right) \underline{B} - c_2\right) \|z\| \, |e_2| - \left(k_4 \underline{m}\left(k_m\right) \underline{B} - c_3\right) \|z\|^2 |e_2|. \end{aligned} \tag{4–20}$$

From (11), it can be demonstrated that the inequality in (4–20) holds for all subsets $\mathcal{Q}_m$ of the controlled region $\mathcal{Q}_c$, so it can be concluded that V_L is a common Lyapunov function in the controlled region. Provided the gain conditions in (4–14) are satisfied, (4–11) can be used to rewrite (4–20) as

$$\dot{V}_L \overset{a.e.}{\leq} -\frac{\gamma_1}{\lambda_2} V_L, \tag{4–21}$$

where γ_1 was defined in (4–13). The inequality in (4–21) can be rewritten as

$$\exp\left(\frac{\gamma_1}{\lambda_2}\left(t-t_n^{on}\right)\right)\left(\dot{V}_L+\frac{\gamma_1}{\lambda_2}V_L\right)\overset{a.e.}{\leq}0,$$

which is equivalent to the following expression:

$$\frac{d}{dt}\left(V_L\exp\left(\frac{\gamma_1}{\lambda_2}\left(t-t_n^{on}\right)\right)\right)\overset{a.e.}{\leq}0. \tag{4–22}$$

Taking the Lebesgue integral of (4–22) and recognizing that the integrand on the left-hand side is absolutely continuous allows the Fundamental Theorem of Calculus to be used to yield

$$V_L\left(z\left(t\right)\right)\leq V_L\left(z\left(t_n^{on}\right)\right)\exp\left(-\frac{\gamma_1}{\lambda_2}\left(t-t_n^{on}\right)\right), \tag{4–23}$$

for all $t\in\left[t_n^{on},\,t_n^{off}\right)$ and for all n. Using (4–11) to rewrite (4–23) and performing some algebraic manipulation yields (4–12). □

Remark 4.1. Theorem 4.1 guarantees that desired crank trajectories can be tracked with exponential convergence, provided that the crank angle does not exit the controlled region. Thus, if the controlled regions and desired trajectories are designed appropriately, the controller in (4–7) yields exponential tracking of the desired trajectories for all time. If the crank position exits the controlled region, the system becomes uncontrolled and the following theorem details the resulting error system behavior.

Theorem 4.2. *For $q\in\mathcal{Q}_u$, the tracking error can be bounded as follows:*

$$\left\|z\left(t\right)\right\| \;\leq\; \frac{1}{\sqrt{\lambda_1}}\tan\left(3\gamma_2\left(t-t_n^{off}\right)+\tan^{-1}\left(\lambda_2\left\|z\left(t_n^{off}\right)\right\|^2\right)\right)^{\frac{1}{2}}, \tag{4–24}$$

for all $t\in\left[t_n^{off},\,t_{n+1}^{on}\right)$ and for all n, where $\gamma_2\in\mathbb{R}_{>0}$ is a known constant defined as

$$\gamma_2\triangleq\max\left\{c_3\left(\frac{1}{\lambda_1}\right)^{\frac{3}{2}},\;\left(c_2+\frac{1}{2}\right)\left(\frac{1}{\lambda_1}\right),\;c_1\left(\frac{1}{\lambda_1}\right)^{\frac{1}{2}}\right\}, \tag{4–25}$$

provided the reverse dwell-time $\Delta t_n^{off}\triangleq t_{n+1}^{on}-t_n^{off}$ is sufficiently small such that

$$\Delta t_n^{off}<\frac{\pi}{6\gamma_2}, \tag{4–26}$$

for all n, and provided γ_1, defined in (4–13), is sufficiently large such that

$$\gamma_1 > \frac{\lambda_2}{\Delta t_n^{on}} \ln\left(V_L\left(t_n^{on}\right) \tan\left(3\gamma_2 \Delta t_n^{off}\right)\right), \tag{4–27}$$

for all n, where $\Delta t_n^{on} \triangleq t_n^{off} - t_n^{on}$.

Proof. The time derivative of (3–7) for $t \in \left[t_n^{off},\ t_{n+1}^{on}\right)$ can be expressed using (4–2), (3–6), Property 11, and Property 13 as

$$\dot{V}_L = -\alpha e_1^2 + e_1 e_2 + \chi e_2. \tag{4–28}$$

Young's inequality, (3–4), and (4–6) allow (4–28) to be upper bounded as

$$\dot{V}_L \leq c_3 \|z\|^3 + \left(c_2 + \frac{1}{2}\right)\|z\|^2 + c_1 \|z\|. \tag{4–29}$$

Using (3–8), (4–29) can be upper bounded as

$$\dot{V}_L \leq c_3 \left(\frac{1}{\lambda_1} V_L\right)^{\frac{3}{2}} + \left(c_2 + \frac{1}{2}\right)\left(\frac{1}{\lambda_1} V_L\right) + c_1 \left(\frac{1}{\lambda_1} V_L\right)^{\frac{1}{2}}. \tag{4–30}$$

To simplify the resulting expression, (4–30) can be upper bounded as

$$\dot{V}_L \leq 3\gamma_2 \left(V_L^2 + 1\right), \tag{4–31}$$

where γ_2 was defined in (4–25). Utilizing (4–31) and the Comparison Lemma in [49], the following upper bound on V_L in the uncontrolled region can be found:

$$V_L\left(z\left(t\right)\right) \leq \tan\left(3\gamma_2\left(t - t_n^{off}\right) + \tan^{-1}\left(V_L\left(z\left(t_n^{off}\right)\right)\right)\right), \tag{4–32}$$

for all $t \in \left[t_n^{off},\ t_{n+1}^{on}\right)$ and for all n. The bound in (4–32) exhibits finite escape time and therefore is only valid if the argument of $\tan\left(\cdot\right)$ in (4–32) lies on the interval $\left[0,\ \frac{\pi}{2}\right)$, i.e.,

$$3\gamma_2\left(t - t_n^{off}\right) + \tan^{-1}\left(V_L\left(z\left(t_n^{off}\right)\right)\right) < \frac{\pi}{2}. \tag{4–33}$$

Using (3–20), it can be demonstrated that (4–27) is a sufficient condition for (4–33). Also, (4–26) is sufficient to ensure that (4–27) can be satisfied. Finally, using (3–8) to rewrite (4–32) and performing some algebraic manipulation yields (4–24). □

Remark 4.2. The bound in (4–32) has a finite escape time, so V_L may become unbounded unless the reverse dwell-time condition in (4–26) is satisfied. The following assumption and subsequent remark detail how the reverse dwell-time condition may be satisfied.

Assumption 4. The time spent in the n^{th} controlled region $\Delta t_n^{on} \triangleq t_n^{off} - t_n^{on}$ has a known, constant lower bound $\Delta t_{min}^{on} \in \mathbb{R}_{>0}$ such that

$$\min_n \Delta t_n^{on} \geq \Delta t_{min}^{on} > 0.$$

Likewise, the time spent in the n^{th} uncontrolled region Δt_n^{off} has a known, constant upper bound $\Delta t_{max}^{off} \in \mathbb{R}_{>0}$ that satisfies $\max_n \Delta t_n^{off} \leq \Delta t_{max}^{off}$ and (4–26) for all n, i.e.,

$$\Delta t_{max}^{off} < \frac{\pi}{6\gamma_2}. \tag{4–34}$$

Remark 4.3. Assumption 4 can be validated through appropriate design of the desired crank velocity $\dot{q}_d$. First consider Δt_{min}^{on}. The time spent in the n^{th} controlled region Δt_n^{on} can be described using the Mean Value Theorem as

$$\Delta t_n^{on} = \frac{\Delta q_n^{on}}{\dot{q}_{avg,n}^{on}}, \tag{4–35}$$

where $\Delta q_n^{on} \triangleq q\left(t_n^{off}\right) - q\left(t_n^{on}\right)$ is the length of the n^{th} controlled region, which is constant for all $n \geq 1$ in this development and is smallest for $n = 0$, and $\dot{q}_{avg,n}^{on} \in \mathbb{R}$ is the average crank velocity through the n^{th} controlled region. Using (4–1) and (4–2) and assuming $\dot{e}_1 < 0$, $\dot{q}$ can be upper bounded as

$$\dot{q} \leq \dot{q}_d + (1+\alpha)\|z\|. \tag{4–36}$$

Using the fact that $\|z\|$ monotonically decreases in the controlled regions together with (4–11) and (4–36) allows the average crank velocity $\dot{q}_{avg,n}^{on}$ to be upper bounded as

$$\dot{q}_{avg,n}^{on} \leq \max_{t \in \left[t_n^{on},\, t_n^{off}\right]} \dot{q}_d(t) + (1+\alpha)\sqrt{\frac{\lambda_2}{\lambda_1}}\left\|z\left(t_n^{on}\right)\right\|. \tag{4–37}$$

Therefore, (4–35) can be lower bounded using (4–37) as

$$\Delta t_n^{on} \geq \frac{\Delta q_n^{on}}{\max\limits_{t \in \left[t_n^{on},\, t_n^{off}\right]} \dot{q}_d(t) + (1+\alpha)\left\|z\left(t_n^{on}\right)\right\|}. \tag{4–38}$$

Suppose now that a desired Δt_{min}^{on} was specified. Then the right-hand side of (4–38) would need to be greater than or equal to the selected Δt_{min}^{on}, i.e.,

$$\frac{\Delta q_n^{on}}{\max\limits_{t \in \left[t_n^{on},\, t_n^{off}\right]} \dot{q}_d(t) + (1+\alpha)\left\|z\left(t_n^{on}\right)\right\|} \geq \Delta t_{min}^{on},$$

which can be rewritten as follows:

$$\max_{t \in \left[t_n^{on},\, t_n^{off}\right]} \dot{q}_d(t) \leq \frac{\Delta q_n^{on}}{\Delta t_{min}^{on}} - (1+\alpha)\left\|z\left(t_n^{on}\right)\right\|. \tag{4–39}$$

From (4–39) an upper bound on the desired velocity at each on-time is given which guarantees that on-duration Δt_n^{on} is greater than a specified minimum on-duration Δt_{min}^{on}. Therefore, designing the desired velocity to satisfy (4–39) for all n is sufficient to validate the first part of Assumption 4.

Now consider Δt_{max}^{off}. The crank's entrance into the uncontrolled region can be likened to a ballistic event, where the crank is carried by the controller to $q\left(t_n^{off}\right)$ and released with initial velocity $\dot{q}\left(t_n^{off}\right)$. In that sense, specifying a desired Δt_{max}^{off} is equivalent to requiring the crank to ballistically (i.e., only under the influence of passive dynamics) traverse the length of the uncontrolled region, Δq_n^{off}, in a sufficiently short amount of time. Since the only controllable factors affecting the behavior of the crank in the uncontrolled region are the initial conditions, of which $q\left(t_n^{off}\right)$ is predetermined by selection of ε_m, then only the initial velocity $\dot{q}\left(t_n^{off}\right)$ can be used to guarantee that

the total time spent in the n^{th} uncontrolled region is less than Δt_{max}^{off}. If it is reasonably assumed that $\Delta t_n^{off} \propto \dot{q}\left(t_n^{off}\right)^{-1}$, then it can be assumed that there exists a sufficiently large initial velocity – a critical velocity $\dot{q}^{crit} \in \mathbb{R}_{>0}$ – which guarantees $\Delta t_n^{off} \leq \Delta t_{max}^{off} < \frac{\pi}{6\gamma_2}$. More specifically, suppose there exists $\dot{q}^{crit}$ such that

$$\dot{q}\left(t_n^{off}\right) \geq \dot{q}^{crit} \Rightarrow \Delta t_n^{off} \leq \Delta t_{max}^{off} < \frac{\pi}{6\gamma_2}. \tag{4–40}$$

Using (4–1) and (4–2) and assuming $\dot{e}_1 > 0$, $\dot{q}\left(t_n^{off}\right)$ can be lower bounded as

$$\dot{q}\left(t_n^{off}\right) \geq \dot{q}_d\left(t_n^{off}\right) - (1+\alpha)\left\|z\left(t_n^{off}\right)\right\|. \tag{4–41}$$

Then, combining (4–40) and (4–41), the following sufficient condition for the desired crank velocity at the n^{th} off-time which guarantees (4–40) can be developed:

$$\dot{q}_d\left(t_n^{off}\right) \geq \dot{q}^{crit} + (1+\alpha)\left\|z\left(t_n^{off}\right)\right\|. \tag{4–42}$$

Furthermore, (4–12) can be used to obtain a sufficient condition for (4–42) in terms of the initial conditions of each cycle as

$$\dot{q}_d\left(t_n^{off}\right) \geq \dot{q}^{crit} + (1+\alpha)\sqrt{\frac{\lambda_2}{\lambda_1}}\left\|z\left(t_n^{on}\right)\right\| \exp\left(-\frac{\gamma_1}{2\lambda_2}\Delta t_{min}^{on}\right). \tag{4–43}$$

Note that increasing γ_1 via selection of α and k_1 relaxes (4–43) to a limit where only $\dot{q}_d\left(t_n^{off}\right) \geq \dot{q}^{crit}$ is required.

Therefore, satisfaction of both (4–39) and (4–43) for all n is sufficient to validate Assumption 4. However, (4–43) depends on knowledge of $\dot{q}^{crit}$, leading to the following additional assumption.

Assumption 5. The critical velocity $\dot{q}^{crit}$ is known a priori for all n. This assumption is mild in the sense that the critical velocity can be experimentally determined for an individual system configuration or numerically calculated for a wide range of individual or cycle configurations.

Theorem 4.3. *The tracking error is ultimately bounded in the sense that, as the number of crank cycles approaches infinity (i.e., as $n \to \infty$), $\|z(t)\|$ converges to a ball with constant radius $d \in \mathbb{R}_{>0}$, defined as*

$$d \triangleq \sqrt{\frac{1 - B - \sqrt{(1-B)^2 - 4A^2B}}{2AB\lambda_1}} \tag{4–44}$$

where $A,\ B \in \mathbb{R}_{\geq 0}$ are constants defined as

$$A \triangleq \tan\left(3\gamma_2 \Delta t_{max}^{off}\right), \quad B \triangleq \exp\left(-\frac{\gamma_1}{2\lambda_2}\Delta t_{min}^{on}\right),$$

provided Assumption 4 holds and the following conditions are satisfied:

$$\|z(t_0^{on})\| < \sqrt{\frac{1 - B + \sqrt{(1-B)^2 - 4A^2B}}{2AB\lambda_2}}, \tag{4–45}$$

$$A < \frac{1-B}{2\sqrt{B}}. \tag{4–46}$$

Proof. Assuming the worst case scenario where $\Delta t_n^{on} = \Delta t_{min}^{on}$ and $\Delta t_n^{off} = \Delta t_{max}^{off}$ for all n, (3–20) and (3–26) can be used to write

$$V_L\left(z\left(t_n^{off}\right)\right) \leq V_L\left(z\left(t_n^{on}\right)\right) \exp\left(-\frac{\gamma_1}{2\lambda_2}\Delta t_{min}^{on}\right), \tag{4–47}$$

$$V_L\left(z\left(t_{n+1}^{on}\right)\right) \leq \tan\left(3\gamma_2 \Delta t_{max}^{off} + \tan^{-1}\left(V_L\left(z\left(t_n^{on}\right)\right) \exp\left(-\frac{\gamma_1}{2\lambda_2}\Delta t_{min}^{on}\right)\right)\right), \tag{4–48}$$

provided

$$0 < 3\gamma_2 \Delta t_{max}^{off} + \tan^{-1}\left(V_L\left(z\left(t_n^{on}\right)\right) \exp\left(-\frac{\gamma_1}{2\lambda_2}\Delta t_{min}^{on}\right)\right) < \frac{\pi}{2},$$

which is sufficiently satisfied by (4–34) and

$$ABV_L\left(z\left(t_n^{on}\right)\right) < 1. \tag{4–49}$$

Then, the sequence of switching points $\{V\left(z\left(t_n^{on}\right)\right) \in \mathbb{R}_{\geq 0}\}_{n=0}^{N}$, for $N \in \{0,\ 1,\ 2,\ ...\}$, can be upper bounded as

$$\left\{V_L\left(z\left(t_n^{on}\right)\right)\right\} \leq \{x_n\},$$

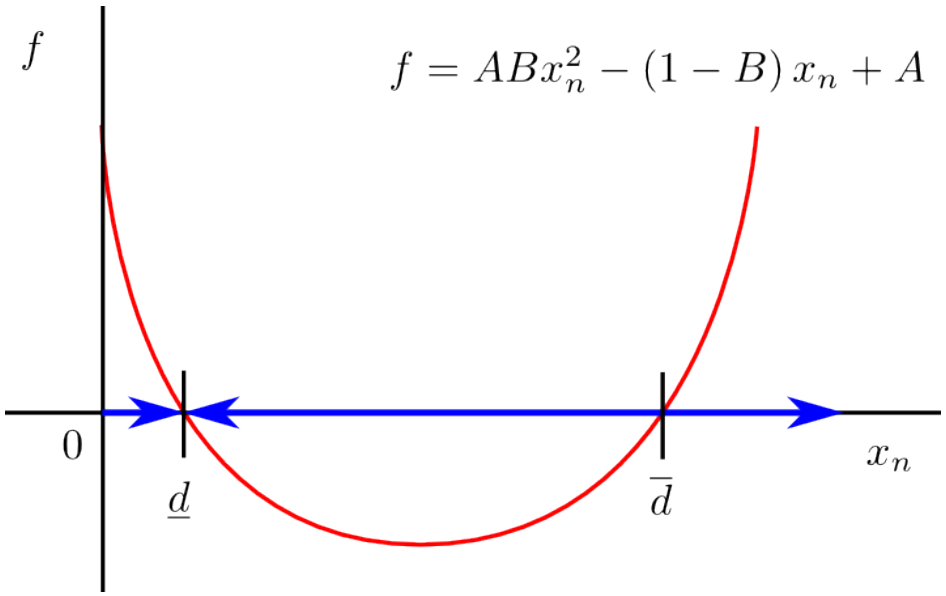

Figure 4-1. Illustration of convergence behavior of the bounding sequence.

where the sequence $\{x_n \in \mathbb{R}_{\geq 0}\}_{n=0}^{N}$, for $N \in \{0,\ 1,\ 2,\ ...\}$, is defined such that

$$x_0 \triangleq V_L\left(z\left(t_0^{on}\right)\right), \quad x_{n+1} = \frac{A + Bx_n}{1 - ABx_n}.$$

The sequence $\{x_n\}$ converges if it is positive, bounded, and monotonic. For a decaying convergence, it can be demonstrated that the following condition is sufficient to satisfy $x_{n+1} \leq x_n$:

$$ABx_n^2 - (1-B)\,x_n + A \leq 0. \tag{4–50}$$

The inequality in (4–50) is satisfied for the range of x_n for which a concave upward parabola defined by $f\left(x_n\right) = ABx_n^2 - (1-B)\,x_n + A$ is non-positive, i.e., for x_n such that

$$\underline{d} \leq x_n \leq \overline{d},$$

where the bounds $\underline{d},\ \overline{d} \in \mathbb{R}_{>0}$ are defined as

$$\underline{d} \triangleq \frac{1 - B - \sqrt{(1-B)^2 - 4A^2B}}{2AB}, \tag{4–51}$$

$$\overline{d} \triangleq \frac{1 - B + \sqrt{(1-B)^2 - 4A^2B}}{2AB}. \tag{4–52}$$

The polynomial roots in (4–51) and (4–52) are real and distinct if (4–46) is satisfied. Therefore, provided (4–34), (4–49), and (4–46) are satisfied, and given that $\underline{d} \leq x_0 \leq \overline{d}$, then the sequence $\{x_n\}$ has a limit that can be calculated as

$$\lim_{n\to\infty} x_{n+1} = \begin{cases} \overline{d} & \text{if } x_0 = \overline{d} \\ \\ \underline{d} & \text{if } \underline{d} \leq x_0 < \overline{d} \end{cases}.$$

In addition, it can be demonstrated that, given any $x_n < \underline{d}$, it is guaranteed that $x_{n+1} \leq \underline{d}$. The behavior of the sequence $\{x_n\}$ is illustrated in Fig. 4-1.

Finally, it has been demonstrated that $\{x_n\} \to \overline{d}$ if $x_0 = \overline{d}$, and $\{x_n\} \to \underline{d}$ if $x_0 < \overline{d}$, provided (4–34), (4–49), and (4–46) are satisfied. Since the sequence of switching points $\{V_L(z(t_n^{on}))\}$ is upper bounded by $\{x_n\}$, then it can be concluded that $\{V_L(z(t_n^{on}))\} \to L_V$, where the limit $L_V \in \mathbb{R}_{>0}$ can be upper bounded as

$$L_V \leq \begin{cases} \overline{d} & \text{if } V_L(z(t_0^{on})) = \overline{d} \\ \\ \underline{d} & \text{if } V_L(z(t_0^{on})) < \overline{d} \end{cases}.$$

Using (4–11), it can then be demonstrated that $\|z\|$ converges to a ball with constant radius d, defined in (4–44), as $n \to \infty$, provided (4–45), (4–34), and (4–46) are satisfied, noting that (4–45) is a sufficient condition for (4–49). □

Remark 4.4. The condition in (4–46) can be rewritten as

$$\tan\left(3\gamma_2 \Delta t_{max}^{off}\right) < \sinh\left(\frac{\gamma_1}{2\lambda_2}\Delta t_{min}^{on}\right), \tag{4–53}$$

which could lead to another reverse dwell-time condition, gain condition on γ_1, or dwell-time condition on Δt_{min}^{on}, depending on the approach. Consider a reverse dwell-time approach, so that (4–53) can be rewritten as

$$\Delta t_{max}^{off} < \frac{1}{3\gamma_2}\tan^{-1}\left(\sinh\left(\frac{\gamma_1}{2\lambda_2}\Delta t_{min}^{on}\right)\right). \tag{4–54}$$

Table 4-1. Experimental protocols used.

Protocol	ε^{s}_{quad}
A	$0.5T^{max}_{*Knee}$
B	$0.7T^{max}_{*Knee}$
C	$0.9T^{max}_{*Knee}$

The right-hand side of (4–54) is upper-bounded by $\frac{\pi}{6\gamma_2}$, so that (4–54) is a sufficient condition for (4–34).

4.3 Experiments

Five able-bodied subjects age 25-42 years participated in this chapter's experiments. Subject recruitment, the FES-cycling test bed, and the experimental setup were the same in this chapter as in Chapter 3, with the exception that only the quadriceps femoris muscle groups were stimulated in these experiments.

4.3.1 Methods

The goal of these experiments was to demonstrate the tracking performance and robustness of the controller in (3–5) and to compare the effect of ε_{*Quad} on the control input and performance. For each trial, ε_{*Quad} was chosen randomly from Table 4-1, where $T^{max}_{*Knee} \triangleq \max_{q\in\mathcal{Q}} T_{*Knee}(q)$ was the maximum value of the subject's torque transfer ratio. The protocols used for each subject and trial are tabulated in 4-2, and the stimulation regions used for Subject 4 are illustrated in 4-2.

Prior to the trials was a two minute warm-up period, during which the subject was shown a graph of the desired crank velocity on a computer screen along with the measured crank velocity. Each subject was asked to track the desired crank velocity to the best of their ability. This pre-trial provided a measure of volitional cycling ability, which was used as a performance benchmark.

During each FES-cycling trial, the subjects were instructed to relax and were not shown the computer screen, and at least five minutes of rest was allotted between each trial to mitigate the effects of fatigue. Stimulation was conducted at a frequency of

Table 4-2. T^{max}_{*Knee} for each subject, protocol, and corresponding ε_{*Quad} used for each trial.

Subject	T^{max}_{*Knee}	Trial	Protocol	ε_{*Quad}
		1	B	0.34
1	0.49	2	A	0.25
		3	C	0.44
		1	A	0.27
2	0.55	2	B	0.38
		3	C	0.49
		1	B	0.37
3	0.53	2	C	0.47
		3	A	0.26
		1	C	0.45
4	0.50	2	B	0.35
		3	A	0.25
		1	C	0.47
5	0.52	2	B	0.36
		3	A	0.26

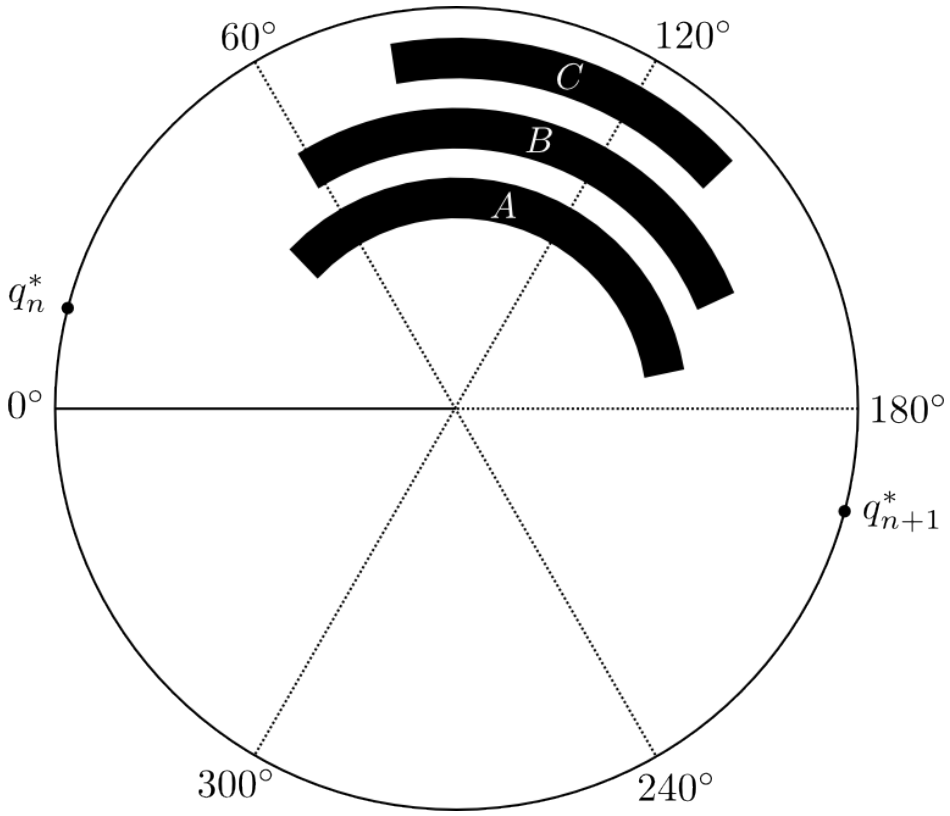

Figure 4-2. Stimulation regions used for Subject 4.

40 Hz with a constant amplitude of 100 mA and a variable pulsewidth dictated by the controller in (3–5). Trials were ended if 90 revolutions had been completed, the control input saturated at 400 microseconds, or the subject reported significant discomfort. After each FES-cycling trial, subjects were asked the following comfort rating question: "On a scale from one to ten, one being as comfortable as pedaling by yourself and ten being painful, how comfortable was the FES-induced pedaling?"

The desired crank position and velocity were given in radians and radians per second, respectively, as

$$q_d \triangleq \phi\left(t - t_0^{on}\right) - \dot{q}_d + q_0^{on}, \tag{4–55}$$

$$\dot{q}_d \triangleq \phi\left(1 - \exp\left(t_0^{on} - t\right)\right), \tag{4–56}$$

where $\phi \in \mathbb{R}_{>0}$ was a selectable constant defined as $\phi \triangleq \frac{7}{6}\pi$ radians per second. The trajectories in (4–55) and (4–56) ensured that the desired velocity started at 0 RPM and exponentially approached 35 RPM. The following control gains were found in preliminary testing and used for all subjects:

$$\alpha = 7,\ k_1 = 10,\ k_2 = 0.1,\ k_3 = 0.1,\ k_4 = 0.1,\ k_{*Quad} = 1.$$

4.3.2 Results

Fig. 4-3 depicts representative cadence tracking error, $\dot{e}_1$, and switched control input, u_{*Quad}, across the three trials for one subject (Subject 4). Fig. 4-4 presents the control input from the first trial for the same subject over the interval between 20 and 25 seconds, for the purpose of illustrating the behavior of the switched control input. Fig. 4-5 compares the position and cadence tracking errors, e_1 and $\dot{e}_1$, respectively, during FES-cycling and volitional cycling, again for Subject 4. The mean, standard deviation, and root mean square (RMS) cadence tracking error from all subjects over all trials, including the volitional warm-up, are presented in Table 4-3, along with the reported comfort scale rating for each trial.

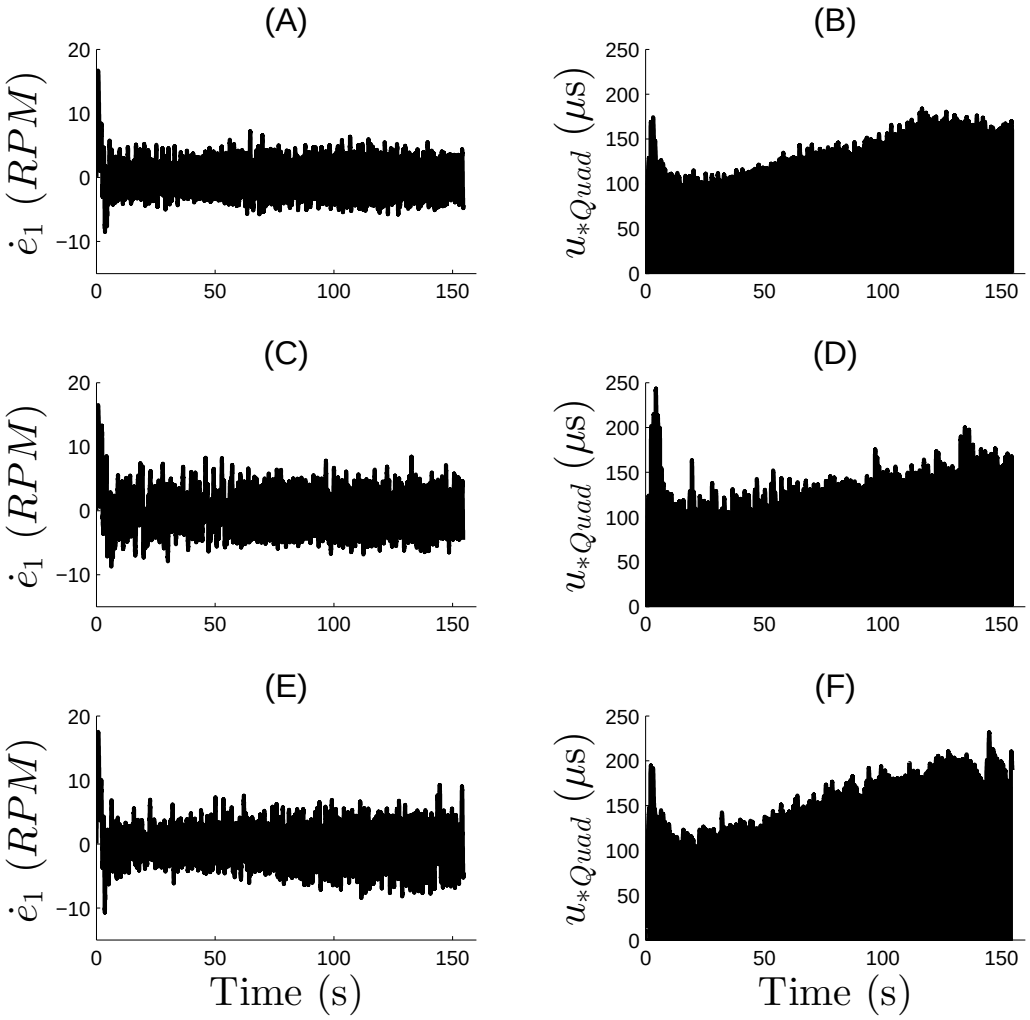

Figure 4-3. Cadence tracking error and switched control input across the three trials for Subject 4. A) Cadence error, Trial 1, Protocol C. B) Control input, Trial 1, Protocol C. C) Cadence error, Trial 2, Protocol B. D) Control input, Trial 2, Protocol B. E) Cadence error, Trial 3, Protocol A. F) Control input, Trial 3, Protocol A.

Table 4-3. Tracking performance in revolutions per minute (RPM) and comfort scale rating from all subjects over all trials

Subject	Protocol	$\dot{e}_1$ mean (RPM)	$\dot{e}_1$ standard deviation (RPM)	$\dot{e}_1$ RMS (RPM)	Comfort scale rating
1	Volitional	-0.53	2.35	2.41	1.0
	A	0.192	3.12	3.13	4.0
	B	0.122	2.66	2.66	3.0
	C	0.41	3.65	3.68	5.0
2	Volitional	-0.003	1.511	1.511	1.0
	A	0.061	1.92	1.92	2.5
	B	0.079	2.12	2.12	3.5
	C	0.48	3.02	3.06	6.0
3	Volitional	0.47	3.54	3.58	1.0
	A	0.54	4.21	4.25	4.0
	B	0.24	2.58	2.59	5.0
	C	0.24	2.39	2.40	3.0
4	Volitional	-0.58	1.830	1.92	1.0
	A	0.153	3.31	3.32	5.0
	B	0.132	3.43	3.44	4.0
	C	0.131	2.82	2.82	3.0
5	Volitional	-0.19	1.45	1.46	1.0
	A	0.25	3.16	3.17	3.0
	B	0.49	4.23	4.26	6.0
	C	0.69	4.17	4.23	7.0

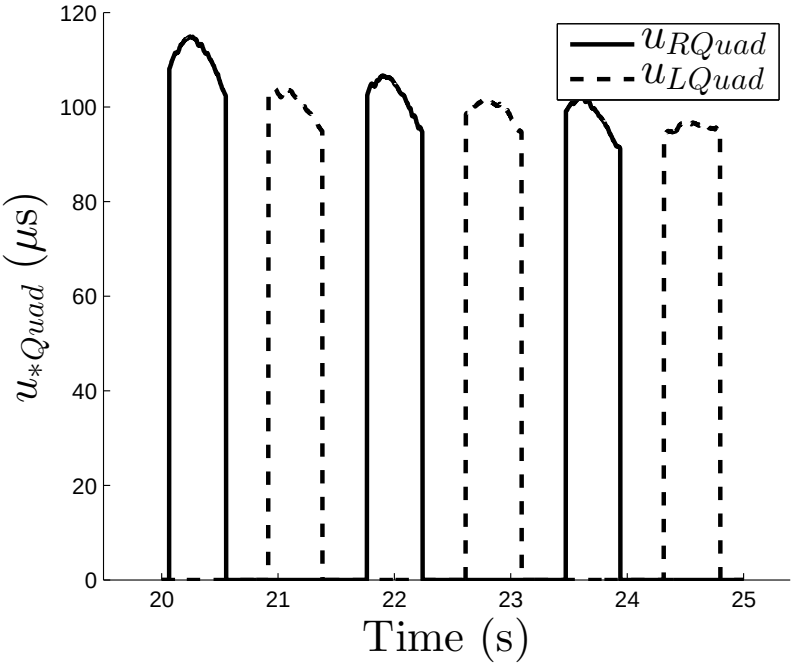

Figure 4-4. Switched control input from the first trial of Subject 4.

4.3.3 Discussion

The FES-cycling controller in (4–7) yields simultaneous crank position and cadence tracking with ultimately bounded tracking error similar to that of volitional cycling by able-bodied subjects across all three protocols and subjects, despite using the same control gains for each subject and only stimulating the quadriceps femoris muscle groups. While there is not enough data to determine statistical significance between the tracking performance of the FES-cycling and volitional trials, the same characteristics can be observed in both the FES-cycling and volitional tracking experiments. However, although both FES-cycling and volitional tracking experiments demonstrated mean tracking errors near zero RPM, the volitional tracking error had less standard deviation for all subjects except Subject 3, whose volitional tracking performance was poor when compared to that of the other subjects. Lower standard deviation in the tracking error suggests better performance due to smoothness in pedaling, which is to be expected considering that volitional cycling can make use of all the muscle groups in the lower

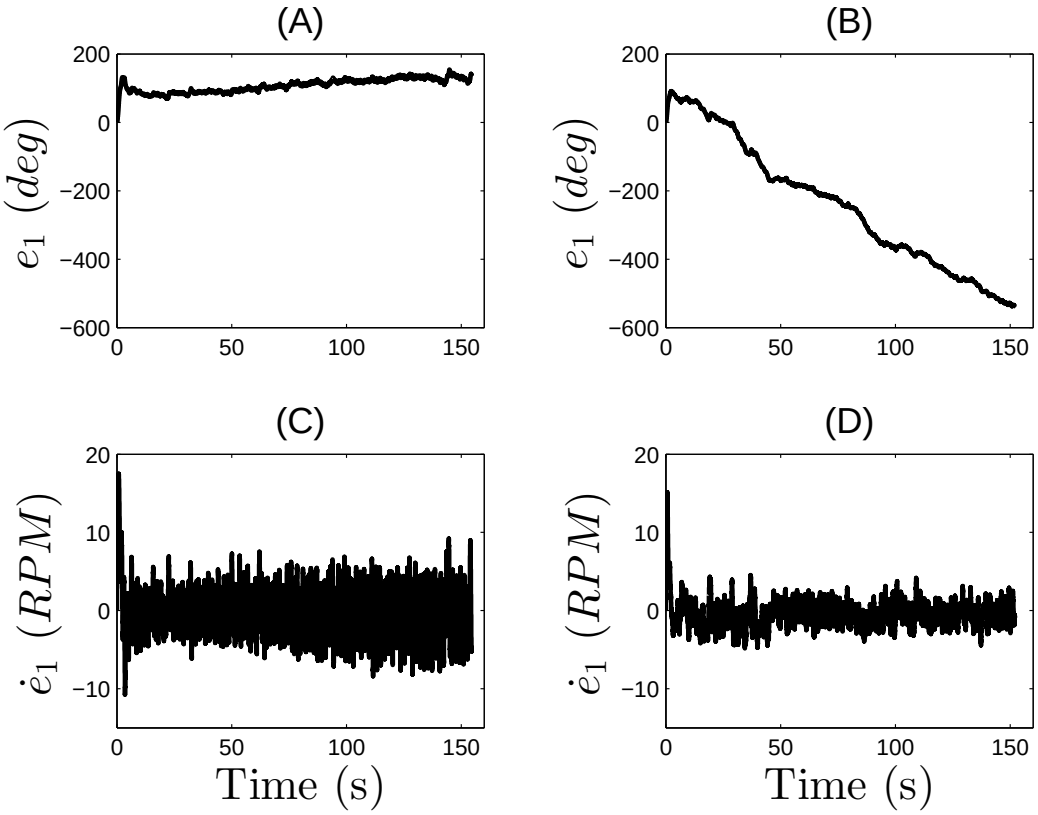

Figure 4-5. Comparison of the position and cadence tracking errors during FES-cycling and volitional cycling for Subject 4. A) FES-cycling crank position error. B) Volitional cycling crank position error. C) FES-cycling cadence error. D) Volitional cycling cadence error.

extremities, whereas these FES-cycling trials only used the quadriceps femoris muscle groups. Motivation arises, therefore, to repeat these experiments using stimulation of the hamstrings and gluteal muscle groups in addition to the quadriceps femoris. It should be noted that, while the FES-cycling trials yielded significantly reduced crank position tracking error when compared to volitional cycling, subjects were not asked to minimize the crank position tracking error during volitional cycling trials.

It was observed that the effectiveness of each protocol in minimizing the tracking error, as well as the subject's comfort during each protocol, was subject-dependent. For example, Protocol C for Subject 4 yielded the best tracking performance of the three protocols, and, perhaps as a consequence, was also reported by the subject as being the most comfortable, whereas Protocol A yielded the best tracking performance and greatest comfort for Subject 5. From Protocol A to Protocol C, the length of the stimulation region decreased, requiring an increase in stimulation intensity to make up for the decrease in stimulation duration. Some subjects appeared to tolerate higher intensities but not longer durations, making it likely that they would report Protocol C as being the most comfortable. On the other hand, some subjects preferred longer durations of lower intensity stimulation, making it likely that they would report Protocol B as being most comfortable. Regardless of the subject's preference, it was always true that the subject reported the protocol that yielded the best tracking performance as being the most comfortable, suggesting a correlation between tracking performance and subject comfort during FES-cycling. More data is needed to explore this correlation as well as the effect of the selection of ε_m on tracking performance.

When compared to the control input and tracking performance from Chapter 3, the control input in this chapter was smoother and yielded better tracking performance by reducing steady state tracking error. The controller in Chapter 3 used a sliding mode strategy with $r = \dot{q}_d - \dot{q}$ as its input, causing the control input to change signs frequently, whereas the controller in this chapter used a filtered tracking error, e_2, as the input to

the sliding mode term and so rarely did the control input change signs (only during the uncontrolled regions). It was observed that tuning α could increase or decrease the frequency of sign changes. The result was better tracking performance here than in Chapter 3, since the actual velocity could oscillate around the desired velocity without chattering.

4.4 Concluding Remarks

A common Lyapunov-like function was used to prove that the developed controller, given in (4–7), yields ultimately bounded tracking of both a desired crank position and cadence (i.e., crank velocity), provided the desired cadence, control gains, initial conditions, and stimulation pattern satisfy sufficient conditions. Experiments were conducted on five able-bodied subjects, and the results both demonstrate the robustness and stability of the developed switched controller and corroborate the theoretical relationships between the desired cadence, control gains, and stimulation pattern that were developed in the stability analysis. The experimental results suggest that there exist correlations between the size of the stimulation regions, determined by selection of ε_m, the tracking performance, and subject comfort during FES-cycling, though more data is needed to determine statistical significance. While the theoretical outcome of the stability analysis in this chapter, ultimately bounded tracking error, is the same as in Chapter 3, the controller developed in this chapter experimentally demonstrated improved tracking performance over the controller developed in Chapter 3, likely due to the addition of an integrator into the control input as well as the use of a filtered tracking error for the sliding mode control term.

The next chapter includes an electric motor to provide control effort during the uncontrolled regions, removing the constraints on the desired cadence, the initial conditions, and the stimulation pattern from Chapter 3 and this chapter, since the electric motor grants controllability of the system throughout the entire crank cycle.

CHAPTER 5
SWITCHED CONTROL OF STATIONARY CYCLING INDUCED BY FUNCTIONAL ELECTRICAL STIMULATION WITH ELECTRIC MOTOR ASSISTANCE

Building on the results in Chapters 3 and 4, which do not consider electric motor input, in this chapter, a novel strategy for electric motor assistance is developed that only provides control input in the regions around the dead points where no FES control input is provided. Based on this model, a switched, sliding-mode controller is developed for both the FES and the motor that yields global, exponentially stable tracking of a desired crank trajectory, despite the switching effects, uncertainty in the system parameters, and the presence of unknown, bounded disturbances. Experimental results with five able-bodied subjects are presented to validate the controller and to demonstrate practical application of the theoretical insights.

5.1 Switched Control Input

For motorized FES-cycling systems in a rehabilitative setting, it is preferred that the muscles exert as much work to complete the cycling task as possible to maximize therapeutic effect; therefore, motivation arises to activate the electric motor only as needed. In the present development, the human-machine effort is balanced by only activating the muscle groups where they can effectively contribute to pedaling and activating the electric motor everywhere else. In other words, the electric motor control region is defined as $\mathcal{Q}_e \triangleq \mathcal{Q} \backslash \mathcal{Q}_c$, which was defined to be the uncontrolled region $\mathcal{Q}_u$ in the previous chapters. Defining $\mathcal{Q}_e$ in this way allows (2–55) to be rewritten as

$$J_{cycle}\ddot{q}(t) + b_{cycle}\dot{q}(t) + M(q(t))\ddot{q}(t) + V(q(t), \dot{q}(t))\dot{q}(t) + G(q(t)) \\ +P(q(t), \dot{q}(t)) + d_{cycle}(t) + d_{rider}(t) = \tau_r(t) + B_\sigma(q(t), \dot{q}(t))u(t), \tag{5–1}$$

where $u \triangleq u_{FES} = u_{motor}$ and $B_\sigma : \mathcal{Q} \times \mathbb{R} \to \mathbb{R}_{>0}$ is the lumped, switched control effectiveness term defined as

$$B_\sigma \triangleq B_{FES} + B_{motor}.$$

In general, stimulation of six muscle groups allows for $2^6 = 64$ possible combinations of active muscle groups, including the empty set (i.e., the region where no stimulation is applied). The definitions in (2–50)-(2–54) introduce constraints that permit at most 28 different subsystems (i.e., B_σ may switch up to 28 times over a crank cycle), so that an auxiliary switching signal can be defined as $\sigma \in \mathcal{P} \triangleq \{1,\ 2,\ 3,\ ...,\ 28\}$, where the first 27 subsystems represent some combination of active muscle groups and the 28^{th} represents only electric motor activation. The switching signal σ specifies the index of B_σ and switches according to the crank position. For example, if only the right and left quadriceps femoris muscle groups were stimulated according to (2–51) and the electric motor was activated elsewhere, there would be only three subsystems, and σ would be defined as

$$\sigma \triangleq \begin{cases} 1 & \text{if } q \in \mathcal{Q}_{RQuad} \\ 2 & \text{if } q \in \mathcal{Q}_{LQuad} \\ 3 & \text{if } q \in \mathcal{Q}_e. \end{cases}$$

The switched control effectiveness B_σ has the following property.

Property 14. $\underline{B}_\sigma \leq B_\sigma \leq \overline{B}_\sigma, \forall \sigma \in \mathcal{P}$, where $\underline{B}_\sigma,\ \overline{B}_\sigma \in \mathbb{R}_{>0}$ are known constants.

In this development, the known sequence of switching states, which are the limit points of $\mathcal{Q}_m$, for all $m \in \mathcal{M}$, is defined as $\left\{q_n \in \mathcal{Q}\right\}_{n=0}^{\infty}$, and the corresponding sequence of unknown switching times $\left\{t_n \in \mathbb{R}_{\geq 0}\right\}_{n=0}^{\infty}$ is defined such that each t_n denotes the instant when q reaches the corresponding switching state q_n. The switching signal σ is assumed to be continuous from the right (i.e., $\sigma(q) = \lim_{q \to q_n^+} \sigma(q)$).

5.2 Control Development

In this development, the cycle inertia J_{cycle} is lumped together with the rider inertia M (i.e., here $M \triangleq M + J_{cycle}$).

5.2.1 Open-Loop Error System

As in Chapter 4, the control objective is to track a desired crank trajectory with performance quantified by the tracking error signals $e_1,\ e_2\ :\ \mathbb{R}_{\geq 0} \to \mathbb{R}$, defined as

$$e_1(t) \triangleq q_d(t) - q(t), \tag{5–2}$$

$$e_2(t) \triangleq \dot{e}_1(t) + \alpha e_1(t), \tag{5–3}$$

where $q_d\ :\ \mathbb{R}_{\geq 0} \to \mathbb{R}$ is the desired crank position, designed so that its derivatives exist and $|\dot{q}_d| \leq c_{d1},\ |\ddot{q}_d| \leq c_{d2}$, where $c_{d1},\ c_{d2} \in \mathbb{R}_{>0}$ are known constants, and $\alpha \in \mathbb{R}_{>0}$ is a selectable constant. Without loss of generality, q_d is designed to monotonically increase, i.e., backpedaling is not desired. Taking the time derivative of (5–3), multiplying by M, and using (5–1)-(5–3) yields

$$\begin{aligned} M(q(t))\,\dot{e}_2(t) &= \chi(q(t),\ \dot{q}(t),\ t) - e_1(t) \\ &\quad -V(q(t),\ \dot{q}(t))\,e_2(t) - B_\sigma(q(t),\ \dot{q}(t))\,u(t), \end{aligned} \tag{5–4}$$

where the auxiliary term $\chi\ :\ \mathcal{Q} \times \mathbb{R} \times \mathbb{R}_{\geq 0} \to \mathbb{R}$ is defined as

$$\begin{aligned} \chi \triangleq\ & M(q(t))\,(\ddot{q}_d(t) + \alpha\dot{e}_1(t)) + V(q(t),\ \dot{q}(t))\,(\dot{q}_d(t) + \alpha e_1(t)) \\ & + G(q(t)) + P(q(t),\ \dot{q}(t)) + b_{cycle}\dot{q}(t) + d_{cycle}(t) + d_{rider}(t) \\ & + e_1(t) - \tau_r(t). \end{aligned} \tag{5–5}$$

Based on Assumption 1 and Properties 5-12, χ can be bounded as

$$|\chi(q(t),\ \dot{q}(t),\ t)| \leq c_1 + c_2\|z(t)\| + c_3\|z(t)\|^2, \tag{5–6}$$

where $c_1,\ c_2,\ c_3 \in \mathbb{R}_{>0}$ are known constants defined as

$$\begin{aligned} c_1 &\triangleq \overline{M} c_{d2} + c_G + c_{P1} + c_{d,cycle} + c_{d,rider} + c_r + c_V c_{d1}^2 + c_{P2} c_{d1} + \overline{b} c_{d1}, \\ c_2 &\triangleq \alpha \overline{M} (1+\alpha) + c_V c_{d1} + \alpha c_V c_{d1} + c_{P2} + \overline{b} + 1, \\ c_3 &\triangleq \alpha c_V, \end{aligned}$$

and the error vector $z : \mathbb{R}_{\geq 0} \to \mathbb{R}^2$ is defined as

$$z \triangleq \begin{bmatrix} e_1 & e_2 \end{bmatrix}^T.$$

5.2.2 Closed-Loop Error System

Based on (5–4) and the subsequent stability analysis, the control input is designed as

$$u \triangleq k_1 e_2 + \left(k_2 + k_3 \|z\| + k_4 \|z\|^2\right) \text{sgn}(e_2), \tag{5–7}$$

where sgn $: \mathbb{R} \to [-1,\ 1]$ denotes the signum function and $k_1,\ k_2,\ k_3,\ k_4 \in \mathbb{R}_{>0}$ are constant control gains. Substituting (5–7) into (5–4) yields

$$M \dot{e}_2 = \chi - e_1 - V e_2 - B_\sigma \left(k_1 e_2 + \left(k_2 + k_3 \|z\| + k_4 \|z\|^2\right) \text{sgn}(e_2)\right). \tag{5–8}$$

5.3 Stability Analysis

Let $V_L : \mathbb{R}^2 \to \mathbb{R}$ denote a continuously differentiable, positive definite, radially unbounded, common Lyapunov-like function defined as

$$V_L(z(t)) \triangleq \frac{1}{2} z^T(t) W(q(t)) z(t), \tag{5–9}$$

where the positive definite matrix $W : \mathcal{Q} \to \mathbb{R}^{2\times 2}$ is defined as

$$W \triangleq \begin{bmatrix} 1 & 0 \\ 0 & M \end{bmatrix}. \tag{5–10}$$

V_L satisfies the following inequalities:

$$\lambda_1 \|z\|^2 \leq V_L \leq \lambda_2 \|z\|^2, \tag{5–11}$$

where $\lambda_1,\ \lambda_2 \in \mathbb{R}_{>0}$ are known constants defined as

$$\lambda_1 \triangleq \min\left\{\frac{1}{2},\ \frac{1}{2}\underline{M}\right\}, \quad \lambda_2 \triangleq \max\left\{\frac{1}{2},\ \frac{1}{2}\overline{M}\right\}.$$

Theorem 5.1. *The tracking error is bounded by an exponentially decaying envelope given by*

$$\|z(t)\| \leq \sqrt{\frac{\lambda_2}{\lambda_1}}\|z(t_0)\| \exp\left(-\frac{1}{2}\lambda_s(t-t_0)\right), \tag{5–12}$$

for all $t \in [t_0,\ \infty)$*, where* $t_0 \in \mathbb{R}_{\geq 0}$ *is the initial time, and* $\lambda_s \in \mathbb{R}_{>0}$ *is defined as*

$$\lambda_s \triangleq \frac{1}{\lambda_2} \min\left\{\alpha,\ c_{B_p} k_1\right\}, \tag{5–13}$$

where $c_{B_p} \in \mathbb{R}_{>0}$ *is a known constant defined as*

$$c_{B_p} \triangleq \min\left\{\min_{m\in\mathcal{M}}\left(B_{FES}\right),\ B_{motor}\right\},$$

provided the following gain conditions are satisfied:

$$k_2 \geq \frac{c_1}{c_{B_p}}, \quad k_3 \geq \frac{c_2}{c_{B_p}}, \quad k_4 \geq \frac{c_3}{c_{B_p}}. \tag{5–14}$$

Proof. Consider $\sigma = p$ for some arbitrary $p \in \mathcal{P}$ such that B_p is continuous. Because of the signum function in u, the time derivative of (5–9) exists almost everywhere (a.e.), i.e., for almost all $t \in [t_n,\ t_{n+1})$, $n \in \{0,\ 1,\ 2,\ ...\}$, as detailed in the analysis in Chapter 4. Therefore, after substituting (5–8), utilizing Property 13, and rearranging terms, the time derivative of (5–9) can be expressed as

$$\dot{V}_L \overset{a.e.}{=} \dot{e}_1 e_1 - e_1 e_2 + \chi e_2 - B_p\left(k_1 e_2 + \left(k_2 + k_3\|z\| + k_4\|z\|^2\right)\text{sgn}\left(e_2\right)\right)e_2.$$

Using (5–3), (5–6), and Property 11, it can be demonstrated that

$$\dot{V}_L \overset{a.e.}{\leq} -\alpha e_1^2 - c_{B_p} k_1 e_2^2 - \left(c_{B_p} k_2 - c_1\right) |e_2| - \left(c_{B_p} k_3 - c_2\right) \|z\| |e_2| - \left(c_{B_p} k_4 - c_3\right) \|z\|^2 |e_2| . \tag{5–15}$$

Provided the gain conditions in (5–14) are satisfied, (5–11) can be used to rewrite (5–15) as

$$\dot{V}_L \overset{a.e.}{\leq} -\lambda_s V_L, \tag{5–16}$$

where λ_s was defined in (5–13). The inequality in (5–16) can be rewritten as

$$\exp\left(\lambda_s \left(t - t_n\right)\right) \left(\dot{V}_L + \lambda_s V_L\right) \overset{a.e.}{\leq} 0,$$

for $t \in [t_n,\ t_{n+1})$, which is equivalent to the following expression:

$$\frac{d}{dt}\left(V_L \exp\left(\lambda_s \left(t - t_n\right)\right)\right) \overset{a.e.}{\leq} 0. \tag{5–17}$$

Taking the Lebesgue integral of (5–17) and recognizing that the integrand on the left-hand side is absolutely continuous allows the Fundamental Theorem of Calculus to be used to yield

$$V_L \leq V_L\left(t_n\right) \exp\left(-\lambda_s \left(t - t_n\right)\right), \tag{5–18}$$

for $t \in [t_n,\ t_{n+1})$. Since (5–18) was proven to hold for an arbitrary σ, (5–18) holds for all $\sigma \in \mathcal{P}$. Therefore, V_L is indeed a common Lyapunov function, and (5–18) holds for all $t \in [t_0,\ \infty)$. In other words,

$$V_L \leq V_L\left(t_0\right) \exp\left(-\lambda_s \left(t - t_0\right)\right). \tag{5–19}$$

Using (5–11) to bound (5–19) and performing some algebraic manipulation yields (5–12). □

Remark 5.1. The exponential decay rate λ_s represents the most conservative (i.e., smallest) decay rate for the closed-loop, switched error system. In practice, each

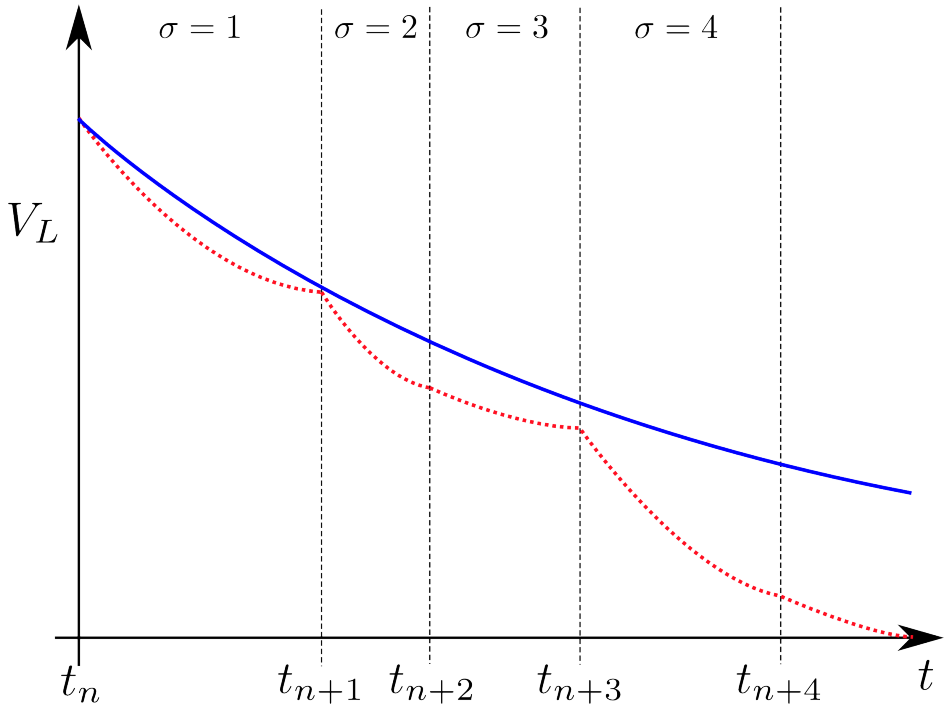

Figure 5-1. Illustration of the behavior of V_L.

subsystem has its own decay rate dependent on the lower bound of the corresponding B_σ, but in the preceding stability analysis, c_{B_p} was used as the lower bound on B_σ for all $\sigma \in \mathcal{P}$. Figure 5-1 illustrates how V_L may behave in practice (dotted red line) versus the conservative bound given in (5–19) (solid blue line).

5.4 Experiments

Experiments were conducted with the primary objective of evaluating the performance of the controller given in (5–7) and distributed as FES and electric motor current according to (2–51)-(2–54). Five able-bodied subjects (four male, one female) 21-43 years old participated in the experiments. Each subject gave written informed consent approved by the University of Florida Institutional Review Board. During the subsequent experiments, the subjects were instructed to relax and make no volitional effort to either assist or inhibit the FES or the electric motor input (i.e., passive riders).

5.4.1 Methods

A commercially available recumbent tricycle (TerraTrike Rover) was modified for the purposes of the FES-cycling experiments. A 250 Watt, brushed, 24 VDC electric motor (Unite Motor Co. Ltd. MY1016Z2) was mounted to the frame and coupled to the drive chain. Orthotic boots (Össur Rebound Air Tall) were affixed to custom pedals; these orthotic pedals served to fix the rider's feet to the pedals, prevent dorsiflexion and plantarflexion of the ankles, and maintain sagittal alignment of the lower legs. An optical encoder with an angular resolution of 0.018 degrees (US Digital H1) was coupled to the cycle crank via spur gears to measure the crank position. To make the system stationary, a stationary cycling trainer and riser rings (Kinetic by Kurt) were used to lift the tricycle's drive wheel off the ground. Current control of the cycle's motor was enabled by a general purpose linear amplifier (AE Techron LVC 5050) interfacing with the data acquisition hardware (Quanser Q8-USB), which also measured the encoder signal. The controller was implemented on a personal computer running real-time control software (QUARC, MATLAB/Simulink, Windows 7) at a sampling rate of 500 Hz. Figure 5-2 depicts the motorized FES-cycling test bed.

Stimulation was applied using the stimulator and electrodes described in Chapter 3. The stimulation amplitudes were fixed at 90 mA for the quadriceps and 80 mA for the hamstrings muscle groups, and the stimulation pulse width for each muscle group was determined by u_m and commanded to the stimulator by the control software. Stimulation frequency was fixed at 60 Hz to leverage the results found in [48]. For safety, an emergency stop switch was attached to the tricycle that enabled the subject to stop the experiment immediately if necessary, though no subjects found it necessary.

Electrodes were placed over the subjects' quadriceps femoris and hamstrings muscle groups according to Axelgaard's electrode placement manual[1] . In these

[1] http://www.palsclinicalsupport.com/videoElements/videoPage.php

Figure 5-2. Motorized FES-cycling test bed. Photo courtesy of author.

experiments, only the quadriceps and hamstrings muscle groups were stimulated to better demonstrate the balance between the FES and motor inputs. Each subject's legs were measured to obtain the distance from the greater trochanter to the lateral femoral condyle and from the lateral femoral condyle to the sole of the foot while the ankle was held in the anatomically neutral position. Subjects were then seated on the tricycle, and their feet were inserted securely into the orthotic pedals. The tricycle's seat position was adjusted for each subject's comfort while ensuring that full extension of the knees could not be achieved while cycling, and the distance from the cycle crank to the subject's right greater trochanter was measured. These measurements were used to calculate the torque transfer ratios for the subjects' muscle groups and to thereby determine the stimulation pattern.

Two experimental protocols were conducted with each subject, and each trial lasted 180 seconds. In Protocol 1, the desired cadence rose to 50 rpm and remained there for the duration of the experiment, while in Protocol 2 the desired cadence first rose to 50

rpm, then varied sinusoidally from 40 rpm to 60 rpm to demonstrate the robustness of the developed control system. For Protocol 1 the desired crank velocity $\dot{q}_d$ and position q_d were designed as

$$\dot{q}_d \triangleq \frac{5\pi}{3}\left(1-\exp\left(-\frac{2}{5}\left(t-t_0\right)\right)\right), \tag{5–20}$$

$$q_d \triangleq \frac{5\pi}{3}\left(t-t_0\right)-\frac{5}{2}\dot{q}_d+q\left(t_0\right), \tag{5–21}$$

where $t_0 = 0$ seconds. The trajectories in (5–20) and (5–21) ensured that the desired cadence started at 0 rpm and smoothly approached 50 rpm. For Protocol 2, the desired crank velocity $\dot{q}_d$ and position q_d were designed as

$$\dot{q}_d \triangleq \begin{cases} \frac{5\pi}{3}\left(1-\left(\frac{t-t_1}{t_1}\right)^4\right) & t < t_1 \\ \frac{5\pi}{3} & t_1 \le t < t_2 \\ \frac{\pi}{6}\cos\left(\frac{\pi}{15}\left(t-t_2\right)\right)+\frac{3\pi}{2} & t_2 \le t < t_3 \\ -\frac{\pi}{3}\cos\left(\frac{\pi}{15}\left(t-t_3\right)\right)+\frac{5\pi}{3} & t \ge t_3, \end{cases} \tag{5–22}$$

$$q_d \triangleq \begin{cases} \frac{5\pi}{3}\left(t-\frac{\left(t-t_1\right)^5+t_1^5}{5t_1^4}\right)+q\left(t_0\right) & t < t_1 \\ \frac{5\pi}{3}\left(t-t_1\right)+q_d\left(t_1\right) & t_1 \le t < t_2 \\ \frac{5}{2}\sin\left(\frac{\pi}{15}\left(t-t_2\right)\right)+\frac{3\pi}{2}\left(t-t_2\right)+q_d\left(t_2\right) & t_2 \le t < t_3 \\ -5\sin\left(\frac{\pi}{15}\left(t-t_3\right)\right)+\frac{5\pi}{3}\left(t-t_3\right)+q_d\left(t_3\right) & t \ge t_3, \end{cases} \tag{5–23}$$

where $t_1 \triangleq 16$ seconds, $t_2 \triangleq 26$ seconds, and $t_3 \triangleq 41$ seconds. The trajectories in (6–39) and (6–40) ensured that the desired cadence started at 0 rpm, smoothly approached 50 rpm, then varied sinusoidally from 40 rpm to 60 rpm with a period of 30 seconds.

For both protocols, the signals ε_m were designed for $m \in \mathcal{M}$ as

$$\varepsilon_m \triangleq \max\left(T_m\right)\gamma, \tag{5–24}$$

where $\gamma \in \mathbb{R}$ was a scaling factor designed as

$$\gamma \triangleq \begin{cases} 1 & t < t_1 \\ 1.4 - \frac{t}{40} & t_1 \leq t < t_2 \\ 0.75 & t \geq t_2. \end{cases} \tag{5–25}$$

By defining ε_m as in (5–24), the stimulation pattern was consistent across all subjects, despite differences in cycle-rider geometry. For example, Subject 1 had $l_t = 18$ inches and $l_l = 22.5$ inches and sat 31.4 inches away from the crank, whereas Subject 2 had $l_t = 15.5$ inches and $l_l = 22$ inches and sat 28.8 inches away from the crank. Despite the difference in cycle-rider geometry between subjects, Subject 1 had $\mathcal{Q}_{RQuad} = (68,\ 161)$ degrees[2] , and Subject 2 had $\mathcal{Q}_{RQuad} = (69,\ 163)$ degrees. In addition to maintaining consistency in the stimulation pattern across subjects, the definitions in (5–24) and (5–25) determined the stimulation pattern and FES-to-motor switching according to (2–51)-(2–54), so that only the motor was active during the first 16 seconds of each trial (i.e., while the desired trajectory rose to 50 rpm). Then the stimulation of the muscle groups was added and the stimulation regions increased in size for 10 seconds until they reached the desired steady state stimulation pattern[3] . This method for defining the stimulation pattern was selected because large muscle forces are required to pedal at low speeds [50], so the motor was used to bring the system to the desired cadence before FES was added. A constant input of 0.5 A was added to the motor current input to mitigate the effect of friction in the motor gearbox. The control gains, introduced

[2] A crank angle of zero degrees was defined as the position where the right crank was horizontal and pointing towards the rider.

[3] Values of 16 and 26 seconds were selected to ensure that only the motor was active while the trajectory rose to 50 rpm and to allow for a smooth transition from passive (i.e., motor-only) cycling to FES-cycling.

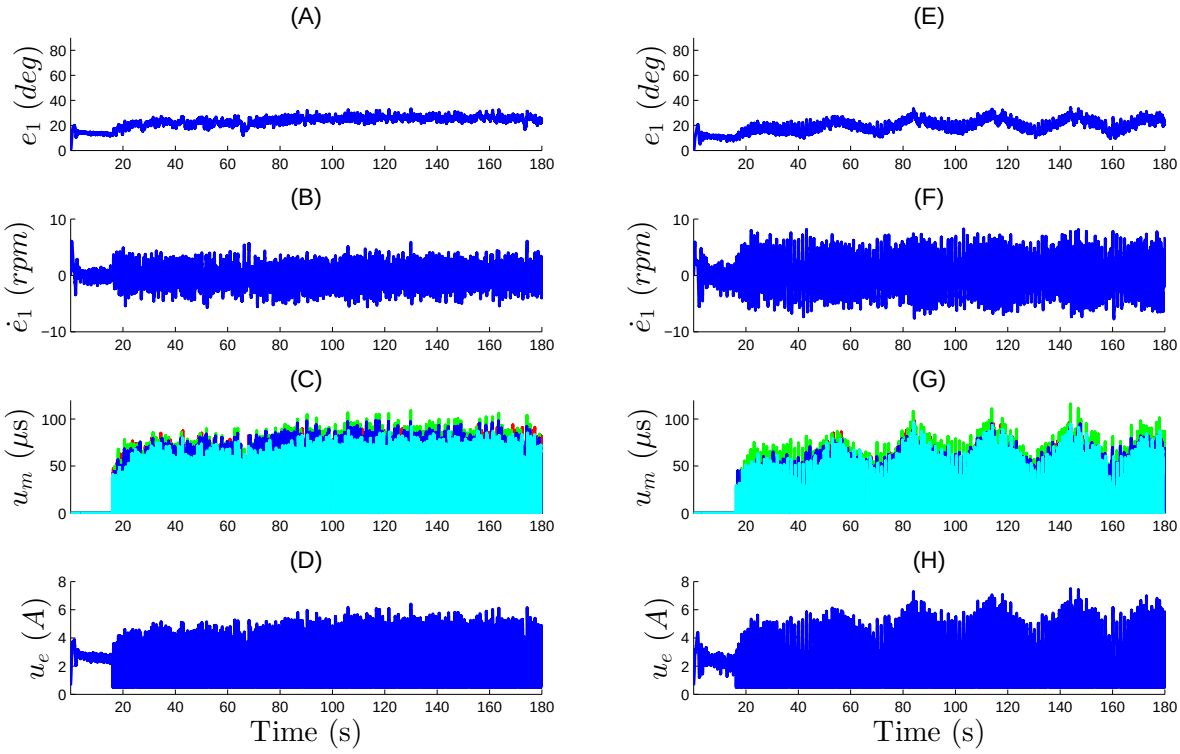

Figure 5-3. Tracking performance for Subject 1 during Protocol 1 and Protocol 2. A) Protocol 1 position tracking error. B) Protocol 1 cadence tracking error. C) Protocol 1 stimulation input. D) Protocol 1 motor input. E) Protocol 2 position tracking error. F) Protocol 2 cadence tracking error. G) Protocol 2 stimulation input. H) Protocol 2 motor input.

in (2–54) and (5–7), and the constant α, introduced in (5–3), were tuned to yield acceptable tracking performance prior to each trial and ranged as follows: $\alpha \in [7,\ 10]$, $k_m = 0.25\ \forall m \in \mathcal{M}$, $k_e \in [5.75 \times 10^{-3},\ 13.2]$, $k_1 \in [80,\ 100]$, $k_2 \in [4,\ 100]$, $k_3 = 0.01$, $k_4 = 0.001$.

5.4.2 Results

Figure 5-3 depicts one subject's tracking performance during both protocols, quantified by e_1, $\dot{e}_1$, the stimulation intensity input to each muscle group u_m, and the electric motor current input u_e. Figure 5-4 provides an enhanced view of the distribution of the control input between FES and the motor across one crank cycle. Table 5-1 summarizes the mean and standard deviation (st. dev.) of the position and cadence

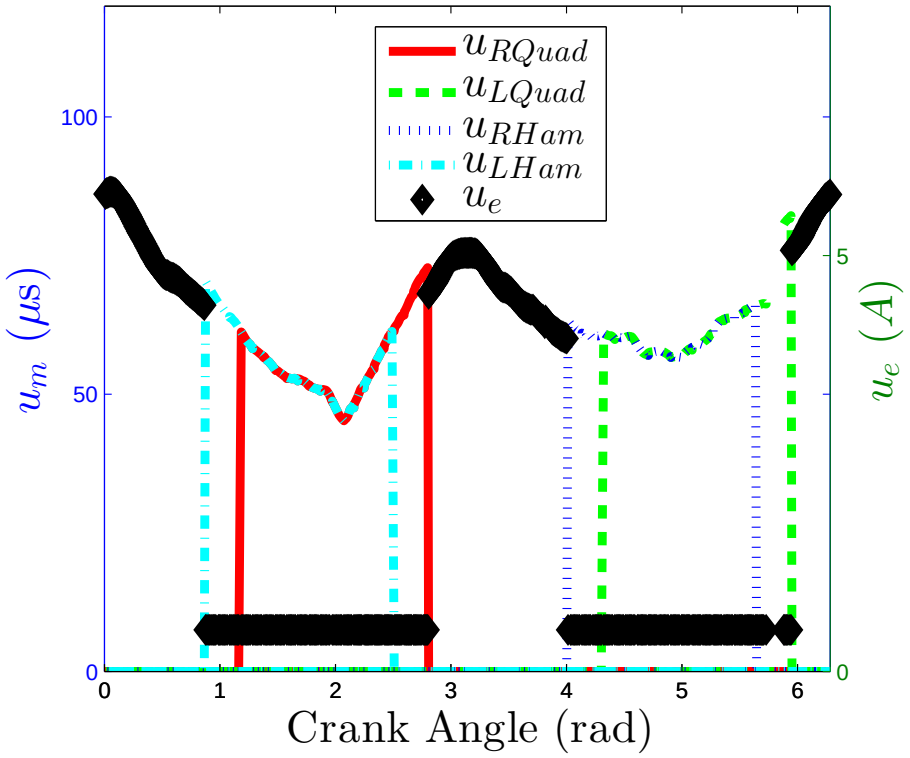

Figure 5-4. FES control inputs and motor current input from one motorized FES-cycling trial over a single crank cycle.

tracking error for each subject during the motor-only ($t \in [t_0,\ t_1)$ seconds), transitory ($t \in [t_1,\ t_2)$ seconds), and FES/motor ($t \in [t_2,\ 180]$ seconds) periods of Protocol 1. Similarly, Table 5-2 summarizes the tracking performance for each subject during Protocol 2.

5.4.3 Discussion

The experimental results successfully demonstrate the ability of the controller in (5–7), distributed between FES of the rider's muscle groups and electric motor current according to (2–54), to achieve exponentially stable tracking performance despite parametric uncertainty (e.g., uncertain rider limb mass) and unknown disturbances. However, the results indicate exponential convergence to an ultimate bound on the tracking error, instead of convergence to zero, which could be due to unmodeled effects such as electromechanical delay between muscle activation and force production [51].

Table 5-1. Summary of motorized FES-cycling performance for all five subjects during Protocol 1.

		Motor-only		Transitory		FES/Motor	
Subject	Error	mean	st. dev.	mean	st. dev.	mean	st. dev.
1	e_1(deg.)	13.70	2.36	18.72	2.86	24.38	2.90
	$\dot{e}_1$ (rpm)	0.34	1.32	0.11	2.12	0.00	2.07
2	e_1(deg.)	12.04	2.19	18.64	3.91	26.13	3.69
	$\dot{e}_1$ (rpm)	0.33	1.34	0.20	1.97	0.00	2.68
3	e_1(deg.)	10.61	2.73	15.13	3.29	17.48	2.80
	$\dot{e}_1$ (rpm)	0.31	1.73	0.13	2.77	0.00	3.44
4	e_1(deg.)	13.83	2.57	21.85	3.77	33.25	4.59
	$\dot{e}_1$ (rpm)	0.36	1.75	0.24	2.56	0.01	2.82
5	e_1(deg.)	5.98	2.55	10.74	3.36	15.18	2.69
	$\dot{e}_1$ (rpm)	0.25	2.11	0.13	3.09	0.01	3.52

Table 5-2. Summary of motorized FES-cycling performance for all five subjects during Protocol 2.

		Motor-only		Transitory		FES/Motor	
Subject	Error	mean	st. dev.	mean	st. dev.	mean	st. dev.
1	e_1(deg.)	11.00	2.84	14.99	2.92	20.55	4.62
	$\dot{e}_1$ (rpm)	0.33	1.75	0.06	2.71	0.01	2.98
2	e_1(deg.)	6.70	1.81	10.28	2.44	13.96	5.23
	$\dot{e}_1$ (rpm)	0.28	1.35	0.12	2.38	0.01	3.11
3	e_1(deg.)	9.32	2.23	13.24	2.74	18.95	5.59
	$\dot{e}_1$ (rpm)	0.30	1.53	0.15	2.04	0.00	2.79
4	e_1(deg.)	8.99	3.19	13.96	2.53	22.04	5.15
	$\dot{e}_1$ (rpm)	0.31	2.08	0.13	2.52	0.01	3.28
5	e_1(deg.)	5.61	2.51	10.26	3.06	14.72	4.29
	$\dot{e}_1$ (rpm)	0.25	1.85	0.14	2.97	0.00	3.62

The results for Subject 1, presented in Figure 5-3, demonstrate typical performance during the motorized FES-cycling task, as corroborated by the data in Table 5-1 and Table 5-2. Of particular note is the mean and standard deviation of the cadence tracking error during the FES/motor period for all subjects, where the average cadence tracking error across all five subjects was 0.00 ± 2.91 rpm (i.e., the actual cadence was centered about the desired cadence with less than 3 rpm in standard deviation) for Protocol 1 and 0.01 ± 3.15 rpm for Protocol 2. In comparison, the average position tracking error across all five subjects was 23.28 ± 3.33 degrees for Protocol 1 and 18.05 ± 4.98 degrees for Protocol 2, indicating that the actual crank trajectory lagged the desired trajectory consistently across all experiments. The steady state offset in the position tracking error was likely caused by a bias in the tuning of the control gains towards improving cadence tracking performance, as cadence error is generally considered to be the main performance criterion during cycling tasks.

As indicated in the experimental data plotted in Figure 5-4, the electric motor provided assistance as needed in the regions of the FES-cycling joint space where the rider's torque transfer ratios were small, and stability was maintained throughout the trial despite the discontinuous switching in the torque input to the system. The subjects reported that the cycling motion felt comfortable and natural and that they perceived their muscles as contributing significantly to the cycling task, though neither metabolic nor relative torque contribution (i.e., comparing FES torque input to motor torque input) measurements were available to quantify these effects.

5.5 Concluding Remarks

A novel switching strategy was developed that applies FES to the rider's muscle groups in regions of the crank cycle where the rider's muscles contribute significantly to the cycling task and utilizes an electric motor for assistance only as needed (i.e., in regions of poor kinematic efficiency). A switched sliding-mode controller was designed to yield global, exponentially stable tracking of a desired crank trajectory, provided

sufficient gain conditions are satisfied. The control design was validated in experiments with five able-bodied subjects, where an average cadence tracking error of 0.00 ± 2.91 rpm ($0.00 \pm 5.82\%$ error) was demonstrated when tracking a constant desired cadence of 50 rpm.

The developed control system for motorized FES-cycling systems has the potential to enhance therapeutic outcomes in a rehabilitative setting and to improve the performance of assistive cycling devices; however, clinical implementation of the developed control system may present additional challenges not considered in this chapter. While the theoretical development in this chapter considers a generalized cycle-rider system, applying the developed control system to a particular patient population may require disorder-specific tuning of the system parameters or the addition of disorder-specific functionality. As discussed in the concluding chapter of this dissertation, future work will focus on applying the developed control system to people with neurological disorders and will necessarily consider such disorder-specific challenges to implementation. Further work also needs to involve clinical trials in clinically relevant patient populations to investigate training benefits.

CHAPTER 6
SWITCHED CONTROL OF CADENCE AND POWER OUTPUT DURING STATIONARY CYCLING INDUCED BY FUNCTIONAL ELECTRICAL STIMULATION

This chapter presents the development of an FES-cycling control system that utilizes an electric motor to maintain a desired cadence while FES is used to control the power output at the cycle crank by the rider's electrically stimulated muscles. As described in [8], for FES exercise testing, it is crucial to control both the cycling cadence and the work done by the muscle groups. In the present development, the electric motor is tasked with tracking a desired crank trajectory while FES of the muscle groups is used to track a desired torque about the crank axis. It is assumed that the torque applied by the rider τ_{rider} is measurable along with the crank position q and velocity $\dot{q}$. A sliding mode controller is developed for the electric motor that guarantees globally, exponentially stable tracking of the desired crank trajectory. Similarly, a sliding mode controller is developed for the FES control input that guarantees ultimately bounded tracking of the desired active torque, averaged over the crank cycle, provided sufficient gain conditions are satisfied, despite the switching effects, uncertainty in the system parameters, and the presence of unknown, bounded disturbances. Experimental results from three able-bodied individuals demonstrate the control system's performance under typical FES-cycling conditions.

6.1 Cadence Control

6.1.1 Controller Development

The electric motor torque τ_{motor} can be modeled as in (2–49) where, here, B_e is assumed to be a known constant. The control objective for the electric motor torque is to track a desired crank trajectory with performance quantified by the tracking error signals $e_i : \mathbb{R}_{\geq 0} \to \mathbb{R},\ i \in \{1,\ 2\}$, defined as

$$e_1(t) \triangleq q_d(t) - q(t), \tag{6–1}$$

$$e_2(t) \triangleq \dot{e}_1(t) + \alpha e_1(t), \tag{6–2}$$

where $\alpha \in \mathbb{R}_{>0}$ is a selectable constant, and $q_d : \mathbb{R}_{\geq 0} \to \mathbb{R}$ denotes the desired crank position, designed such that its first two time derivatives exist and are bounded as $|\dot{q}_d| \leq c_{q1}$ and $|\ddot{q}_d| \leq c_{q2}$, where $c_{qi} \in \mathbb{R}_{\geq 0},\ i \in \{1,\ 2\}$, are known constants. Taking the time derivative of (6–2), multiplying by J_{cycle}, substituting (2–42), (2–43), (2–49) and (6–1), and rearranging terms yields

$$J_{cycle}\dot{e}_2 = J_{cycle}\left(\ddot{q}_d + \alpha\dot{e}_1\right) + b_{cycle}\dot{q} + d_{cycle} + \tau_{rider} - B_e u_e. \tag{6–3}$$

Based on (6–3) and the subsequent stability analysis, the electric motor control current is designed as

$$u_e \triangleq B_e^{-1}\left(\tau_{rider} + k_1 e_2 + \left(k_2 + k_3\left|e_1\right|\right)\text{sgn}\left(e_2\right)\right), \tag{6–4}$$

where $k_1,\ k_2 \in \mathbb{R}_{>0}$ are constant control gains, and sgn $: \mathbb{R} \to [-1,\ 1]$ is the signum function. Substituting (6–4) into (6–3) yields

$$J_{cycle}\dot{e}_2 = J_{cycle}\left(\ddot{q}_d + \alpha\dot{e}_1\right) + b_{cycle}\dot{q} + d_{cycle} - k_1 e_2 - \left(k_2 + k_3\left|e_1\right|\right)\text{sgn}\left(e_2\right). \tag{6–5}$$

6.1.2 Stability Analysis

Let $V_q : \mathbb{R}^2 \to \mathbb{R}_{\geq 0}$ denote a continuously differentiable, positive definite, Lyapunov function candidate defined as

$$V_q\left(z\left(t\right)\right) \triangleq \frac{1}{2}e_1^2\left(t\right) + \frac{1}{2}J_{cycle}e_2^2\left(t\right), \tag{6–6}$$

where the error vector $z : \mathbb{R}_{\geq 0} \to \mathbb{R}^2$ is defined as

$$z\left(t\right) \triangleq \begin{bmatrix} e_1\left(t\right) & e_2\left(t\right) \end{bmatrix}^T.$$

The Lyapunov function candidate V_q satisfies the following inequalities:

$$\lambda_1\left\|z\right\|^2 \leq V_q \leq \lambda_2\left\|z\right\|^2, \tag{6–7}$$

where $\lambda_1,\ \lambda_2 \in \mathbb{R}_{>0}$ are known constants defined as

$$\lambda_1 \triangleq \min\left(\frac{1}{2},\ \frac{1}{2}\underline{J}\right), \quad \lambda_2 \triangleq \max\left(\frac{1}{2},\ \frac{1}{2}\overline{J}\right).$$

Theorem 6.1. *The tracking error is bounded by an exponentially decaying envelope given by*

$$\|z(t)\| \ \leq\ \sqrt{\frac{\lambda_2}{\lambda_1}}\|z(t_0)\| \exp\left(-\frac{1}{2}\lambda_q(t-t_0)\right), \tag{6–8}$$

for all $t \in [t_0,\ \infty)$*, where* $t_0 \in \mathbb{R}_{\geq 0}$ *is the initial time, and* $\lambda_q \in \mathbb{R}_{>0}$ *is defined as*

$$\lambda_q \triangleq \frac{1}{\lambda_2}\min\left\{\alpha,\ \alpha\overline{J} - k_1\right\}, \tag{6–9}$$

provided the following gain conditions are satisfied:

$$k_1 > \alpha\overline{J}, \quad k_2 \geq \overline{J}c_{q2} + \overline{b}c_{q1} + c_{d,cycle}, \quad k_3 \geq 1 + \left(\overline{J} + \overline{b}\right)\alpha. \tag{6–10}$$

Proof. Because of the signum function in (6–5), the time derivative of V_q exists almost everywhere (a.e.), i.e., for almost all $t \in [t_0,\ \infty)$. Using (6–2) and (6–5), the time derivative of (6–6) can be expressed as

$$\dot{V}_q \overset{a.e.}{=} -\alpha e_1^2 + e_1e_2 + \left(J_{cycle}\left(\ddot{q}_d + \alpha\dot{e}_1\right) + b_{cycle}\dot{q} + d_{cycle} - k_1e_2 - \left(k_2 + k_3|e_1|\right)\text{sgn}\left(e_2\right)\right)e_2. \tag{6–11}$$

Using Assumption 1 and Properties 5-6, (6–11) can be bounded above as

$$\dot{V}_q \overset{a.e.}{\leq} -\alpha e_1^2 + \left(\alpha\overline{J} - k_1\right)e_2^2 + \left(\overline{J}c_{q2} + \overline{b}c_{q1} + c_{d,cycle} - k_2\right)|e_2| + \left(1 + \alpha\overline{J} + \overline{b}\alpha - k_3\right)|e_1||e_2|. \tag{6–12}$$

Provided the conditions in (6–10) are satisfied, (6–7) can be used to bound (6–12) as

$$\dot{V}_q \overset{a.e.}{\leq} -\lambda_q V_q, \tag{6–13}$$

where λ_q was defined in (6–9). From (6–13), it can be demonstrated that

$$V_q(z(t)) \leq V_q(z(t_0))\exp\left(-\lambda_q(t-t_0)\right) \tag{6–14}$$

for $t \in [t_0,\ \infty)$. Using (6–7) to bound (6–14) and performing some algebraic manipulation yields (6–8). □

Remark 6.1. Using (6–1), (6–2), (6–5), and (6–8), it can be demonstrated that the crank velocity $\dot{q}$ and acceleration $\ddot{q}$ are bounded as

$$|\dot{q}| \leq c_{q1} + (\alpha + 1)\sqrt{\frac{\lambda_2}{\lambda_1}}\left\|z\left(t_0\right)\right\|, \tag{6–15}$$

$$|\ddot{q}| \leq \underline{J}^{-1}\left(\left(k_1 + k_3 + \bar{b}\right)\sqrt{\frac{\lambda_2}{\lambda_1}}\left\|z\left(t_0\right)\right\| + k_2 + c_{d,cycle}\right). \tag{6–16}$$

6.2 Power Control

6.2.1 Controller Development

In this development, the control objective for the FES control input is: (1) to track a desired active torque trajectory that yields a desired active power output at the cycle crank in the controlled regions (i.e., for $q \in \mathcal{Q}_c$) and (2) to ensure boundedness of the torque tracking error system in the uncontrolled regions (i.e., for $q \in \mathcal{Q}_u$). Here, as in [8, 29, 52, 53], the desired torque is defined based on the average torque over one crank cycle instead of the instantaneous torque, because, as noted in [52], the limited bandwidth of electrically stimulated muscle groups makes tracking an instantaneous crank torque unfeasible. Ideally, to achieve the active-torque-tracking objective, an error system and controller would be designed based on the difference between the desired torque and τ_a. However, noninvasive torque-sensing devices can only measure the net torque produced by the rider, τ_{rider}, which includes the rider's passive limb dynamics and disturbances, as in (2–44). Therefore, in this development, a measure of τ_{rider} is taken while the rider's active torque $\tau_a = 0$ (i.e., the rider is passive and is not electrically stimulated), thereby achieving a measure of τ_p along a desired trajectory, as done in [10, 29, 52]. This estimate of τ_p, denoted here as $\hat{\tau}_p : \mathcal{Q} \times \mathbb{R} \to \mathbb{R}$, is added to the torque sensor measurement to obtain an estimate of the active rider torque thereafter.

Then, the active torque estimate $\hat{\tau}_a : \mathbb{R}_{\geq 0} \to \mathbb{R}$ is defined as

$$\hat{\tau}_a(t) \triangleq \hat{\tau}_p(q(t),\ \dot{q}_c) - \tau_{rider}(q(t),\ \dot{q}(t),\ \ddot{q}(t),\ t), \tag{6–17}$$

where $\dot{q}_c \in \mathbb{R}$ is a known, constant crank velocity. The following assumption is made about the passive torque estimate $\hat{\tau}_p$.

Assumption 6. An estimate of the rider's passive limb dynamics $\hat{\tau}_p$ can be generated during preliminary testing such that the estimate error $\tilde{\tau}_p : \mathbb{R}_{\geq 0} \to \mathbb{R}$, defined as

$$\tilde{\tau}_p(t) \triangleq \tau_p(q(t),\ \dot{q}(t),\ \ddot{q}(t)) - \hat{\tau}_p(q(t),\ \dot{q}_c), \tag{6–18}$$

and its first time derivative can be bounded as $|\tilde{\tau}_p| \leq c_{\tilde{\tau}_p}$, and $\left|\dot{\tilde{\tau}}_p\right| \leq c_{\dot{\tilde{\tau}}_p}$, where $c_{\tilde{\tau}_p},\ c_{\dot{\tilde{\tau}}_p} \in \mathbb{R}_{\geq 0}$ are known constants. This assumption is reasonable provided that τ_a and d_{rider} are sufficiently small when $\hat{\tau}_p$ is generated and that the value of $\dot{q}_c$ used when generating $\hat{\tau}_p$ is the same used when subsequently applying the estimate.

The average of the active torque estimate over the crank cycle $\hat{\tau}_a^{avg} : \mathbb{R}_{\geq 0} \to \mathbb{R}$ is a discrete signal defined as

$$\hat{\tau}_a^{avg}(t = kT) \triangleq \frac{1}{T} \int_{(k-1)T}^{kT} \hat{\tau}_a(t)\, dt, \tag{6–19}$$

where $k \in \mathbb{Z}$ denotes the number of crank cycles and is incremented when the crank reaches zero degrees, and $T \in \mathbb{R}_{>0}$ is the nominal cycling period, defined as $T \triangleq \frac{2\pi}{\dot{q}_c}$. Hereafter, for simplicity of notation, discrete signals are denoted as functions of k, rather than kT (e.g., $\hat{\tau}_a^{avg}(k) \triangleq \hat{\tau}_a^{avg}(t = kT)$). In this development, the desired torque $\tau_d : \mathbb{R}_{\geq 0} \to \mathbb{R}$ is based on the desired, average power output at the crank $\psi_d : \mathbb{R}_{\geq 0} \to \mathbb{R}$ and is defined as

$$\tau_d(t) \triangleq \begin{cases} 0 & \dot{q}_d(t) < \dot{\bar{q}}_d \\ \frac{\psi_d(t)}{\dot{q}_d(t)} & \dot{q}_d(t) \geq \dot{\bar{q}}_d, \end{cases} \tag{6–20}$$

where $\dot{\bar{q}}_d \in \mathbb{R}_{>0}$ is a selectable, positive constant. The desired torque is designed to be continuous and bounded as $|\tau_d| \leq c_{\tau_d}$ with its first time derivative bounded as $|\dot{\tau}_d| \leq c_{\dot{\tau}_d}$. The average torque tracking error signal $e_\tau : \mathbb{R}_{\geq 0} \to \mathbb{R}$ is defined as

$$e_\tau(k) \triangleq \tau_d(k) - \hat{\tau}_a^{avg}(k). \tag{6–21}$$

Substituting (2–44), (2–46), (6–17), (6–18), and (6–19) into (6–21) and rearranging terms yields

$$e_\tau(k) = \tau_d(k) + D(k) - \frac{1}{T} \int_{(k-1)T}^{kT} \left(\sum_{m \in \mathcal{M}} B_m(q(t), \dot{q}(t)) u_m(t) \right) dt, \tag{6–22}$$

where $D : \mathbb{Z} \to \mathbb{R}$ is defined as

$$D(k) \triangleq \frac{1}{T} \int_{(k-1)T}^{kT} (\tilde{\tau}_p(t) + d_{rider}(t) - \tau_r(t)) dt.$$

Using Assumptions 1 and 6, Property 12

$$|\Delta D(k)| \leq \left(c_{\dot{\tilde{\tau}}_p} + c_{\dot{d},rider} + c_{\dot{r}} \right) T,$$

where the operator Δ indicates the forward difference (i.e., $\Delta D(k) \triangleq D(k+1) - D(k)$).

Because the feedback signal, torque averaged over the crank cycle, is only updated once per crank cycle, the torque tracking error system is discretized. Therefore, the control input is also discretized in the sense that a constant control input is applied throughout each crank cycle and is updated once a new measurement of the tracking error is available. If u_m were defined as in (2–54), the stimulation applied to each muscle group would essentially be a square wave. In previous FES-cycling studies, a ramping envelope for the stimulation was used to avoid the large jump discontinuities that arise from a square input to the muscle groups (e.g., [4, 19]). Motivated to do likewise while simultaneously maximizing efficiency of the FES-evoked joint torques, in this

development, u_m is defined as

$$u_m(t) \triangleq k_m T_m(q(t)) \sigma_m(q(t)) u_{FES}(k), \tag{6–23}$$

for $t \in [kT,\ (k+1)T)$, where k_m, T_m, σ_m, and u_{FES} were defined in Chapter 2. Substituting (6–23) into (6–22) and rearranging terms yields

$$e_\tau(k) = \tau_d(k) + D(k) - \frac{1}{T} B(k) u_{FES}(k), \tag{6–24}$$

where $B : \mathbb{Z} \to \mathbb{R}_{>0}$ is defined as

$$B(k) \triangleq \int_{(k-1)T}^{kT} \left(\sum_{m \in \mathcal{M}} B_m(q(t), \dot{q}(t)) k_m T_m(q(t)) \sigma_m(q(t)) \right) dt.$$

Note that the design of the switching signals σ_m ensures that B is positive.

Assumption 7. $B(0) = B(1) = B(2) = ... = B(k) = B_k$, where $B_k \in \mathbb{R}_{>0}$ is an uncertain constant and $\underline{B} \leq B_k \leq \overline{B}$, where $\underline{B},\ \overline{B} \in \mathbb{R}_{>0}$ are known constants. This assumption is reasonable provided that the cadence is nearly constant from cycle to cycle.

Using Assumption 7, the forward difference of (6–24) can be expressed as

$$\Delta e_\tau(k) = \Delta \tau_d(k) + \Delta D(k) - \frac{1}{T} B_k \Delta u_{FES}(k). \tag{6–25}$$

Based on (6–25) and the subsequent stability analysis, the electrical stimulation control input is defined as

$$\Delta u_{FES}(k) \triangleq k_4 e_\tau(k) + (k_5 + k_6 |\Delta \tau_d(k)|) \operatorname{sgn}(e_\tau(k)), \tag{6–26}$$

where $k_4,\ k_5,\ k_6 \in \mathbb{R}_{>0}$ are constant control gains.

6.2.2 Stability Analysis

Theorem 6.2. *The torque tracking error is ultimately bounded in the sense that* $|e_\tau(k)|$ *converges to a ball with constant radius* $d \in \mathbb{R}_{>0}$ *as the number of crank cycles approaches infinity (i.e., as* $k \to \infty$*), where* d *is defined as*

$$d \triangleq \sqrt{\frac{2c_\tau}{\lambda_\tau}}, \tag{6–27}$$

where $c_\tau,\ \lambda_\tau \in \mathbb{R}_{>0}$ *are constants defined as*

$$c_\tau \triangleq \frac{1}{2}\left(\left(1+\frac{1}{T}\overline{B}k_6\right)c_{\dot{\tau}_d} + c_{\dot{\bar{\tau}}_p} + c_{\dot{d},rider} + c_{\dot{r}} + \frac{1}{T^2}\overline{B}k_5\right)^2 T^2,$$

$$\lambda_\tau \triangleq \frac{2}{T}B_k k_4 - \left(\frac{1}{T}B_k k_4\right)^2, \tag{6–28}$$

$$c_\tau \triangleq \frac{1}{2}\left(\left(1+\frac{1}{T}\overline{B}k_6\right)c_{\dot{\tau}_d} + c_{\dot{\bar{\tau}}_p} + c_{\dot{d},rider} + c_{\dot{r}} + \frac{1}{T^2}\overline{B}k_5\right)^2 T^2, \tag{6–29}$$

provided the following gain conditions are satisfied:

$$k_4 < T\overline{B}^{-1}, \tag{6–30}$$

$$k_5 \geq \left(\frac{T\underline{B}^{-1}+k_4}{T\overline{B}^{-1}-k_4}\right)\left(c_{\dot{\bar{\tau}}_p} + c_{\dot{d},rider} + c_{\dot{r}}\right)T^2\underline{B}^{-1}, \tag{6–31}$$

$$k_6 \geq \left(\frac{T\underline{B}^{-1}+k_4}{T\overline{B}^{-1}-k_4}\right)T\underline{B}^{-1}. \tag{6–32}$$

Proof. Let $V_\tau : \mathbb{R} \to \mathbb{R}_{\geq 0}$ denote a discrete, positive definite Lyapunov function candidate defined as

$$V_\tau\left(e_\tau(k)\right) \triangleq \frac{1}{2}e_\tau^2(k). \tag{6–33}$$

The forward difference of (6–33) can be expressed using the property $\Delta(ab) = b\Delta a + a\Delta b + \Delta a\Delta b$ as

$$\Delta V_\tau\left(e_\tau(k)\right) = \left(\Delta e_\tau(k)\right)e_\tau(k) + \frac{1}{2}\left(\Delta e_\tau(k)\right)^2. \tag{6–34}$$

Substituting (6–25) and (6–26) into (6–34) and performing some algebraic manipulation yields

$$\begin{aligned}\Delta V_\tau\left(e_\tau\left(k\right)\right) &= \left(\frac{1}{2}\left(\frac{1}{T}B_k\right)^2 k_4^2 - \frac{1}{T}B_k k_4\right) e_\tau^2\left(k\right) + \left(\left(\frac{1}{T}B_k\right)^2 k_4 k_5 - \frac{1}{T}B_k k_5\right)\left|e_\tau\left(k\right)\right| \\ &+ \left(1 - \frac{1}{T}B_k k_4\right)\Delta\tau_d\left(k\right) e_\tau\left(k\right) + \left(1 - \frac{1}{T}B_k k_4\right)\Delta D\left(k\right) e_\tau\left(k\right) \\ &+ \left(\left(\frac{1}{T}B_k\right)^2 k_4 k_6 - \frac{1}{T}B_k k_6\right)\left|\Delta\tau_d\left(k\right)\right|\left|e_\tau\left(k\right)\right| \\ &+ \frac{1}{2}\left(\Delta\tau_d\left(k\right) + \Delta D\left(k\right) - \left(k_5 + k_6\left|\Delta\tau_d\left(k\right)\right|\right)\frac{1}{T}B_k \mathrm{sgn}\left(e_\tau\left(k\right)\right)\right)^2. \quad (6\text{–}35)\end{aligned}$$

Provided the gain conditions in (6–30)-(6–32) are satisfied, (6–35) can be bounded using (6–33) as

$$\Delta V_\tau\left(k\right) \leq -\lambda_\tau V_\tau\left(k\right) + c_\tau, \quad (6\text{–}36)$$

where λ_τ and c_τ were defined in (6–28) and (6–29), respectively. Applying (6–36) sequentially from the first to the k^{th} crank cycle yields the following bound on $V_\tau\left(k\right)$:

$$V_\tau\left(k\right) \leq \left(1 - \lambda_\tau\right)^k V_\tau\left(0\right) + \sum_{n=0}^{k-1}\left(1 - \lambda_\tau\right)^n c_\tau. \quad (6\text{–}37)$$

The summation in (6–37) is a geometric series that converges for $\lambda_\tau \in \left(0,\ 2\right)$, which is satisfied provided (6–30) is satisfied, so that (6–37) can be expressed as

$$V_\tau\left(k\right) \leq \left(1 - \lambda_\tau\right)^k\left(V_\tau\left(0\right) - \frac{c_\tau}{\lambda_\tau}\right) + \frac{c_\tau}{\lambda_\tau}. \quad (6\text{–}38)$$

Then, as the number of crank cycles approaches infinity (i.e., as $k \to \infty$), $V_\tau\left(k\right)$ is ultimately bounded in the sense that

$$\lim_{k\to\infty} V_\tau\left(k\right) \leq \frac{c_\tau}{\lambda_\tau},$$

and, after using (6–33) and performing some algebraic manipulation, it can be determined that $|e_\tau(k)|$ is ultimately bounded in the sense that

$$\lim_{k\to\infty} |e_\tau(k)| \leq d,$$

where d was defined in (6–27). □

6.3 Experiments

Experiments were conducted with the primary objective of evaluating the performance of the controllers defined by (6–4) and (6–26), with the FES distributed to the muscle groups according to (2–51), (2–50), and (6–23). Three able-bodied, male subject (21-26 years old) participated in the experiments after giving written informed consent approved by the University of Florida Institutional Review Board. During the subsequent experiments, the subjects were instructed to relax and make no volitional effort to either assist or inhibit the FES or the electric motor input (i.e., passive riders).

6.3.1 Methods

The test bed used for these experiments was the same one used for the experiments described in Chapter 5, except that a torque-measuring crank set (SRM PowerMeter) was added to provide instantaneous feedback of the rider torque τ_{rider}. The torque signal was filtered using a discrete, second-order low pass filter with a cut-off frequency of 25 radians per second (the principal frequency of the cycle-rider dynamics is equal to the crank velocity, which remained well below 8 radians per second throughout the experiments). The filtered torque signal was used in (6–4), while its average value, obtained by averaging over the period T and only sampling when the crank passed through zero degrees, was used for feedback in (6–26).

The desired crank velocity $\dot{q}_d$ and position q_d were designed as

$$\dot{q}_d \triangleq \begin{cases} \dot{q}_c \left(1 - \left(\frac{t-t_1}{t_1}\right)^4\right) & t_0 \leq t < t_1 \\ \dot{q}_c & t_1 \leq t \leq t_f, \end{cases} \tag{6–39}$$

$$q_d \triangleq \begin{cases} \dot{q}_c \left(t - \frac{(t-t_1)^5 + t_1^5}{5t_1^4}\right) + q\left(t_0\right) & t_0 \leq t < t_1 \\ \dot{q}_c \left(t - t_1\right) + q_d\left(t_1\right) & t_1 \leq t \leq t_f, \end{cases} \tag{6–40}$$

where $t_0 \triangleq 0$ seconds, $t_1 \triangleq 30$ seconds, $t_f \triangleq 180$ seconds, and $\dot{q}_c \triangleq \frac{5\pi}{3}$ radians per second. The trajectories in (6–39) and (6–40) ensured that the desired cadence started at 0 rpm and smoothly approached 50 rpm over a period of 30 seconds, after which it remained constant for the remainder of the trial. The motor control effectiveness was determined to be $B_e = 3.87$ Newton-meters (Nm) per ampere (A), and an offset of 0.5 A was added to the electric motor control input to offset the effects of static friction in the gearing. The control gains for the electric motor were selected as: $k_1 = 15$, $k_2 = 1.5$, $k_3 = 7.5$, $\alpha = 1$.

The desired average torque at the crank τ_d was designed as

$$\tau_d \triangleq \begin{cases} 0 & t_0 \leq t < t_1 \\ \frac{\psi_d}{\dot{q}_d} \left(1 - \left(\frac{t-t_2}{t_2-t_1}\right)^4\right) & t_1 \leq t < t_2 \\ \frac{\psi_d}{\dot{q}_d} & t_2 \leq t \leq t_f, \end{cases} \tag{6–41}$$

where $t_2 \triangleq 60$ seconds and $\psi_d \triangleq 20$ Watts. The trajectory in (6–41) ensured that the desired torque started at 0 Nm and smoothly approached 3.8 Nm to achieve an average, active power output of 20 Watts at 50 rpm. For reference, in previous literature (e.g., [8, 23]), the desired power output typically varies between 5 and 15 Watts. Preliminary testing revealed that, relative to the quadriceps and gluteal muscle groups, the hamstrings muscle groups did not yield a significant torque about the crank

when stimulated, primarily because of low tolerance of the stimulation by the rider; therefore, only the quadriceps and gluteal muscle groups were stimulated in these experiments. The stimulation pattern was designed according to (2–51) and (2–50) with $\varepsilon_m \triangleq 0.1\text{max}\left(T_m\right)$, where T_m was determined based on measurements of the rider's thigh (l_t) and shank (l_l) lengths as well as his seat position (l_x and l_y), as described in Chapter 5. The stimulation pattern was shifted backward with respect to the crank rotation to account for delay in the torque response of the muscle groups to the electrical stimulation, as was done in [7, 8, 15, 19, 23, 54]. Here, the magnitude of the backward shift was $0.1\dot{q}$ radians, assuming a delay of 100 milliseconds. The stimulation amplitude was set to 90 mA for the quadriceps and 80 mA for the gluteal muscle groups, and the stimulation frequency was set to 60 Hz to leverage the results in [48]. The gains for the FES control input were tuned for each subject and ranged as follows: $k_4 = [4,\ 10]$, $k_5 = [2.5,\ 5]$, $k_6 = [25,\ 70]$, $k_{*Quad} = 1$, $k_{*Glute} = [1,\ 1.50]$.

Prior to beginning the tracking trial, a calibration procedure was conducted to obtain $\hat{\tau}_p\left(q\left(t\right),\ \dot{q}_c\right)$ for each subject. The electric motor was used to track the trajectories in (6–39) and (6–40) while τ_{rider} was measured using the cycle's torque sensor and the rider remained passive (i.e., $\tau_a = 0$). The collected torque data was analyzed for $t_1 \leq t \leq t_f$ (i.e., for $\dot{q} \cong \dot{q}_c$), and an eight-term Fourier series was fit to the data to obtain the passive torque estimate as

$$\hat{\tau}_p = \sum_{n=0}^{8} \left(a_n \text{cos}\left(n\omega q\right) + b_n \text{sin}\left(n\omega q\right)\right).$$

where $a_i \in \mathbb{R}, i \in \{0,\ 1,\ 2,\ ...,\ 8\}$, $b_j \in \mathbb{R}, j \in \{1,\ 2,\ 3,\ ...,\ 8\}$, and $\omega \in \mathbb{R}$ are fit parameters given in Table 6-1 for Subject 1. The results of the fit over a single crank cycle for Subject 1 are illustrated in Figure 6-1, where the thick dashed line depicts the rider torque averaged over the calibration trial, the thin dashed lines depict one standard deviation from the mean, and the thick solid line depicts $\hat{\tau}_p$. The estimate obtained for each subject was used in the subsequent trial to calculate $\hat{\tau}_a$.

Table 6-1. Passive torque estimate parameters for Subject 1.

Parameter	Value	Parameter	Value
a_0	-1.1108	b_1	0.1286
a_1	-0.1226	b_2	0.4559
a_2	-0.4834	b_3	0.0020
a_3	0.0112	b_4	-0.1664
a_4	-0.4055	b_5	0.0121
a_5	0.0131	b_6	-0.0370
a_6	-0.0763	b_7	0.0068
a_7	0.0142	b_8	-0.0011
a_8	-0.0102	ω	1

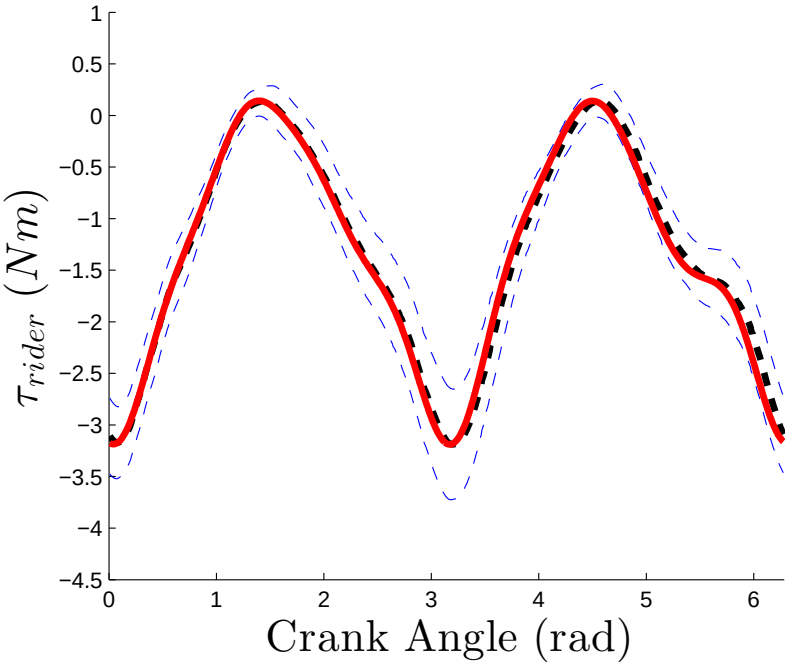

Figure 6-1. Measured versus estimated passive rider torque.

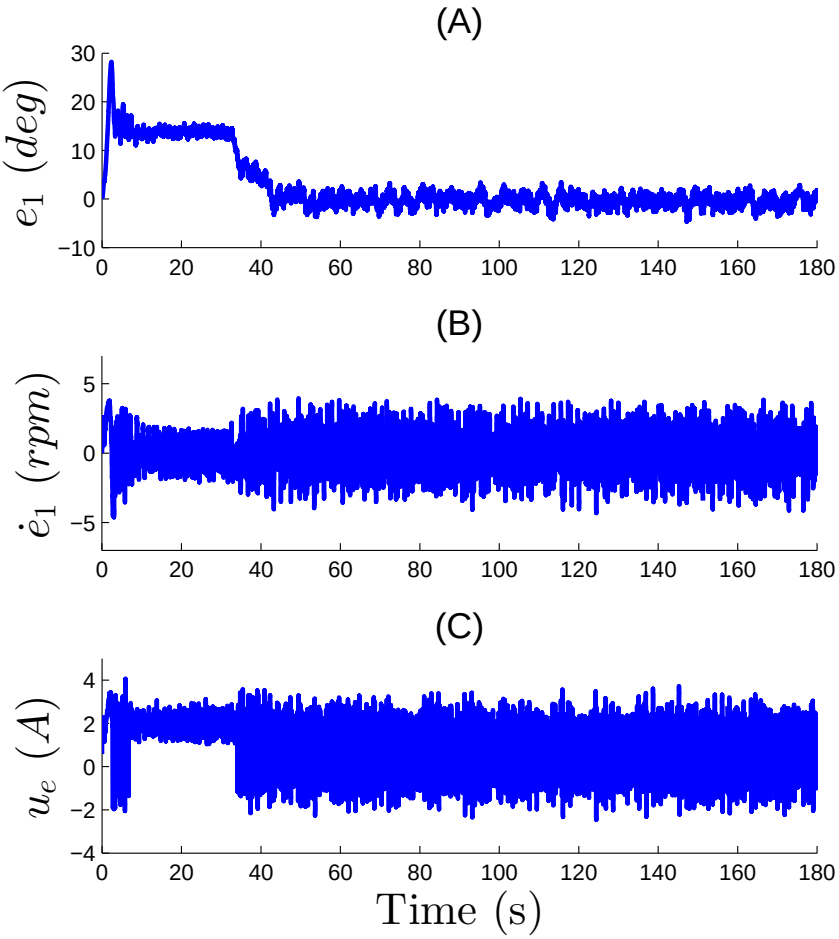

Figure 6-2. Electric motor controller's tracking performance. A) Position tracking error. B) Cadence tracking error. C) Motor input.

6.3.2 Results

Figure 6-2 depicts the electric motor controller's tracking performance for Subject 1, quantified by e_1, $\dot{e}_1$, and the electric motor current input u_e. Note that in the first 30 seconds of the trial (i.e., for $t < t_1$), there was a steady state error in the position tracking that was minimized after torque tracking began, since the electrical stimulation pushed the crank forward and essentially assisted the motor controller in catching up to the desired crank position. Across the trial for Subject 1, the motor maintained a position tracking error of 2.7 ± 5.8 degrees and a cadence tracking error of 0.0165 ± 1.5 rpm.

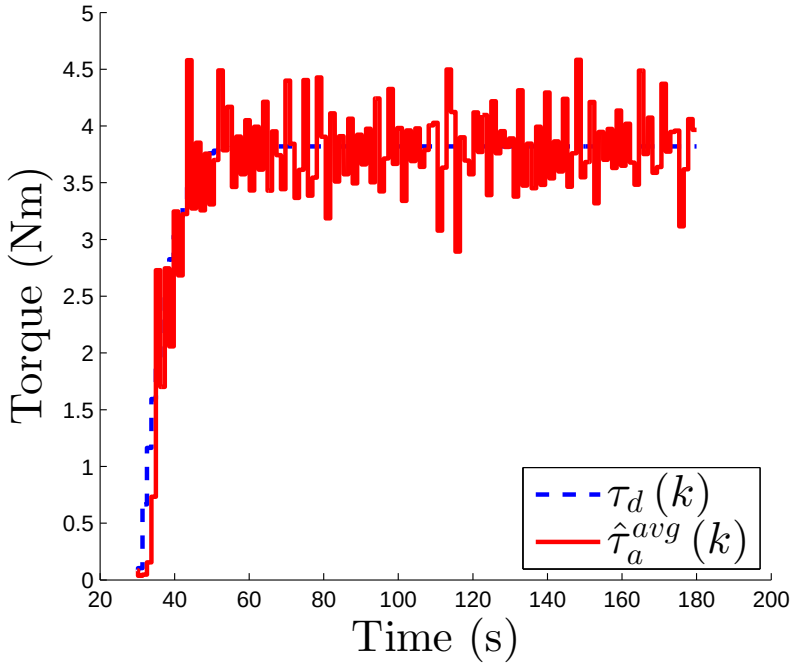

Figure 6-3. Desired versus actual active torque averaged over the crank cycle.

Figure 6-3 depicts the desired torque and the actual, active torque estimate, averaged over the crank cycle $\hat{\tau}_a^{avg}(k)$. Figure 6-4 depicts the FES controller's torque tracking performance, quantified by $e_\tau(k)$ and the stimulation applied to each muscle group u_m. Note that torque tracking did not begin until $t_1 = 30$ seconds, so no data is displayed in the first 30 seconds of Figure 6-4. Figure 6-5 provides an enhanced view of the stimulation input, depicted over a single crank cycle. Across the trial for Subject 1, the FES controller maintained an average active torque tracking error of 0.031 ± 0.38 Nm.

To quantify the overall performance of the power tracking system, the average, active power tracking error $e_\psi : \mathbb{R}_{\geq 0} \to \mathbb{R}$ is defined as

$$e_\psi(k) \triangleq \psi_d(k) - \hat{\tau}_a^{avg}(k)\, \dot{q}^{avg}(k),$$

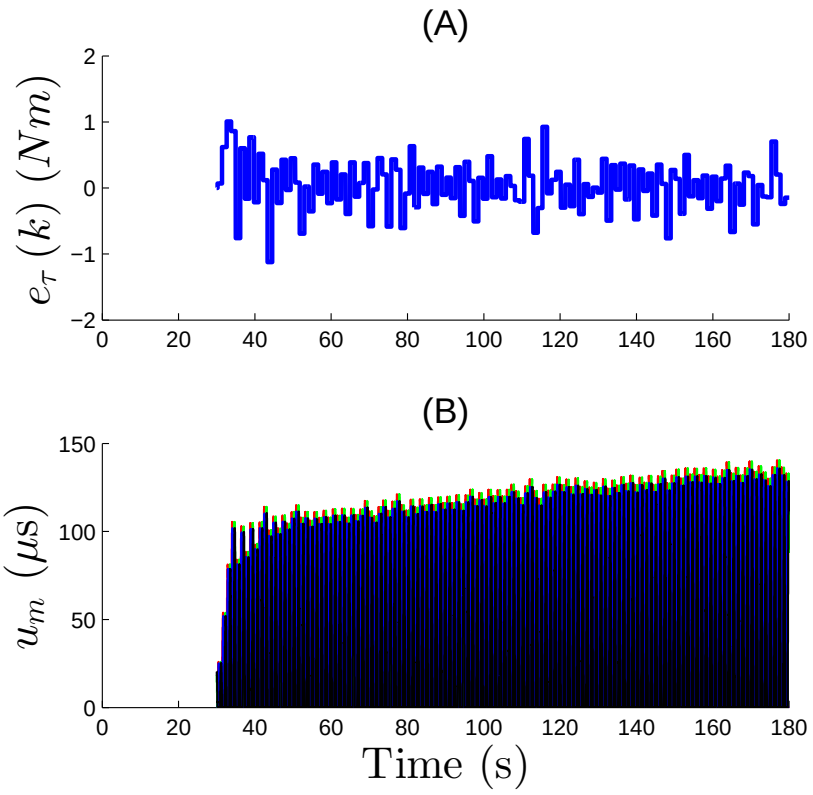

Figure 6-4. FES controller's torque tracking performance. A) Torque tracking error. B) Stimulation input.

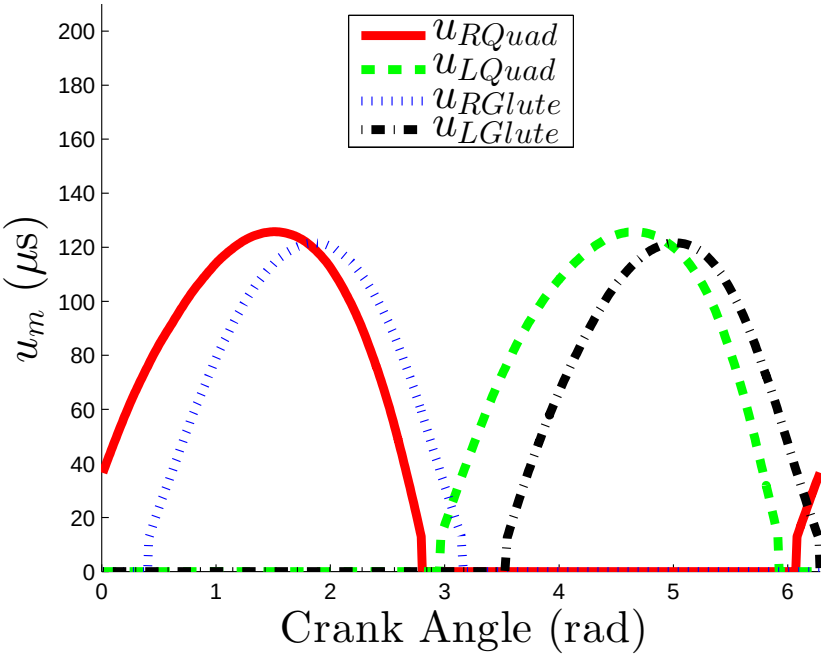

Figure 6-5. FES control input over a single crank cycle.

Table 6-2. Mean and standard deviation of tracking performance for all subjects.

Subject	e_1 (deg.)	$\dot{e}_1$ (rpm)	e_τ (Nm)	e_ψ (Watts)
1	2.7$\pm$5.8	0.0165$\pm$1.5	0.031$\pm$0.38	0.12$\pm$2.1
2	3.9$\pm$5.6	0.0199$\pm$2.3	0.066$\pm$0.56	0.29$\pm$3.0
3	2.9$\pm$6.3	0.0198$\pm$2.0	0.193$\pm$0.52	0.96$\pm$2.8

where $\dot{q}^{avg} : \mathbb{R}_{\geq 0} \to \mathbb{R}$ is defined as

$$\dot{q}^{avg}(k) \triangleq \int_{(k-1)T}^{kT} \dot{q}(t)\, dt.$$

Across the trial for Subject 1, the electric motor and FES controllers worked together to maintain an average, active power tracking error of 0.12 ± 2.1 Watts for a desired trajectory of 20 Watts at 50 rpm.

Table 6-2 reports the mean and standard deviation of the position, cadence, torque, and power tracking errors across the trial for each subject.

6.3.3 Discussion

The experimental results demonstrate ultimately bounded tracking of a desired active power output, averaged over the crank cycle, at a desired cadence. To compare the results with a recent study with the same tracking objectives, the normalized root-mean-square (NRMS) of the power tracking error was calculated for each subject as 10.3%, 15.3%, and 14.7%, respectively, for a desired trajectory of 20 Watts at 50 rpm, while in [23] the NRMS of the power tracking error ranged from 4.6% to 11.1% for a desired trajectory of 5-10 Watts at 40-45 rpm. In [23], the subjects had motor and sensory complete spinal cord injuries, and a fuzzy logic scheme was used to vary the pulse amplitude over the course of each trial. These differences, especially the use of spinal cord injured subjects, along with the slower and less powerful desired trajectories, likely lead to slightly better tracking performance. In the experiments described throughout this dissertation, it was observed that able-bodied subjects often have difficulty remaining completely passive during the experiments and sometimes

involuntarily resisted the stimulation because of discomfort, which was more easily observed in this chapter given feedback of the rider torque. More experiments must be conducted under similar conditions to truly compare the results with other works. Nevertheless, the results described herein demonstrate successful achievement of the control objective, and the developed control system provides a stepping stone for future work.

6.4 Concluding Remarks

Controllers for an electric motor and FES control inputs were developed that guarantee ultimately bounded tracking of a desired, average, active power output at a desired cycling cadence. As in the previous chapters, sliding mode controllers are used to achieve exponential convergence of the tracking error when the system is controlled. Unlike the previous chapters, the switching dynamics are due to quantization of the feedback signal, which is only measurable once per crank cycle, and the resulting discrete system has no uncontrolled regions. Stability is proven by means of discrete Lyapunov methods, and experimental results on three subjects demonstrate the electric motor and FES controllers' ability to track the desired trajectories.

Future work must investigate the practical implications of the developed control system, especially when applied to impaired individuals (e.g., spinal cord injured persons), as neurological impairments are likely to influence the magnitude of the power output that can be achieved by the rider. Another future direction along this line of work would be to investigate varying the stimulation pattern, in addition to the stimulation intensity, to achieve the desired torque output, as suggested in [26].

CHAPTER 7
CONCLUSION

Investigating the control of FES-cycling from the perspective of switched systems theory may yield insights into methods for improving the efficiency and power output of FES-cycling. In Chapter 2, a nonlinear, uncertain model of the cycle-rider system with pedaling induced by a switched FES control input was developed. In Chapters 3 and 4, switched sliding mode controllers were developed that yielded exponential convergence of the tracking error during periods where muscle groups were activated and divergence of the tracking error during periods where muscle groups were not activated. Chapter 5 built on the results of Chapters 3 and 4 by including electric motor input in the regions of the crank cycle where the muscle groups of the rider were not activated, thereby guaranteeing global, exponentially stable tracking of the desired crank position and cadence and removing the constraints on the desired cadence, initial conditions, and stimulation pattern that arose when unstable modes were present in the switched system. Chapter 6 detailed the development of an FES-cycling control system that uses an electric motor to control the cycling cadence while FES is used to achieve a desired active power output at the crank, and ultimately bounded tracking of a desired cycling workrate is achieved. Experiments were conducted on able-bodied individuals and an individual with Parkinson's disease to validate the developed control systems and to demonstrate how the control systems might impact clinical outcomes in a rehabilitative setting.

Throughout the development of these control systems, several challenges were encountered that could not be addressed in the scope of this dissertation.

Delay in the activation of stimulated muscle groups and their relaxation presents a significant challenge to effective FES-cycling. For example, if the delay is 100 milliseconds and the crank is rotating at 60 rpm, then the crank will have traveled 36 degrees before the stimulated muscle outputs the desired force or before the force dissipates.

The latter case is especially problematic, as the force may continue up to and beyond a dead point and cause backpedaling. Several past FES-cycling studies have attempted to address this issue by shifting the stimulation regions backwards proportional to the cadence scaled by an estimated delay [8, 15, 19], as was done in Chapter 6, or by using more sophisticated methods [21]. None of these studies considered that delay changes as a function of fatigue or analyzed the effects of the delay on the stability of the FES-cycling control system, so there is much room for further explorations in to how the stimulation pattern might be modulated as a function of the cycling cadence, fatigue, or other factors.

While the control systems developed in this dissertation utilized a model of both sides of the cycle-rider system as well as control gains for each muscle group, asymmetries in the system often caused degradations in the experimental control performance. Asymmetries in the system arise from differences in the rider's leg lengths and mass, muscle fiber type composition, muscle strength, location of motor units, electrode placement, joint stiffness and impedance, and other factors. Practically, the most significant factor affecting performance was the difference in B_{FES} between the right and left muscle groups, as the response by the muscle to electrical stimulation was always different when stimulating, for example, the quadriceps of the right leg versus the left. This issue would be exacerbated if a subject with extreme asymmetry, as would be the case for a subject with hemiparetic stroke, were to participate in FES-cycling. Experience indicates that tuning of the control gains for each muscle group could aid in combating the issue of asymmetry, as was done in the experiments for Chapter 3, but more sophisticated strategies, such as the one employed in [55], are likely to yield greater improvements in the control performance and should be explored further in the context of the methods developed in this dissertation.

A significant limitation of the switched systems approach applied in this dissertation is the necessity for stability results where the rate of convergence to or divergence

from the desired trajectory has a known bound (e.g., exponential convergence). This requirement led to the use of sliding mode control throughout this dissertation, which, while theoretically effective and robust, is certainly not the optimal or even the safest control strategy for FES-cycling. Adaptive control methods (e.g., neural networks, iterative control) have the potential to improve the experimental results, despite the inevitably weaker theoretical result (i.e., asymptotically stable tracking), because of the model knowledge they contribute to the control system by means of learning. Iterative learning control is a promising technique for FES-cycling because of the cyclical nature of the system and is especially promising for a tracking objective like that described in Chapter 6. However, applying adaptive control methods to switched systems with uncertainty and disturbances represents a significant challenge in terms of controller development and analysis. Nevertheless, explorations into the topic should be made, as adaptive control methods could not only improve the control performance but may also facilitate the adoption of FES-cycling into the clinical setting, as adaptive controllers could accommodate a wider range of subjects without requiring the tuning of control gains and other subject-specific parameters of the system.

In addition to investigating the challenges encountered in this dissertation, there remain challenges beyond the scope of this work that should be undertaken. In this work, only stationary cycling was considered, but mobile FES-cycling has the potential to provide people with paralysis a new form of mobility and recreation in addition to the already stated health benefits of FES-cycling. Mobile cycling presents its own set of engineering challenges, particularly when considering the effects of sloped terrain, turning, and safety despite environmental factors such as rain. The work in this dissertation could also serve as a stepping stone towards the concept of FES-walking. A natural progression from cycling to walking could occur through FES-cycling with ankle actuation, bodyweight-supported FES-cycling on an elliptical machine, bodyweight-supported FES-walking on a treadmill, and finally to bodyweight-supported

FES-walking over ground, likely with support from an exoskeleton or similar bracing system. Whatever the paths may be that lead from this dissertation, the clinical impact of FES-enhanced technologies should remain at the forefront of the researcher's mind, as there does exist a great need in the world beyond the laboratory for assistive technologies that can improve the quality of life for millions of people with paralysis.

APPENDIX: DETAILED EXPRESSIONS FOR CYCLE-RIDER DYNAMICS

The Euler-Lagrange dynamics for one side s of the cycle-rider system can be expressed as in (2–36) as

$$M^s\left(q\left(t\right)\right)\ddot{q}\left(t\right)+V^s\left(q\left(t\right),\ \dot{q}\left(t\right)\right)\dot{q}\left(t\right)+G^s\left(q\left(t\right)\right)=\tau^s_{crank}\left(t\right).$$

Detailed expressions for M^s, V^s, and G^s are provided as follows:

$$\begin{aligned}
M^s &= \left(m^s_t\left(l^s_{c,t}\right)^2+I^s_t+m^s_l\left(l^s_t\right)^2\right)\left(S^s_1\right)^2+\left(m^s_l\left(l^s_{c,l}\right)^2+I^s_l\right)\left(S^s_2\right)^2\\
&\quad -2m^s_l l^s_t l^s_{c,l}\cos\left(q^s_k-q^s_h\right)S^s_1S^s_2+m^s_c\left(l^s_{c,c}\right)^2+I^s_c,\\
V^s &= \left(\left(m^s_t\left(l^s_{c,t}\right)^2+I^s_t+m^s_l\left(l^s_t\right)^2\right)S^s_1\frac{l^s_c}{l^s_t}\left(\frac{\left(S^s_2-1\right)\cos\left(q^s_k-q\right)\sin\left(q^s_k+q^s_h\right)}{\sin^2\left(q^s_k+q^s_h\right)}\right)\right.\\
&\quad \left(m^s_t\left(l^s_{c,t}\right)^2+I^s_t+m^s_l\left(l^s_t\right)^2\right)S^s_1\frac{l^s_c}{l^s_t}\left(\frac{-\sin\left(q^s_k-q\right)\cos\left(q^s_k+q^s_h\right)\left(S^s_2+S^s_1\right)}{\sin^2\left(q^s_k+q^s_h\right)}\right)\\
&\quad -\left(m^s_l\left(l^s_{c,l}\right)^2+I^s_l\right)S^s_2\frac{l^s_c}{l^s_l}\left(\frac{\left(S^s_1+1\right)\cos\left(q^s_h+q\right)\sin\left(q^s_k+q^s_h\right)}{\sin^2\left(q^s_k+q^s_h\right)}\right)\\
&\quad -\left(m^s_l\left(l^s_{c,l}\right)^2+I^s_l\right)S^s_2\frac{l^s_c}{l^s_l}\left(\frac{-\sin\left(q^s_h+q\right)\cos\left(q^s_k+q^s_h\right)\left(S^s_2+S^s_1\right)}{\sin^2\left(q^s_k+q^s_h\right)}\right)\\
&\quad +m^s_l l^s_t l^s_{c,l}\sin\left(q^s_k-q^s_h\right)\left(S^s_2-S^s_1\right)S^s_1S^s_2\\
&\quad +m^s_l l^s_t l^s_{c,l}\cos\left(q^s_k-q^s_h\right)S^s_1\frac{l^s_c}{l^s_l}\left(\frac{\left(S^s_1+1\right)\cos\left(q^s_h+q\right)\sin\left(q^s_k+q^s_h\right)}{\sin^2\left(q^s_k+q^s_h\right)}\right)\\
&\quad +m^s_l l^s_t l^s_{c,l}\cos\left(q^s_k-q^s_h\right)S^s_1\frac{l^s_c}{l^s_l}\left(\frac{-\sin\left(q^s_h+q\right)\cos\left(q^s_k+q^s_h\right)\left(S^s_2+S^s_1\right)}{\sin^2\left(q^s_k+q^s_h\right)}\right)\\
&\quad -m^s_l l^s_t l^s_{c,l}\cos\left(q^s_k-q^s_h\right)S^s_2\frac{l^s_c}{l^s_t}\left(\frac{\left(S^s_2-1\right)\cos\left(q^s_k-q\right)\sin\left(q^s_k+q^s_h\right)}{\sin^2\left(q^s_k+q^s_h\right)}\right)\\
&\quad \left.-m^s_l l^s_t l^s_{c,l}\cos\left(q^s_k-q^s_h\right)S^s_2\frac{l^s_c}{l^s_t}\left(\frac{-\sin\left(q^s_k-q\right)\cos\left(q^s_k+q^s_h\right)\left(S^s_2+S^s_1\right)}{\sin^2\left(q^s_k+q^s_h\right)}\right)\right)\dot{q},\\
G^s &= -\left(m^s_t l^s_{c,t}\cos\left(q^s_h\right)S^s_1+m^s_l l^s_t\cos\left(q^s_h\right)S^s_1+m^s_l l^s_{c,l}\cos\left(q^s_k\right)S^s_2+m^s_c l^s_{c,c}\cos\left(q\right)\right)g.
\end{aligned}$$

REFERENCES

[1] C. A. Phillips, J. S. Petrofsky, D. M. Hendershot, and D. Stafford, “Functional electrical exercise: A comprehensive approach for physical conditioning of the spinal cord injured patient,” *Orthopedics*, vol. 7, no. 7, pp. 1112–1123, 1984.

[2] C.-W. Peng, S.-C. Chen, C.-H. Lai, C.-J. Chen, C.-C. Chen, J. Mizrahi, and Y. Handa, “Review: Clinical benefits of functional electrical stimulation cycling exercise for subjects with central neurological impairments,” *J. Med. Biol. Eng.*, vol. 31, pp. 1–11, 2011.

[3] J. S. Petrofsky, H. Heaton, and C. A. Phillips, “Outdoor bicycle for exercise in paraplegics and quadriplegics,” *J. Biomed. Eng.*, vol. 5, pp. 292–296, October 1983.

[4] D. J. Pons, C. L. Vaughan, and G. G. Jaros, “Cycling device powered by the electrically stimulated muscles of paraplegics,” *Med. Biol. Eng. Comput.*, vol. 27, no. 1, pp. 1–7, 1989.

[5] J. S. Petrofsky and J. Smith, “Three-wheel cycle ergometer for use by men and women with paralysis,” *Med. Biol. Eng. Comput.*, vol. 30, pp. 364–369, 1992.

[6] M. Gföhler, M. Loicht, and P. Lugner, “Exercise tricycle for paraplegics,” *Med. Biol. Eng. Comput.*, vol. 36, pp. 118–121, 1998.

[7] T. A. Perkins, N. N. Donaldson, N. A. C. Hatcher, I. D. Swain, and D. E. Wood, “Control of leg-powered paraplegic cycling using stimulation of the lumbro-sacral anterior spinal nerve roots,” *IEEE Trans. Neural Syst. Rehabil. Eng.*, vol. 10, no. 3, pp. 158–164, September 2002.

[8] K. J. Hunt, B. Stone, N.-O. Negård, T. Schauer, M. H. Fraser, A. J. Cathcart, C. Ferrario, S. A. Ward, and S. Grant, “Control strategies for integration of electric motor assist and functional electrical stimulation in paraplegic cycling: Utility for exercise testing and mobile cycling,” *IEEE Trans. Neural Syst. Rehabil. Eng.*, vol. 12, no. 1, pp. 89–101, March 2004.

[9] T. Watanabe, T. Murakami, and Y. Handa, “Preliminary tests of a prototype FES control system for cycling wheelchair rehabilitation,” in *Proc. 13th Int. Conf. of the IEEE ICORR*, June 2013, pp. 1–6.

[10] K. J. Hunt, D. Hosmann, M. Grob, and J. Saengsuwan, “Metabolic efficiency of volitional and electrically stimulated cycling in able-bodied subjects,” *Med. Eng. Phys.*, vol. 35, no. 7, pp. 919–925, July 2013.

[11] T. E. Johnston, “Biomechanical considerations for cycling interventions in rehabilitation,” *Phys. Ther.*, vol. 87, pp. 1243–1252, 2007.

[12] D. J. Newham and N. d. N. Donaldson, “FES cycling,” *Acta. Neurochir. Suppl.*, vol. 97, no. 1, pp. 395–402, 2007.

[13] K. J. Hunt, J. Fang, J. Saengsuwan, M. Grob, and M. Laubacher, “On the efficiency of FES cycling: A framework and systematic review,” *Technol. Health Care*, vol. 20, no. 5, pp. 395–422, 2012.

[14] L. M. Schutte, M. M. Rodgers, F. E. Zajac, and R. M. Glaser, “Improving the efficacy of electrical stimulation-induced leg cycle ergometry: An analysis based on a dynamic musculoskeletal model,” *IEEE Trans. Rehabil. Eng.*, vol. 1, no. 2, pp. 109–125, June 1993.

[15] M. Gföhler, T. Angeli, T. Eberharter, P. Lugner, W. Mayr, and C. Hofer, “Test bed with force-measuring crank for static and dynamic investigation on cycling by means of functional electrical stimulation,” *IEEE Trans. Neural Syst. Rehabil. Eng.*, vol. 9, no. 2, pp. 169–180, June 2001.

[16] J. S. Petrofsky, “New algorithm to control a cycle ergometer using electrical stimulation,” *Med. Biol. Eng. Comput.*, vol. 41, no. 1, pp. 18–27, January 2003.

[17] K. J. Hunt, M. Rothe, T. Schauer, A. Ronchi, and N. O. Negåard, “Automatic speed control in FES cycling,” in *Proc. 6th Conf. of the IFESS*, 2001, pp. 300–302.

[18] E. Ambrosini, S. Ferrante, T. Schauer, G. Ferrigno, F. Molteni, and A. Pedrocchi, “Design of a symmetry controller for cycling induced by electrical stimulation: preliminary results on post-acute stroke patients,” *Artif. Organs*, vol. 34, no. 8, pp. 663–667, August 2010.

[19] J.-J. J. Chen, N.-Y. Yu, D.-G. Huang, B.-T. Ann, and G.-C. Chang, “Applying fuzzy logic to control cycling movement induced by functional electrical stimulation,” *IEEE Trans. Neural Syst. Rehabil. Eng.*, vol. 5, no. 2, pp. 158–169, June 1997.

[20] Y. Ogawa, T. Inoue, T. Inada, Y. Tagawa, K. Yoshimitsu, and N. Shiba, “Locomotion assistance for the person with mobility impairment: fuzzy control of cycling movement by means of surface electrical-stimulation,” in *Proc. 29th Int. Conf. of the IEEE EMBS*, August 2007, pp. 2420–2423.

[21] C.-S. Kim, G.-M. Eom, K. Hase, G. Khang, G.-R. Tack, J.-H. Yi, and J.-H. Jun, “Stimulation pattern-free control of FES cycling: Simulation study,” *IEEE Trans. Syst. Man Cybern. Part C Appl. Rev.*, vol. 38, no. 1, pp. 125–134, January 2008.

[22] P.-F. Li, Z.-G. Hou, F. Zhang, M. Tan, H.-B. Wang, Y. Hong, and J.-W. Zhang, “An FES cycling control system based on CPG,” in *Proc. 31st Ann. Int. Conf. of the IEEE EMBS*, 2009, pp. 1569–1572.

[23] A. Farhoud and A. Erfanian, “Fully automatic control of paraplegic FES pedaling using higher-order sliding mode and fuzzy logic control,” *IEEE Trans. Neural Syst. Rehabil. Eng.*, vol. 22, no. 3, pp. 533–542, 2014.

[24] K. J. Hunt, C. Ferrario, S. Grant, B. Stone, A. N. McLean, M. H. Fraser, and D. B. Allan, “Comparison of stimulation patterns for FES-cycling using measures of

oxygen cost and stimulation cost," *Med. Eng. Phys.*, vol. 28, no. 7, pp. 710–718, September 2006.

[25] M. Gföhler and P. Lugner, "Dynamic simulation of FES-cycling: Influence of individual parameters," *IEEE Trans. Neural Syst. Rehabil. Eng.*, vol. 12, no. 4, pp. 398–405, December 2004.

[26] E. S. Idsø, T. Johansen, and K. J. Hunt, "Finding the metabolically optimal stimulation pattern for FES-cycling," in *Proc. Conf. of the Int. Funct. Electrical Stimulation Soc.*, Bournemouth, UK, September 2004.

[27] N. A. Hakansson and M. L. Hull, "Can the efficacy of eletrically stimulated pedaling using a commercially available ergometer be improved by minimizing the muscle stress-time integral?" *Muscle Nerve*, vol. 45, no. 3, pp. 393–402, March 2012.

[28] L. A. Bremner, K. E. Sloan, R. E. Day, E. R. Scull, and T. Ackland, "A clinical exercise system for paraplegics using functional electrical stimulation," *Paraplegia*, vol. 30, pp. 647–655, 1992.

[29] C. Fornusek, G. M. Davis, P. J. Sinclair, and B. Milthorpe, "Development of an isokinetic functional electrical stimulation cycle ergometer," *Nueromodulation*, vol. 7, no. 1, pp. 56–64, 2004.

[30] C. G. A. McRae, T. E. Johnston, R. T. Lauer, A. M. Tokay, S. C. K. Lee, and K. J. Hunt, "Cycling for children with neuromuscular impairments using electrical stimulation–development of tricycle-based systems," *Med. Eng. Phys.*, vol. 31, no. 6, pp. 650–659, 2009.

[31] L. D. Duffell, N. d. N. Donaldson, and D. J. Newham, "Power output during functional electrically stimulated cycling in trained spinal cord injured people," *Neuromodulation: Technology at the Neural Interface*, vol. 13, no. 1, pp. 50–57, 2010.

[32] D. Liberzon, *Switching in Systems and Control*. Birkhauser, 2003.

[33] E. S. Idsø, "Development of a mathematical model of a rider-tricycle system," Dept. of Engineering Cybernetics, NTNU, Tech. Rep., 2002.

[34] M. Gföhler and P. Lugner, "Cycling by means of functional electrical stimulation," *IEEE Trans. Rehabil. Eng.*, vol. 8, no. 2, pp. 233–243, June 2000.

[35] I. Carl D. Crane and J. Duffy, *Kinematic Analysis of Robot Manipulators*. Cambridge Uni. Press, 1998.

[36] J. Apkarian, S. Naumann, and B. Cairns, "A three-dimensional kinematic and dynamic model of the lower limb," *J. Biomechanics*, vol. 22, no. 2, pp. 143–155, 1989.

[37] M. Ferrarin and A. Pedotti, “The relationship between electrical stimulus and joint torque: A dynamic model,” *IEEE Trans. Rehabil. Eng.*, vol. 8, no. 3, pp. 342–352, September 2000.

[38] T. Schauer, N. O. Negård, F. Previdi, K. J. Hunt, M. H. Fraser, E. Ferchland, and J. Raisch, “Online identification and nonlinear control of the electrically stimulated quadriceps muscle,” *Control Eng. Pract.*, vol. 13, no. 9, pp. 1207–1219, September 2005.

[39] N. Sharma, K. Stegath, C. M. Gregory, and W. E. Dixon, “Nonlinear neuromuscular electrical stimulation tracking control of a human limb,” *IEEE Trans. Neural Syst. Rehabil. Eng.*, vol. 17, no. 6, pp. 576–584, June 2009.

[40] J. L. Krevolin, M. G. Pandy, and J. C. Pearce, “Moment arm of the patellar tendon in the human knee,” *J. Biomech.*, vol. 37, no. 5, pp. 785–788, 2004.

[41] D. A. Winter, *Biomechanics and Motor Control of Human Movement*. New York: Wiley, 1990.

[42] O. M. Rutherford and D. A. Jones, “Measurement of fibre pennation using ultrasound in the human quadriceps in vivo,” *Eur. J. Appl. Physiol. Occup. Physiol.*, vol. 65, pp. 433–437, 1992.

[43] A. Filippov, “Differential equations with discontinuous right-hand side,” *Am. Math. Soc. Transl.*, vol. 42 no. 2, pp. 199–231, 1964.

[44] B. E. Paden and S. S. Sastry, “A calculus for computing Filippov’s differential inclusion with application to the variable structure control of robot manipulators,” *IEEE Trans. Circuits Syst.*, vol. 34, no. 1, pp. 73–82, January 1987.

[45] C. Cai, A. Teel, and R. Goebel, “Smooth Lyapunov functions for hybrid systems part II: (pre)asymptotically stable compact sets,” *IEEE Trans. Autom. Control*, vol. 53, no. 3, pp. 734–748, 2008.

[46] M. M. Hoehn and M. D. Yahr, “Parkinsonism: onset, progression and mortality,” *Neurology*, vol. 17, no. 5, pp. 427–442, 1967.

[47] J. Szecsi, P. Krause, S. Krafczyk, T. Brandt, and A. Straube, “Functional output improvement in FES cycling by means of forced smooth pedaling,” *Med. Sci. Sports Exerc.*, vol. 39, no. 5, pp. 764–780, May 2007.

[48] P. C. Eser, N. Donaldson, H. Knecht, and E. Stussi, “Influence of different stimulation frequencies on power output and fatigue during FES-cycling in recently injured SCI people,” *IEEE Trans. Neural Syst. Rehabil. Eng.*, vol. 11, no. 3, pp. 236–240, September 2003.

[49] H. K. Khalil, *Nonlinear Systems*, 3rd ed. Upper Saddle River, NJ, USA: Prentice Hall, 2002.

[50] C. Fornusek and G. M. Davis, “Maximizing muscle force via low-cadence functional electrical stimulation cycling,” *J. Rehabil. Med.*, vol. 36, pp. 232–237, 2004.

[51] N. Sharma, C. Gregory, and W. E. Dixon, “Predictor-based compensation for electromechanical delay during neuromuscular electrical stimulation,” *IEEE Trans. Neural Syst. Rehabil. Eng.*, vol. 19, no. 6, pp. 601–611, 2011.

[52] T. Schauer, “Feedback control of cycling in spinal cord injury using functional electrical stimulation,” Ph.D. dissertation, University of Glasgow, 2006.

[53] J. Szecsi, A. Straube, and C. Fornusek, “Comparison of the pedalling performance induced by magnetic and electrical stimulation cycle ergometry in able-bodied subjects,” *Med. Eng. Phys.*, vol. 36, no. 4, pp. 484–489, 2014.

[54] L. Comolli, S. Ferrante, A. Pedrocchi, M. Bocciolone, G. Ferrigno, and F. Molteni, “Metrological characterization of a cycle-ergometer to optimize the cycling induced by functional electrical stimulation on patients with stroke,” *Med. Eng. Phys.*, vol. 32, no. 4, pp. 339 – 348, 2010.

[55] E. Ambrosini, S. Ferrante, G. Ferrigno, F. Molteni, and A. Pedrocchi, “Cycling induced by electrical stimulation improves muscle activation and symmetry during pedaling in hemiparetic patients,” *IEEE Trans. Neural Syst. Rehabil. Eng.*, vol. 20, no. 3, pp. 320–330, May 2012.

BIOGRAPHICAL SKETCH

Matthew Bellman has been a member of the Nonlinear Controls and Robotics group since May 2009, and has since received his bachelor's, master's, and doctoral degrees in mechanical engineering from the University of Florida under the guidance of Dr. Warren E. Dixon. Matthew completed his doctoral degree as a National Defense Science and Engineering Fellow, with a focus on the theoretical development of robust control systems for applications involving functional electrical stimulation, specifically those involving rehabilitation and mobility of the lower extremities. Matthew has started a company, MYOLYN, to bring the results of his research to the millions of people who could benefit from it, and it is there that he serves as MYOLYN's Co-founder and Chief Technology Officer.